Transcriptional Regulation of Gene Expression at Early Stages of Arabidopsis Vein Development

by

Jason Lloyd Gardiner

A thesis submitted in partial fulfillment of the requirements for the degree of

Doctor of Philosophy

in

Plant Biology

Department of Biological Sciences
University of Alberta

ABSTRACT

How multicellular organisms activate gene expression in the correct cells at the correct time is a central question in biology. In animals, in which this question has been investigated extensively, broadly expressed transcription factors activate target gene expression in narrow domains by a combination of differential affinity of such transcription factors for their binding sites in target genes and combinatorial interactions between transcription factors. In plants too, broadly expressed transcription factors often activate target gene expression in narrow domains; however, how broadly expressed plant transcription factors activate target gene expression in narrow domains is unclear. I addressed this question for the *MONOPTEROS* (*MP*)–*ARABIDOPSIS THALIANA HOMEOBOX8* (*ATHB8*) pair of Arabidopsis genes. *ATHB8* expression is activated in files of vascular precursor cells of the leaf. Activation of *ATHB8* expression in such narrow domains depends on binding of the broadly expressed MP transcription factor to a low-affinity MP-binding site in the *ATHB8* promoter. I tested the hypothesis that activation of *ATHB8* expression is restricted to narrow domains by binding of peak levels of the broadly expressed MP to a low-affinity MP-binding site in the *ATHB8* promoter. I found that activation of *ATHB8* expression is restricted to narrow domains by an MP-dependent incoherent feed-forward loop: MP activates *ATHB8* expression, but it also activates expression of the *AUXIN*/*INDOLE-3-ACETIC ACID INDUCIBLE* (*AUX*/*IAA*) gene *IAA12*/*BODENLOS*, which inhibits MP-mediated activation of *ATHB8* expression. In animals, a similar regulatory mechanism is most frequently used to activate gene expression in narrow domains, suggesting conservation of regulatory logic of striped gene expression in animals and plants despite the independent evolution of their multicellularity.

The development of multicellular organisms requires that not only do cells differentiate correctly but that they do so at the correct position. The correct differentiation of cells at the correct position depends on communication between cells; therefore, how cells communicate with one another is a key question in biology. In animals, such cell-cell communication often relies on direct coupling between cells. Direct cell-cell coupling is precluded in plants by a wall that surrounds each cell; yet, precisely because a cell wall holds plant cells in place and prevents their migration, positional signals, rather than lineage, specify cell fate in plants. For example, positional signals from leaf veins have long been known to control the differentiation of the adjacent bundle-sheath cells; however, the nature of such vein-derived signal had remained unclear. My results suggest that in Arabidopsis the SHORT-ROOT (SHR) transcription factor is such signal: the *SHR* gene is expressed in vascular precursor cells but the SHR protein is additionally localized to the adjacent layer of bundle-sheath cell precursors, and *shr* mutants fail to differentiate bundle-sheath cells. Available evidence suggests that restriction of *SHR* expression to vascular cells is critical to *SHR* function; yet what controls *SHR* vascular expression is poorly understood. I addressed this question for the Arabidopsis leaf. I found that *SHR* expression in vascular precursor cells is required for SHR-mediated induction of bundle-sheath differentiation, and that both *SHR* expression in vascular precursor cells and *SHR* function in bundle-sheath cell differentiation are directly and positively controlled by a group of previously functionally uncharacterized transcription factors of the DNA-BINDING WITH ONE FINGER (DOF) family. My results provide long-awaited molecular details of how veins act as source of positional signals that specify fate of adjacent cells—positional signals which are so critical for the development of multicellular organisms such as plants, the cells of which, unlike those of animals, are unable to migrate.

PREFACE

Two chapters of this Ph.D. thesis are published:

Chapter 2 has been published as Odat O., Gardiner J., Sawchuk M.G., Verna C., Donner T.J., and Scarpella E. 2014. "Characterization of an allelic series in the *MONOPTEROS* gene of Arabidopsis". *Genesis* 52(2): 127-133. All authors contributed equally to conceiving, designing and executing of the experiments, analyzing the data, and writing the manuscript. O. Odat and I—the co-first authors—collectively performed 55% of the experiments, while M.G. Sawchuk, C. Verna and T.J. Donner performed 20%, 15%, and 10% of the experiments, respectively.

Chapter 4 has been published as Gardiner J., Donner T.J., and Scarpella E. 2011. "Simultaneous activation of *SHR* and *ATHB8* expression defines switch to preprocambial cell state in Arabidopsis leaf development". *Developmental Dynamics* 240(1): 261-270. All authors contributed equally to conceiving, designing and executing of the experiments, analyzing the data, and writing the manuscript. T.J. Donner and I—the co-first authors—collectively performed all the experiments.

All the authors and publishers have given their permission for the inclusion of these publications in this thesis.

ACKNOWLEDGEMENTS

The opportunity to follow my passion for discovery has required the help and support of many people.

First and foremost, I am greatful for the opportunity given to me by Dr. Enrico Scarpella. His mentorship has opened my eyes to the world of science and helped me develop my mental and technical capabilities. Enrico has been a mentor who has believed in my abilities since the beginning and pushed me to realize my potential as a scientist. It has truly been a privilege and a pleasure to have spent these years working under his supervision.

During my time in the Scarpella lab I have had the opportunity to collaborate with many of the graduate students in the lab. They have helped me to grow and produce research I can be proud of. Ira Sherr, Tyler Donner, Megan Sawchuk, Osama Odat, and Carla de Agostini Verna: thank you for the camaraderie and help over the years in everything we have achieved together.

For kindly providing plasmids and seeds, without which my research would have been impossible, I thank the Arabidopsis Biological Resource Center, Thomas Berleth, Robert Campbell, David Galbraith, Kim Gallagher, Gerd Jürgens, Ben Scheres, Roger Tsien, and Dolf Weijers. I further thank Renze Heidstra for the Vectorette PCR protocol, Dolf Weijers for the *mp-B4149*genotyping strategy, and Viola Willemsen for information on polymorphism between Columbia-0 and Utrecht backgrounds.

For their generous scholarships and funding that have supported me throughout the years, I thank the the Natural Sciences and Engineering Research Council of Canada, the University of Alberta, the Government of Alberta, and the Alberta Society of Professional Biologists.

I thank Dr. Michael Deyholos and Dr. Uwe Hacke for their guidance as members of my supervisory committee.

Finally, I thank my wife, Stephanie Gardiner, and my parents, Lloyd and Wilma Gardiner, for their unwavering support and confidence in me, which has helped to bring me to this point. Without you this journey would have been over before it had started.

TABLE OF CONTENTS

LIST OF TABLES

LIST OF FIGURES

LIST OF ABBREVIATIONS

AD	Activation Domain
ABI3	ABSCISIC ACID INSENSITIVE3
ACL5	ACAULIS5
Arabidopsis	*Arabidopsis thaliana*
ARF	AUXIN RESPONSE FACTOR
ARR	ARABIDOPSIS RESPONSE REGULATOR
Asp	Aspartic Acid
ATHB8	ARABIDOPSIS THALIANA HOMEOBOX8
AUX/IAA	AUXIN/INDOLE-3-ACETIC ACID INDUCIBLE
AuxRE	Auxin Responsive Element
BDL	BODENLOS
bHLH	BASIC HELIX LOOP HELIX
BLH	BEL1-LIKE HOMEODOMAIN
bZIP	BASIC LEUCINE ZIPPER
CBF	C-REPEAT-BINDING FACTOR
CFP	CYAN FLUORESCENT PROTEIN
ChIP	Chromatin Immunoprecipitation
CNA	CORONA
Col-0	Columbia-0
CTD	Carboxyl-Terminal Domain
DAG	Days After Germination
DBD	DNA-Binding Domain
DNA	Deoxyribonucleic Acid
DOF	DNA BINDING WITH ONE ZINC FINGER
DR5	DIRECT REPEAT5
eal1	*endodermal-amyloplast less1*
EAR	ETHYLENE-RESPONSIVE ELEMENT-BINDING FACTOR-Associated Amphiphilic Repression

EIL	ETHYLENE-INSENSITIVE3-LIKE
EP	End Point
erGFP	Endoplasmic-Reticulum-Localized GREEN FLUORESCENT PROTEIN
EYFP	ENHANCED YELLOW FLUORESCENT PROTEIN
Fig	Figure
GAI	GIBBERELLIC ACID INSENSITIVE
GARP	GOLDEN2, TYPE-B ARABIDOPSIS RESPONSE REGULATOR, PHOSPHORUS STARVATION RESPONSE1, PHOSPHATE STARVATION RESPONSE1
GFP	GREEN FLUORESCENT PROTEIN
Gly	Glycine
GRAS	GIBBERELLIC ACID INSENSITIVE, REPRESSOR OF *gibberellic acid1-3,* AND SCARECROW
HD-ZIP	HOMEODOMAIN-LEUCINE ZIPPER
HD-ZIP III	Class III HD-ZIP
HTA6	HISTONE H2A 6
hv	Minor Veins
IAA	Indole-3-Acetic Acid
KAN	KANADI
KNOX	KNOTTED1-LIKE HOMEOBOX
KP	Break Point
l1	First Loop
l2	Second Loop
LAV	LEAFY COTYLEDON2, ABSCISIC ACID INSENSITIVE3, VIVIPAROUS1/ABSCISIC ACID INSENSITIVE3-LIKE
LEC2	LEAFY COTYLEDON2
LHW	LONESOME HIGHWAY
LUT	Look Up Table
miR	MicroRNA

MP	MONOPTEROS
mv	Midvein
nCFP	Nuclear CYAN FLUORESCENT PROTEIN
nGFP	Nuclear GREEN FLUORESCENT PROTEIN
NPA	1-N-Naphthylphthalamic Acid
NPH4	NON-PHOTOTROPIC HYPOCOTYL4
nRFP	Nuclear RED FLUORESCENT PROTEIN
nYFP	Nuclear YELLOW FLUORESCENT PROTEIN
OBE	OBERON
PHB	PHABULOSA
PHD	PLANT HOMEODOMAIN
PHR1	PHOSPHATE STARVATION RESPONSE1
PIN1	PIN-FORMED1
Pro	Proline
RAV	RELATED TO ABI3 AND VP1
REV	REVOLUTA
REM	REPRODUCTIVE MERISTEM
RFP	RED FLUORESCENT PROTEIN
RGA	REPRESSOR OF *gibberellic acid1-3*
RNA	Ribonucleic Acid
RNAi	RNA Interference
RT	Reverse Transcriptase
$SCF^{TIR1/AFB}$	S-PHASE KINASE ASSOCIATED PROTEIN1, CULLIN, F-BOX TRANSPORT INHIBITOR RESISTANT1/AUXIN SIGNALING F-BOX
SCL	SCARECROW-LIKE
SCR	SCARECROW
SEU	SEUSS
SHR	SHORT-ROOT
SPL	SQUAMOSA PROMOTER-BINDING PROTEINS-LIKE

T5L	TMO5-LIKE
TMO5	TARGET OF MONOPTEROS5
TP	Touch Point
UBQ10	UBIQUITIN10
VAL	VIVIPAROUS1/ABI3-LIKE
WOL	WOODEN LEG
WOX	WUSCHEL-RELATED HOMEOBOX
WT	Wild-Type
XP	Exit Point
YFP	YELLOW FLUORESCENT PROTEIN
ZF-HD	ZINC FINGER ASSOCIATED TO A HOMEODOMAIN

LOCUS IDENTIFIERS OF ARABIDOPSIS GENES

ABI3	AT3G24650
ACL5	AT5G19530
ATHB8	AT4G32880
ARF6	AT1G30330
ARF8	AT5G37020
ARF19	AT1G19220
ARR1	AT3G16857
ARR10	AT4G31920
ARR12	AT2G25180
BDL	AT1G04550
BEL1	AT5G41410
CNA	AT1G52150
DOF3.2	AT3G45610
DOF2.1	AT2G28510
DOF5.3	AT5G60200
DOF5.6	AT5G62940
DOF5.8	AT5G66940

GAI	AT1G14920
KAN1	AT5G16560
KAN2	AT1G32240
KAN3	AT4G17695
KAN4	AT5G42630
LEC2	AT1G28300
LHW	AT2G27230
MP	AT1G19850
NPH4	AT5G20730
OBE1	AT3G07780
OBE2	AT5G48160
PHB	AT2G34710
PHR1	AT4G28610
PIN1	AT1G73590
REV	AT5G60690
RGA	AT2G01570
SCL29	At3g13840
SCL3	AT1G50420
SCL32	AT3G49950
SCR	AT3G54220
SEU	AT1G43850
SHR	AT4G37650
T5L1	AT1G68810
T5L2	AT2G41130
T5L3	AT3G56770
TMO5	AT3G25710
UBQ10	AT4G05320
WOL	AT2G01830
WOX14	AT1G20700

WOX4	AT1G46480

ARABIDOPSIS GENE AND PROTEIN NOTATION

Uppercase Italics	WT Gene (e.g., *SHR*)
Uppercase Roman	WT Protein (e.g., SHR)
Lowercase Italics	Mutant Allele (e.g., *shr*)
Double Mutant of Gene *A* and *B*	a;b

GENE FUSION NOTATION

Transcriptional Fusion of Gene *A* to Gene *B* (Fusion of promoter *A* to gene *B*)	A::B
Translational Fusion of Gene *A* to Gene *B* (Fusion of gene *A* to gene *B*)	A:B

CHAPTER 1: GENERAL INTRODUCTION

1.1 The Plant Vascular System

The plant vascular system is a continuous network of vascular strands—cylinders of laterally juxtaposed files of vascular cells—which transport water, nutrients, and signaling molecules throughout the plant (Esau, 1965; Hopkins and Hüner, 2004). Vascular strands are named differently in different organs: veins in flat organs (cotyledons, leaves, sepals, and petals), vascular bundles in the stem, and vascular cylinder in the root.

In Arabidopsis, the dermatogen-stage embryo is composed of 16 cells: eight outer cells and eight inner cells (Mansfield and Briarty, 1991). The eight outer cells are the precursors of the epidermis, while the eight inner cells are the precursors of all the other tissue types (Fig. 1.1A). During embryogenesis, the eight inner cells will divide longitudinally, and the resulting four innermost cells in the basal half of the embryo will elongate to become procambial cells: the precursors of all vascular cells (Esau, 1965; Mansfield and Briarty, 1991)(Fig. 1.1B,C). The de novo formation of procambial cells from within a seemingly identical group of cells does not only occur during embryogenesis but also during the development of flat organs [in leaves for example: (Foster, 1952; Pray, 1955)]. Throughout the life of a plant, procambial cells will continue to divide transversely and longitudinally, thus lengthening and thickening vascular strands (Esau, 1965).

1.2 Vascular Strand Formation and Auxin Transport

Many substances induce vascular differentiation (Aloni, 1987; Caño-Delgado et al., 2010; Clouse and Sasse, 1998; Dettmer et al., 2009; Fukuda, 2004; Furuta et al., 2014; Kondo et al., 2015; Vera-Sirera et al., 2010; Werner and Schmulling, 2009); however, the plant signaling

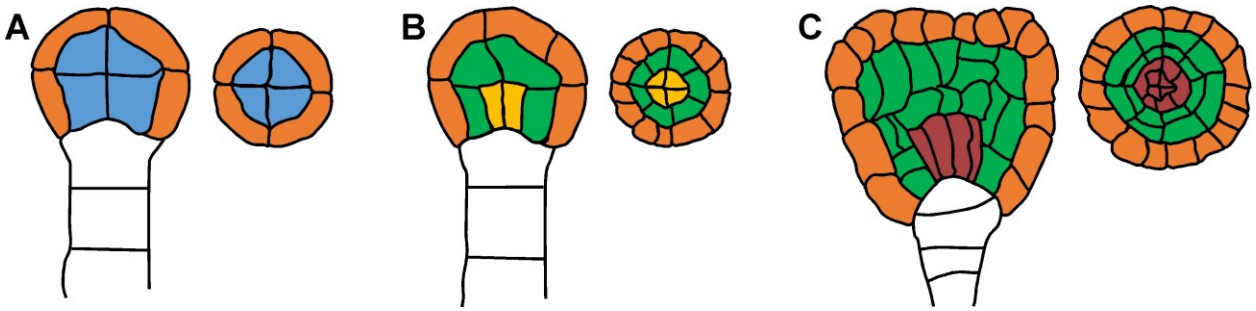

Figure 1.1. Formation of the first vascular cells in the Arbidopsis embryo.
Longitudinal (left) and transverse (right) sections of an Arabidopsis embryo at the dermatogen (A), globular (B), and triangular (C) stage of embryogenesis. Orange, epidermal cell precursors; blue, inner cells; green, ground cell precursors; yellow, procambial cell precursors; brown, procambial cells.

molecule auxin is unique among such compounds because it is the only one that is also capable of organizing vascular differentiation along continuous lines to induce the formation of vascular strands (Berleth et al., 2000; Sachs, 1981). The auxin-induced vascular-strand formation response is characterized by five defining properties (Berleth et al., 2000; Sachs, 1981): (i) the response is local, as vascular strands form from the site of auxin application; (ii) the response is polar, as vascular strands form toward the pre-existing vasculature located basally to the site of auxin application; (iii) the response is continuous, as it gives rise to uninterrupted files of vascular cells; (iv) the response is constrained laterally, as vascular differentiation is restricted to files of cells, rather than clouds of cells surrounding the site of auxin application; (v) the response requires the use of polarly transported auxins and is obstructed by polar auxin-transport inhibitors, suggesting that it is auxin transport and not auxin per se that is required for vascular strand formation.

Auxin is indeed transported, mainly through vascular tissue, from the immature apical regions of the plant, where it is synthesized, to the roots (Michniewicz et al., 2007; Normanly, 2010; Zhao, 2010). This apical-basal transport of auxin has been suggested to be the result of the polar localization of auxin efflux proteins to the basal plasma membrane of auxin-transporting cells (Raven, 1975; Rubery and Sheldrake, 1974). Indeed, indole-3-acetic acid (IAA)—the most common auxin in plants—is non-charged in the acidic extracellular space and can thus freely diffuse into cells through the plasma membrane (Raven, 1975; Rubery and Sheldrake, 1974). However, in the more alkaline intracellular space, IAA becomes negatively charged and can no longer passively diffuse through the plasma membrane but requires efflux proteins to exit the cell (Raven, 1975; Rubery and Sheldrake, 1974).

These observations form the basis of the ‘canalization hypothesis’, which proposes that auxin transport through a cell gradually increases the cell’s ability to transport auxin (Berleth and Sachs, 2001; Sachs, 1981, 1991, 2000). The hypothesis predicts that auxin efflux proteins are initially homogeneously distributed throughout the plasma membrane and that thus any applied auxin is initially transported without a preferred direction. However, pre-existing vascular strands, which efficiently transport auxin toward the root, would act as auxin sinks, soon orienting the movement of auxin in neighboring cells toward the pre-existing strands, thereby polarizing the localization of auxin efflux proteins in neighboring cells. These cells would

gradually become more efficient at transporting auxin and would eventually become auxin sinks for their neighboring cells. Repetition of this process would eventually lead to the selection of files of cells that are the preferred auxin transport routes and that would differentiate into vascular strands.

In Arabidopsis, the plasma-membrane localization of the auxin efflux protein PIN-FORMED1 (PIN1) marks the presumed site of cellular auxin efflux (Petrásek and Friml, 2009). Auxin application activates a broad domain of PIN1 expression connecting the applied auxin with pre-existing vascular strands; over time, this broad domain of PIN1 expression becomes restricted to files of cells through which auxin is preferentially transported and which will differentiate into vascular strands (Sauer et al., 2006). Consistent with the canalization hypothesis, PIN1 is initially homogeneously distributed throughout the plasma membrane and over time becomes polarly localized to the side of the cell closest the pre-existing vasculature (Sauer et al., 2006). Mutation of *PIN* genes or development in the presence of polar auxin-transport inhibitors leads to defects in vein network formation, supporting a role for polar auxin transport in vascular strand formation (Mattsson et al., 1999; Sawchuk et al., 2013; Sieburth, 1999; Verna et al., 2015).

1.3 Vascular Strand Formation and Auxin Signaling

The promoters of auxin inducible genes contain Auxin Responsive Elements (AuxREs) which are bound by AUXIN RESPONSE FACTORs (ARFs) (Ulmasov, 1997). When cellular levels of auxin are low, ARFs are bound by inhibitors belonging to the AUXIN/INDOLE-3-ACETIC ACID INDUCIBLE (AUX/IAA) family, which prevent ARFs from activating gene expression (Ulmasov et al., 1997). When cellular levels of auxin are high, auxin binds to both an AUX/IAA and the F-box subunit of the $SCF^{TIR1/AFB}$ (for S-PHASE KINASE ASSOCIATED PROTEIN1, CULLIN, F-BOX TRANSPORT INHIBITOR RESISTANT1/AUXIN SIGNALING F-BOX) E3 ubiquitin ligase complex; binding of auxin to both an AUX/IAA and the $SCF^{TIR1/AFB}$ brings the AUX/IAA into close proximity with the $SCF^{TIR1/AFB}$, which leads to AUX/IAA ubiquitination and subsequent degradation (Gray et al., 1999; Mockaitis and Estelle, 2008; Tan et al., 2007).

Degradation of the AUX/IAAs releases ARFs from inhibition, allowing them to activate gene expression (Tiwari et al., 2003; Ulmasov et al., 1997; Worley et al., 2000). While this model of auxin-dependent, ARF-mediated activation of gene expression has been well characterized, it only explains the function of ARFs that contain a transcriptional activation domain [for example, in Arabidopsis: ARF5/MONOPTEROS (MP hereafter), ARF6, ARF7/NON-PHOTOTROPIC HYPOCOTYL4 (NPH4 hereafter), ARF8, and ARF19] (Okushima et al., 2005; Tiwari et al., 2003; Ulmasov et al., 1999a) and not the function of the ARFs (17 in Arabidopsis) that act as repressors of transcription (Okushima et al., 2005; Tiwari et al., 2003).

Two pieces of evidence suggest that auxin signaling is key for vascular strand formation: (i) the expression domains of the synthetic auxin-responsive promoter DIRECT REPEAT5 (DR5) and of target genes of activating ARFs overlap with sites of vascular strand formation (Donner et al., 2009; Friml et al., 2003; Hardtke and Berleth, 1998; Mattsson et al., 2003; Okushima et al., 2005; Scarpella et al., 2004; Schlereth et al., 2010); (ii) Mutations in genes encoding auxin signaling components lead to the formation of fewer, if any, vascular strands (Alonso-Peral et al., 2006; Esteve-Bruna et al., 2013; Hardtke and Berleth, 1998; Przemeck et al., 1996).

1.4 Transcriptional Control of Vascular Strand Development

Two pieces of evidence suggest that vascular strand formation can be controlled at the transcriptional level: (i) transcription factors are expressed at sites of vascular strand formation and control vascular strand development; (ii) the vascular-specific expression of genes regulating vascular strand development is controlled by cis-regulatory elements. I will review these two pieces of evidence separately.

1.4.1 Transcription Factors Are Expressed at Sites of Vascular Strand Formation and Control Vascular Strand Development

1.4.1.1 B3 Transcription Factors

ARF, LAV [for LEAFY COTYLEDON2 (LEC2), ABSCISIC ACID INSENSITIVE3 (ABI3), VIVIPAROUS1/ABI3-LIKE (VAL)], RELATED TO ABI3 AND VP1 (RAV), and REPRODUCTIVE MERISTEM (REM) transcription factors share a conserved B3 domain: a ~110-amino-acid-long sequence that contains a DNA-binding domain enriched in basic amino acids (Swaminathan et al., 2008). Of all the B3 transcription factors, only ARFs have been implicated in the control of vascular strand development (Berleth and Jürgens, 1993; Hardtke and Berleth, 1998; Hardtke et al., 2004; Przemeck et al., 1996) (Table 1.1).

1.4.1.1.1 ARF

In Arabidopsis, *MP* and *NPH4* are expressed in vascular strands (Hardtke and Berleth, 1998; Hardtke et al., 2004; Okushima et al., 2005). Reduction of *MP* function by mutation or RNA interference (RNAi) leads to formation of fewer veins (Berleth and Jürgens, 1993; Hardtke and Berleth, 1998; Przemeck et al., 1996); additional *nph4* mutation in an *MP* RNAi background further reduces vein formation (Hardtke et al., 2004), suggesting that both *MP* and *NPH4* are positive regulators of vascular strand formation.

1.4.1.2 bHLH Transcription Factors

BASIC HELIX LOOP HELIX (bHLH) transcription factors share a conserved bHLH domain: a ~60-amino-acid-long sequence that contains a DNA-binding domain enriched in basic amino acids followed by a helix-loop-helix dimerization domain (Toledo-Ortiz et al., 2003). In Arabidopsis, the bHLH-related LONESOME HIGHWAY (LHW) and the bHLH TARGET OF MONOPTEROS5 (TMO5), TMO5-LIKE1 (T5L1), T5L2, and T5L3 have been implicated in the control of vascular strand development (Ohashi-Ito and Bergmann, 2007; Ohashi-Ito et al., 2013; Rybel et al., 2013) (Table 1.1).

Table 1.1. Proportion of Transcription Factors Expressed at Sites of Vascular Strand Formation and Controlling Vascular Strand Development

Transcription factor family	Number of family members in Arabidopsis[1]	Number of family members expressed at sites of vascular strand formation and controlling vascular strand development	Percentage of family members expressed at sites of vascular strand formation and controlling vascular strand development
B3	87	2	2.3%
bHLH	161	5	3.1%
GARP	55	7	12.7%
HOMEODOMAIN	90	8	8.9%
GRAS	33	1	3.0%

[1]Obtained from The Arabidopsis Information Resource (TAIR): https://www.arabidopsis.org/; accessed on September 19, 2016.

1.4.1.2.1 LHW, TMO5, and T5L1-3

In Arabidopsis, *LHW*, *TMO5, T5L1, T5L2,* and *T5L3* are expressed in the procambial cells of the embryo and in their initials, as well as in the vascular cylinder (Ohashi-Ito and Bergmann, 2007; Ohashi-Ito et al., 2013; Rybel et al., 2013). The *lhw* mutant embryo forms fewer procambial cell initials, a defect which will lead to fewer cell files in the vascular cylinder (Ohashi-Ito et al., 2013); fewer cell files in the vascular cylinder are also formed in the *tmo5*;*t5l1;t5l2;t5l3* quadruple mutant (Katayama et al., 2015; Rybel et al., 2013), suggesting that LHW, TMO5*,* T5L1, T5L2, and T5L3 are positive regulators of procambial cell division. In support of this conclusion, simultaneous ectopic expression of *TMO5* and *LHW* leads to more cell files in the vascular cylinder (Rybel et al., 2013).

1.4.1.3 GARP Transcription Factors

The GOLDEN2, KANADI (KAN), TYPE-B ARABIDOPSIS RESPONSE REGULATOR (ARR), and PHOSPHATE STARVATION RESPONSE1 (PHR1) transcription factors share a conserved GARP [for GOLDEN2, ARR, PHOSPHORUS STARVATION RESPONSE1, PHR1] domain: a ~60 amino-acid-long sequence that folds into a helix-turn-helix DNA-binding domain (Hosoda et al., 2002). Both KANs and TYPE-B ARRs have been implicated in control of vascular strand development (Eshed et al., 2001; Imamura et al., 1999; Ishida et al., 2008; Kerstetter et al., 2001; Rubio et al., 2001; Wykoff et al., 1999) (Table 1.1).

1.4.1.3.1 KAN

In Arabidopsis, all four *KAN*s (*KAN1–KAN4*) are expressed in vascular strands (Emery et al., 2003; Eshed et al., 2001; Kerstetter et al., 2001; McAbee et al., 2006). The vascular cylinder of the *kan1;kan2;kan3;kan4* quadruple mutant contains more cell files, suggesting that KANs are negative regulators of procambial cell division (Ilegems et al., 2010). In support of this conclusion, *KAN1* ectopic expression leads to complete loss of vascular tissue (Eshed et al., 2001; Ilegems et al., 2010; Kerstetter et al., 2001).

1.4.1.3.2 TYPE-B ARR

In Arabidopsis, *ARR1*, *ARR10*, and *ARR12* are expressed in vascular strands (Mason et al., 2004; Tajima et al., 2004; Yokoyama et al., 2007). The vascular cylinder of the *arr1*;*arr10*;*arr12* triple mutant contains fewer cell files (Ishida et al., 2008), suggesting that ARR1, ARR10, and ARR12 are positive regulators of procambial cell division.

1.4.1.4 HOMEODOMAIN Transcription Factors

The BEL1, BEL1-LIKE HOMEODOMAIN (BLH), HOMEODOMAIN-LEUCINE ZIPPER (HD-ZIP), KNOTTED1-LIKE HOMEOBOX, PLANT HOMEODOMAIN (PHD), WUSCHEL-RELATED HOMEOBOX (WOX), and ZINC FINGER ASSOCIATED TO A HOMEODOMAIN (ZF-HD) transcription factors share a conserved homeodomain: a ~60-amino-acid-long sequence that folds into a helix-turn-helix DNA-binding domain (Ariel et al., 2007). Of all the homeodomain transcription factors, HD-ZIPs, PHDs, and WOXs have been implicated in vascular strand development (Baima et al., 1995; Carlsbecker et al., 2010; Emery et al., 2003; McConnell et al., 2001; Otsuga et al., 2001; Prigge et al., 2005; Thomas et al., 2009) (Table 1.1).

1.4.1.4.1 HD-ZIP

In Arabidopsis, there are four classes (I–IV) of HD-ZIPs, each containing a unique set of class-specific conserved domains in addition to the DNA-binding homeodomain followed by the leucine zipper dimerization domain (Ariel et al., 2007). Of the five Class III *HD-ZIP* (*HD-ZIP III*) genes, at least four [*ARABIDOPSIS THALIANA HOMEOBOX8* (*ATHB8*), *CORONA* (*CNA*), *PHABULOSA* (*PHB*), and *REVOLUTA* (*REV*)] are expressed in procambial cells of the embryo and of the post-embryonic plant (Baima et al., 1995; Carlsbecker et al., 2010; Emery et al., 2003; McConnell et al., 2001; Otsuga et al., 2001; Prigge et al., 2005).

Mutation of all five *HD-ZIP III*s leads to arrest of vascular development at the procambial stage, suggesting that HD-ZIP IIIs are positive regulators of the differentiation of procambial cells into mature vascular cells (Carlsbecker et al., 2010).

Vascular strands of plants overexpressing *ATHB8* or *CNA* contain more cell files (Baima et al., 2001; Ochando et al., 2008), while vascular strands of plants overexpressing *PHB* contain fewer cells files (Carlsbecker et al., 2010). *CNA* overexpression and *PHB* overexpression

mutually suppress each other's effects on the number of cell files within vascular strands (Ochando et al., 2008), suggesting that *HD-ZIP III*s interact to control procambial cell division, a conclusion also suggested by some mutant combinations (Prigge et al., 2005).

1.4.1.4.2 PHD

In Arabidopsis, the *PHD*s *OBERON1* (*OBE1*) and *OBE2* are expressed in vascular strands (Thomas et al., 2009). The *obe1;obe2* double mutant forms fewer veins, suggesting that OBE1 and OBE2 are positive regulators of vascular strand formation (Thomas et al., 2009).

1.4.1.4.3 WOX

In Arabidopsis, *WOX4* and *WOX14* are expressed in vascular strands (Etchells et al., 2013; Hirakawa et al., 2010; Ji et al., 2010). The vascular bundles of the *wox4;wox14* double mutant contain fewer cell files, suggesting that WOX4 and WOX14 are positive regulators of procambial cell division (Etchells et al., 2013).

1.4.1.5 GRAS Transcription Factors

The GIBBERELLIC ACID INSENSITIVE (GAI), REPRESSOR OF *gibberellic acid1-3* (RGA), AND SCARECROW(SCR) (GRAS) transcription factors share a conserved VHIID domain which has been suggested to mediate DNA binding (Bolle, 2004; Pysh et al., 1999). Of all the GRAS transcription factors, only *SHR* has been implicated in vascular strand development (Cui et al., 2014; Dhondt et al., 2010; Helariutta et al., 2000; Di Laurenzio et al., 1996) (Table1.1).

1.4.1.5.1 SHR

In Arabidopsis, *SHORT-ROOT* (*SHR)* is expressed in the vascular cylinder and in veins (Cui et al., 2014; Dhondt et al., 2010; Helariutta et al., 2000). The vascular cylinder of the *shr* mutant contains fewer cell files (Levesque et al., 2006), suggesting that SHR is a positive regulator of procambial cell division.

1.4.2 The Vascular-Specific Expression of Genes Regulating Vascular Strand Development is Controlled by Cis-Regulatory Elements

1.4.2.1 MP, ATHB8, and ACL5

The vascular-specific expression of *ATHB8* depends on the binding of MP to the *ATHB8* promoter (Donner et al., 2009), and the vascular-specific expression of *ACAULIS5 (ACL5)* depends on the binding of ATHB8 to the *ACL5* promoter (Baima et al., 2014). The vascular strands of the *acl5* mutant contain more cell files (Baima et al., 2014), suggesting that ACL5 is a negative regulator of procambial cell division.

1.4.2.2 MP and *DOF5.8*

The vascular-specific expression of *DNA BINDING WITH ONE ZINC FINGER5.8* (*DOF5.8)* depends on the binding of MP to the *DOF5.8* promoter (Konishi et al., 2015). Mutation of *DOF5.8* in an *mp* mutant background enhances the vein network defects of *mp* (Konishi et al., 2015), suggesting that *MP* function in vein development is mediated, at least in part, by *DOF5.8*. Ectopic expression of *DOF5.8* leads to formation of fewer veins (Konishi and Yanagisawa, 2015), suggesting that DOF5.8 negatively feeds back on *MP* expression.

1.4.2.3 SEU and *SHR*

SHR expression in the vascular cylinder depends on the binding of the SEUSS (SEU) transcription factor to the *SHR* promoter (Gong et al., 2016).

1.5 Scope and Outline of Thesis

The evidence discussed above suggests that vascular strand development can be controlled at the transcriptional level; however, molecular details of such control are scarce. The scope of my Ph.D. thesis was to understand at the molecular level how gene expression is transcriptionally activated at early stages of vascular strand development. I chose to focus my investigations on

leaves because: (i) as in embryos (Mansfield and Briarty, 1991), in leaves, vascular strands form de novo (Foster, 1952; Pray, 1955); (ii) unlike embryos, leaves are readily accessible for imaging; (iii) unlike in other flat organs—such as sepals and petals—in leaves, stages of vascular strand development have been extensively characterized (Kang and Dengler, 2004; Mattsson et al., 1999; Sawchuk et al., 2007; Scarpella et al., 2004, 2006; Sieburth, 1999; Steynen and Schultz, 2003; Wenzel et al., 2007).

As discussed above, the best understood transcriptional control of vascular strand formation seems to rely on the function of the B3 transcription factor ARF5/MP. Accordingly, analyses of vascular defects of *mp* mutants have advanced, and will continue to advance, our understanding of the role of auxin signaling in vascular differentiation. Unfortunately, an *mp* allelic series in the widely used Columbia-0 wild-type background of Arabidopsis had been lacking.

In Chapter 2 (Odat et al., 2014), I addressed this limitation by extending the characterization of two known *mp* mutant alleles in the Columbia-0 background of Arabidopsis, and by identifying and characterizing four new alleles of *mp* in the Columbia-0 background. Among these four new *mp* mutant alleles, I found the first low-expression allele of *mp* and the strongest Columbia-0 allele of *mp*.

The expression of the *HD-ZIP III* gene *ATHB8* is activated in files of isodiametric, polygonal, ground cells of the leaf; *ATHB8*-expressing ground cells will elongate into procambial cells and are therefore referred to as “preprocambial cells” (Kang and Dengler, 2004; Sawchuk et al., 2007; Scarpella et al., 2004). Activation of *ATHB8* expression in files of preprocambial cells exclusively depends on binding of MP to a low-affinity MP-binding site in the *ATHB8* promoter (Donner et al., 2009); however, whereas both *ATHB8* and MP are expressed in files of preprocambial cells, MP is additionally expressed in surrounding ground cells, which fail to activate *ATHB8* expression; why is *ATHB8* expression only activated in a subset of MP-expressing cells?

In Chapter 3, I tested the hypothesis that *ATHB8* preprocambial expression is restricted to narrow domains by binding of peak levels of the broadly expressed MP to a low-affinity MP-binding site in the *ATHB8* promoter; I found that *ATHB8* preprocambial expression is restricted to narrow domains by an MP-dependent incoherent feed-forward loop: MP activates *ATHB8*

expression, but it also activates expression of the *AUX*/*IAA* gene *IAA12*/*BODENLOS* (*BDL*) (Krogan et al., 2014; Lau et al., 2011), which inhibits MP-mediated activation of *ATHB8* expression.

Files of *ATHB8*-expressing preprocambial cells mark sites of vascular strand formation (Kang and Dengler, 2004; Sawchuk et al., 2007; Scarpella et al., 2004). Moreover, changes in leaf vascular pattern by genetic or chemical means are foreshadowed by corresponding changes in *ATHB8* expression pattern (Alonso-Peral et al., 2006; Carland and Nelson, 2004; Carland et al., 2010; Ckurshumova et al., 2011; Cnops et al., 2006; Esteve-Bruna et al., 2013; Gardiner et al., 2010, 2011; Garrett et al., 2012; Hou et al., 2010; Koizumi et al., 2000; Krogan et al., 2012; Petricka and Nelson, 2007; Pineau et al., 2005; Pullen et al., 2010; Robles et al., 2010; Tsugeki et al., 2009) (Chapter 4). Therefore, available evidence suggests that activation of *ATHB8* expression in preprocambial cells is the first indicator of the final vascular pattern of the leaf, and that mechanisms controlling leaf vascular patterning are acting prior to preprocambial stages of vascular strand development. If termination of leaf vascular patterning is marked by activation of *ATHB8* expression, identification of genes the expression of which is activated in preprocambial cells, identification of the regulatory elements required for such preprocambial expression, and identification of the transcription factors binding to these elements should identify transcriptional controls of vascular strand development.

In Chapter 4 (Gardiner et al., 2011), I showed that expression of *SHR* is activated simultaneously with that of *ATHB8* during normal and experimentally manipulated leaf vascular patterning; however, whereas the ATHB8 protein remains confined to leaf vascular strands, as in the root (Nakajima et al., 2001), in the leaf, the SHR protein is additionally localized to the adjacent layer of bundle-sheath cell precursors.

In Chapter 5, I showed that activation of *SHR* expression in preprocambial cells is required for SHR-mediated induction of bundle-sheath differentiation, and that both *SHR* preprocambial expression and *SHR* function in bundle-sheath cell differentiation are directly and positively controlled by a group of previously functionally uncharacterized transcription factors of the DNA-BINDING WITH ONE ZINC FINGER (DOF) family.

Finally, in Chapter 6, I proposed and discussed two non-mutually exclusive hypotheses of how the transcriptional control of *SHR* preprocambial expression could be integrated with that of *ATHB8* preprocambial expression.

CHAPTER 2: CHARACTERIZATION OF AN ALLELIC SERIES IN THE *MONOPTEROS* GENE OF ARABIDOPSIS

2.1 Introduction

Auxin is a central regulator of plant development: during embryogenesis, it controls patterning of the embryo parts; during post-embryonic development, it controls the patterned formation of lateral shoot organs and lateral roots, and of their tissues (De Smet and Jürgens, 2007). The auxin signal is transduced by multiple pathways (Leyser, 2010); best understood is that which ends with the transcriptional activation or repression of auxin-responsive genes by transcription factors of the AUXIN RESPONSE FACTOR (ARF) family (Chapman and Estelle, 2009).

Of the 22 *ARF* genes in *Arabidopsis thaliana* (Guilfoyle and Hagen, 2007), *MONOPTEROS* (*MP*)/*ARF5* is the only one whose mutation results in conspicuous patterning defects in embryos and seedlings (Okushima et al., 2005). In *mp* embryos and seedlings, hypocotyl and root are typically replaced by a conical structure with no apparent cellular organization ("basal peg"), but weak mutant alleles occasionally form a short hypocotyl (Berleth and Jürgens, 1993) or both hypocotyl and root (Cole et al., 2009; Donner et al., 2009; Schlereth et al., 2010). In *mp*, the two cotyledons may be separate—as in wild-type (WT)—they may be fused to varying extents, or a single cotyledon may be formed (Berleth and Jürgens, 1993). Invariably, however, the vein network of *mp* cotyledons is simplified (Berleth and Jürgens, 1993). The severity of these defects has been shown to be inversely proportional to the amount of residual *MP* function and has thus been conventionally used as criterion to define allele strength (Berleth and Jürgens, 1993; Cole et al., 2009; Donner et al., 2009; Hardtke and Berleth, 1998; Schlereth et al., 2010).

Most *mp* alleles are in the Landsberg *erecta* background (Berleth and Jürgens, 1993), and only seven, recessive *mp* alleles have been reported in the widely used Columbia-0 (Col-0) background: two extensively characterized (*mp-G33* and *mp-S319*/*arf5-2*) and five only partially characterized (*mp-G12*, *mp-G25*, *mp-BS1354*, *arf5-1,* and *mp-B4149*) (Cole et al., 2009; Donner et al., 2009; Hardtke and Berleth, 1998; Okushima et al., 2005; Przemeck et al., 1996; Schlereth et al., 2010; Weijers et al., 2005). One of these five *mp* alleles (*mp-G25*) appears to be extinct and thus unavailable for analysis. We show that two of the four remaining, partially characterized *mp* alleles reported to be in the Col-0 background (*mp-BS1354* and *mp-B4149*) are in fact not in this background. We extend characterization of the remaining two Col-0 alleles of *mp* (*mp-G12* and *arf5-1*), and we identify and characterize four new alleles of *mp* in the Col-0 background (*mp-11*, *mp-12*, *mp-13*, and *mp-14*), among which the first low-expression allele of *mp* (*mp-11*) and the strongest Col-0 allele of *mp* (*mp-13*). These genetic resources provide the research community with new experimental opportunities for insight into the function of *MP*-dependent auxin signaling in plant development.

2.2 Results and Discussion

We were unable to induce germination of seed stocks of *mp-G25*; it is therefore possible that this allele has to be considered extinct and thus unavailable for further analysis. Because WT-looking siblings of *mp-BS1354* and *mp-B4149* appeared different from Col-0 plants (not shown), we characterized their background and found that *mp-BS1354* is in a Col-0/Wassilewskija mixed background (Fig. 2.1B) and *mp-B4149* is in the Utrecht background (Fig. 2.1C). We thus excluded these two alleles from further analysis.

The inviability of *mp-G25* seed stocks and the non-Col-0 backgrounds of *mp-BS1354* and *mp-B4149* left only *mp-G12* and *arf5-1* as partially characterized *mp* alleles in the Col-0 background. We thus surveyed available resources and identified seven additional, putative alleles of *mp* in the Col-0 background: lines WiscDsLox489-492C10, SAIL_1265_F06, SALK_144183, SALK_149553, WiscDsLoxHs148_11H, WiscDsLoxHs148_12G, and SALK_001058. None of the 30 plants that grew from the seed stock of line SALK_144183

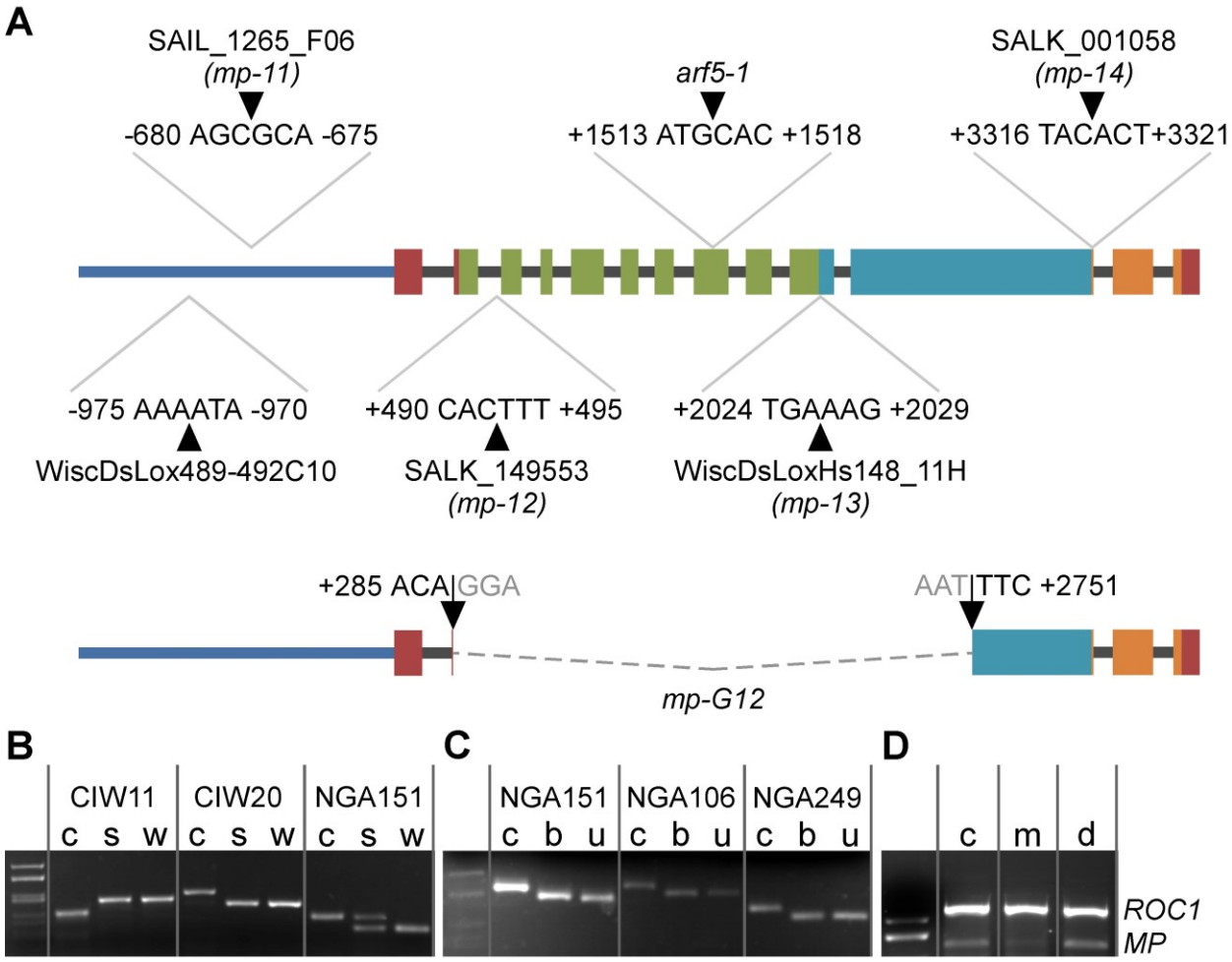

Figure 2.1. Mutations in the *MP* gene.

(A) Schematic diagram of the *MP* gene indicating position of insertions (black triangles) in *mp* mutants (top) or nature of molecular lesion in *mp-G12* (bottom). Coordinates are in nucleotides relative to the first nucleotide of the start codon. Lines depict promoter (blue, -1500 to -1) or introns (grey). Boxes depict translated exons: brown, sequences with unclear function (+1 to +309 and +3744 to +3827); green, sequence encoding the DNA-binding domain (Ulmasov et al., 1999b) (+310 to +2018); teal, sequence encoding the activation domain (Tiwari et al., 2003) (+2019 to +3312); orange, sequence encoding the carboxyl-terminal dimerization domain (Guilfoyle and Hagen, 2012) (+3313 to +3743). Dashed line depicts region of *MP* deleted in *mp-G12* and replaced with a sequence identical to sequences on all chromosomes (grey font, 5'-end of deletion) or with a sequence identical to gene AT1G16400 (grey font, 3'-end of deletion). See text for details. (B) Analysis of SSLP markers CIW11, CIW20, and NGA151 in Columbia-0 (c),

mp-BS1354 (s), and Wassilewskija (w). l, molecular weight marker (*Hae*III-digested pBluescript II). (C) Analysis of SSLP markers NGA151, NGA106, and NGA249 in Columbia-0 (c), *mp-B4149* (b), and Utrecht (u). l, molecular weight marker (*Hae*III-digested pBluescript II). (D) RT-PCR analysis of *MP* expression in 4-day-old seedlings of Columbia-0 (c), SAIL_1265_F06/*mp-11* (m), and WiscDsLox489-492C10 (d). The nearly evenly expressed *ROC1* (Lippuner et al., 1994) was used as control. l, molecular weight marker (*Hae*III-digested pBluescript II).

(predicted to have an insertion in the first intron of *MP*) or of the 60 plants that grew from the seed stock of line WiscDsLoxHs148_12G (predicted to have an insertion in the 10th exon of *MP*) had *mp*-like defects. Furthermore, we were unable to confirm the presence of insertion in *MP* in any of those plants. Finally, none of the progeny of those plants (~50 seedlings/plant) had *mp*-like defects. It is thus possible that lines SALK_144183 and WiscDsLoxHs148_12G are incorrectly annotated or that seeds that have inherited those insertions are extremely infrequent in the currently available stocks.

We found a T-DNA insertion after nucleotide -973 of *MP*—nucleotide coordinates are relative to the first nucleotide of the start codon—in line WiscDsLox489-492C10 (Fig. 2.1A), but seedlings homozygous for such insertion had no defects (not shown) or reduction in *MP* transcript (Fig. 2.1D). We thus excluded line WiscDsLox489-492C10 from further analysis.

Here we extend the characterization of the Col-0 alleles *mp-G12* and *arf5-1*, and we characterize four new alleles of *mp* in the Col-0 background, including the first low-expression allele and the strongest Col-0 allele.

We first determined the precise location of insertion in lines SAIL_1265_F06, SALK_149553, WiscDsLoxHs148_11H, and SALK_001058, and in *arf5-1*. We found a T-DNA insertion after nucleotide -678 of *MP* in line SAIL_1265_F06 (Fig. 2.1A); seedlings homozygous for such insertion had lower levels of *MP* transcript (Fig. 2.1D). Line SALK_149553 has a T-DNA insertion in the second intron of *MP* (Fig. 2.1A). *arf5-1* has a T-DNA insertion in the eighth exon of *MP*, which encodes part of the DNA-binding domain (DBD) (Ulmasov et al., 1999b) (Fig. 2.1A). Line WiscDsLoxHs148_11H has a T-DNA insertion in the 10th exon of *MP*, at the beginning of the sequence encoding the activation domain (AD) (Tiwari et al., 2003; Ulmasov et al., 1999a) (Fig. 2.1A). And line SALK_001058 has a T-DNA insertion in the 11th exon of *MP*, at the beginning of the sequence encoding for the carboxyl-terminal domain (CTD), which mediates interaction with ARF proteins or with repressors of the AUX/IAA family (Guilfoyle and Hagen, 2012) (Fig. 2.1A). Next, we determined by PCR the nature of the *MP* lesion in *mp-G12* and found that in this allele part of the *MP* gene was missing (not shown). By Vectorette PCR, we found that the missing sequence extended from nucleotide +288 to nucleotide +2748 (Fig. 2.1A). We isolated 435 bp of the sequence that preceded nucleotide +2748 of *MP* in *mp-G12* and found it to be identical to the sequence from nucleotide +2076 to

nucleotide +1641 of gene AT1G16400. We also isolated 34 bp of the sequence that followed nucleotide +288 of *MP* in *mp-G12* and found it to be identical to a sequence present on all five chromosomes. Our results are thus consistent with those of RFLP mapping, suggesting that the *mp-G12* allele is the result of a large chromosomal defect (Hardtke and Berleth, 1998).

We next analyzed the axis of seedlings homozygous for *mp-G12* or *arf5-1*, or for insertions SAIL_1265_F06, SALK_149553, WiscDsLoxHs148_11H, or SALK_001058. WT seedlings can be formalized as a top-to-bottom sequence of pattern elements: shoot meristem, cotyledons, and seedling axis—composed of hypocotyl and root (Capron et al., 2009) (Fig. 2.2A). In ~20–25% of the progeny of self-fertilized plants heterozygous for *mp-G12* (*n*=667) or *arf5-1* (*n*=626), or for insertions SAIL_1265_F06 (*n*=823), SALK_149553 (*n*=669), or WiscDsLoxHs148_11H (*n*=735), hypocotyl and root were replaced by a basal peg lacking the central vein typical of WT hypocotyl and root (Fig. 2.2A,B,D,E,G). Approximately 22% (*n*=784) of the progeny of self-fertilized plants heterozygous for insertion SALK_001058 were rootless; the hypocotyl was missing from most rootless seedlings, but a short hypocotyl with its central vein was formed in small proportion (<1%) of them (Fig. 2.2C,F). The proportion of rootless seedlings in the progeny of self-fertilized plants heterozygous for *mp-G12* or *arf5-1*, or for insertions SAIL_1265_F06, SALK_149553, WiscDsLoxHs148_11H, or SALK_001058, was not significantly different from that expected for a recessive phenotype associated with mutation in a single nuclear gene, as tested by Chi-squared test (not shown). We renamed SAIL_1265_F06, SALK_149553, WiscDsLoxHs148_11H, and SALK_001058 as *mp-11*, *mp-12*, *mp-13*, and *mp-14*, respectively.

Next, we analyzed cotyledon patterns of seedlings homozygous for *mp-G12*, *arf5-1*, *mp-11*, *mp-12*, *mp-13*, or *mp-14*. WT seedlings had two separate cotyledons (Fig. 2.3E). Nearly 75% of *mp-11* seedlings had two separate cotyledons, and all *mp-11* seedlings had at least one cotyledon (Fig. 2.3E). Approximately 50% of *mp-G12* seedlings had two separate cotyledons, and all *mp-G12* seedlings had at least one cotyledon (Fig. 2.3E). The spectrum of cotyledon pattern phenotypes of *arf5-1* seedlings was similar to that of *mp-12* seedlings: ~35–45% of seedlings had two separate cotyledons, and ~5% of seedlings had no cotyledons (Fig. 2.3E). And the spectrum of cotyledon pattern phenotypes of *mp-13* seedlings was similar to that of *mp-14*

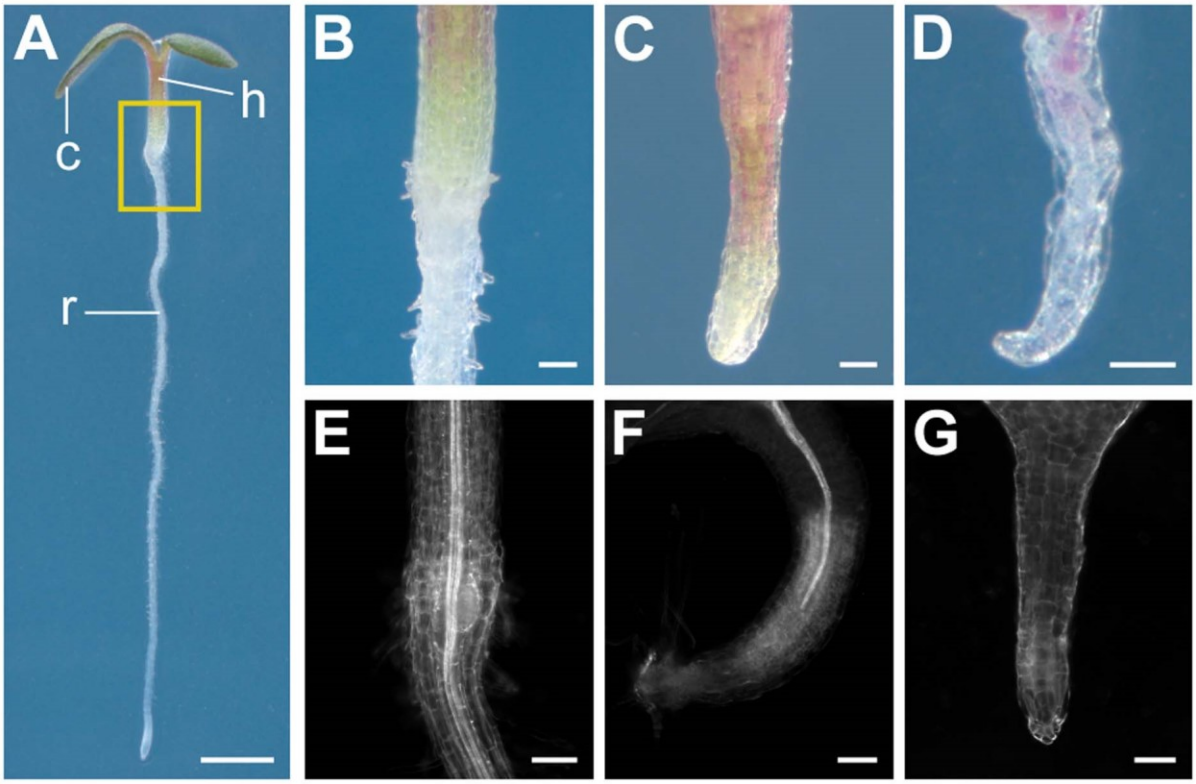

Figure 2.2. Seedling axis defects of *mp* alleles.

(A–G) Dark-field illumination of seedlings 3 days after germination. (A,B,E) WT. c, cotyledon; h, hypocotyl; r, root. (C,D,F,G) *mp*. (A–D) Live. (E–G) Cleared; mature veins appear bright due to their refraction properties. (B,E) Hypocotyl-root transition zone. Detail of an area as boxed in (A). (C,F) Hypocotyl-basal peg transition zone. (D,G) Basal peg. Scale bars: (A) 1 mm; (B–G) 0.1 mm.

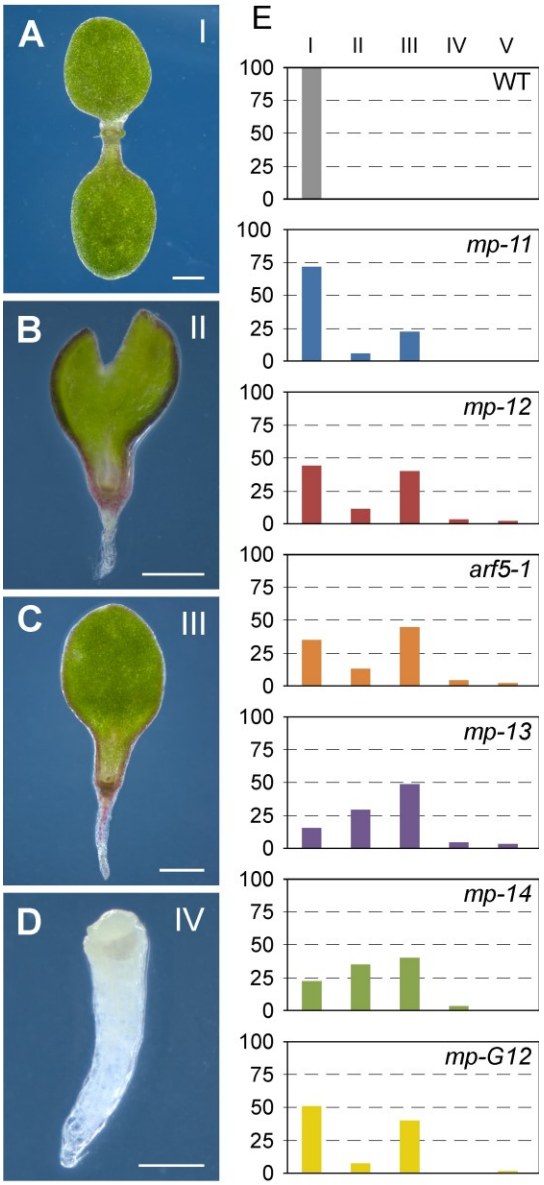

Figure 2.3. Cotyledon pattern defects of *mp* alleles.

(A–D) Dark-field illumination of seedlings 4 days after germination illustrating phenotype classes: Class I, two separate cotyledons (A); Class II, fused cotyledons (B); Class III, single cotyledon (C); Class IV, no cotyledons (D). Other, infrequent cotyledon-pattern defects were grouped in Class V (not shown). (E) Percentage of seedlings in phenotype classes. Sample population sizes: WT, 191; *mp-11*, 168; *mp-12*, 188; *arf5-1*, 164; *mp-13*, 179; *mp-14*, 172; *mp-G12*, 207. Scale bars: (A–C) 0.5 mm; (D) 0.25 mm.

seedlings: ~15–20% of seedlings had two separate cotyledons, and ~5% of seedlings had no cotyledons (Fig. 2.3E).

Finally, we analyzed cotyledon vein patterns of seedlings homozygous for *mp-G12*, *arf5-1*, *mp-11*, *mp-12*, *mp-13*, or *mp-14*. Four days after germination, nearly 75% of WT cotyledons had a central midvein and at least four vein loops (phenotype class I); ~25% had a simpler vein pattern, with a central midvein and up to three loops (class II) (Fig. 2.4A,B,F). Nearly 35% of *mp-11* cotyledons belonged to class I, ~45% belonged to class II, ~5% had no loops (class III), ~10% had a vein pattern in which the midvein bifurcated near the cotyledon tip (class IV), and nearly 5% had no veins (class V) (Fig. 2.4C–F). Most (~55%) of *mp-14* cotyledons belonged to class II, and the remaining ~45% were nearly equally distributed among classes III–V (Fig. 2.4F). The spectrum of vein pattern phenotypes of *mp-12* cotyledons was similar to that of *arf5-1* cotyledons and of *mp-G12* cotyledons: ~5–10% belonged to class II, ~65–70% to class III, and 25–35% to class V (Fig. 2.4F). Approximately 45% of *mp-13* cotyledons belonged to class III, and ~50% belonged to class V (Fig. 2.4F).

Our results suggest that *mp-11* is the weakest of the Col-0 alleles characterized here and the first low-expression allele of *mp*. Insertion after nucleotide -973 of *MP* in line WiscDsLox489-492C10 results in WT-looking individuals with normal levels of MP transcript. By contrast, insertion after nucleotide -678 of *MP* in *mp-11* results in ~30% reduction in levels of *MP* transcript and defects in hypocotyl and root formation, cotyledon separation, and vein patterning. This suggests that the 295-bp region of the *MP* promoter from nucleotide -972 to nucleotide -678—which contains putative binding sites for several transcription-factor families (Fig. 2.5)—might be required for *MP* function in these processes. Though it will be interesting to determine whether any of the putative regulatory elements in this promoter region are required for functional *MP* expression, the low-expression allele *mp-11* could already be used to test the hypothesis that *MP* expression dynamics are dependent on *MP* levels (Lau et al., 2011).

Our results also suggest that *mp-13* is the strongest Col-0 allele available. *mp-13* has an insertion at the beginning of the sequence that encodes MP's AD. It is difficult to explain how such mutation could result in stronger defects than those of *mp-G12*, in which the entire sequence encoding MP's DBD is missing. However, part of the sequence encoding MP's AD

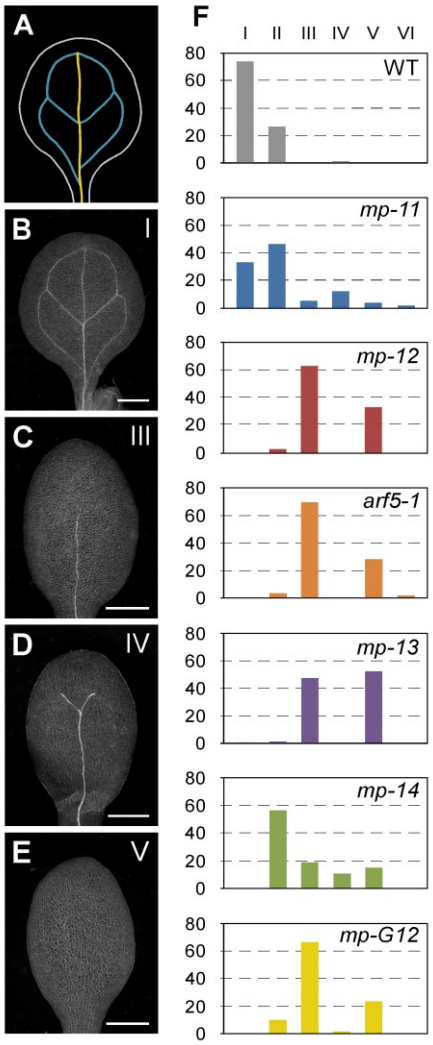

Figure 2.4. Vein pattern defects of *mp* alleles.

(A,B) Vein pattern of WT mature cotyledon. In (A), yellow, midvein; blue, vein loops. (B–E) Dark-field illumination of cleared cotyledons 4 days after germination illustrating phenotype classes: Class I, unbranched midvein and four or more loops (B); Class III, solitary, unbranched midvein (C); Class IV, bifurcated midvein (D); Class V, no veins (E). Class II is defined by unbranched midvein and up to three loops (not shown). Other, infrequent vein-pattern defects were grouped in Class VI (not shown). (F) Percentage of cotyledons in phenotype classes. Samples population sizes: WT, 191; *mp-11*, 168; *mp-12*, 188; *arf5-1*, 164; *mp-13*, 179; *mp-14*, 172; *mp-G12*, 207. Scale bars: (B–E) 0.5 mm.

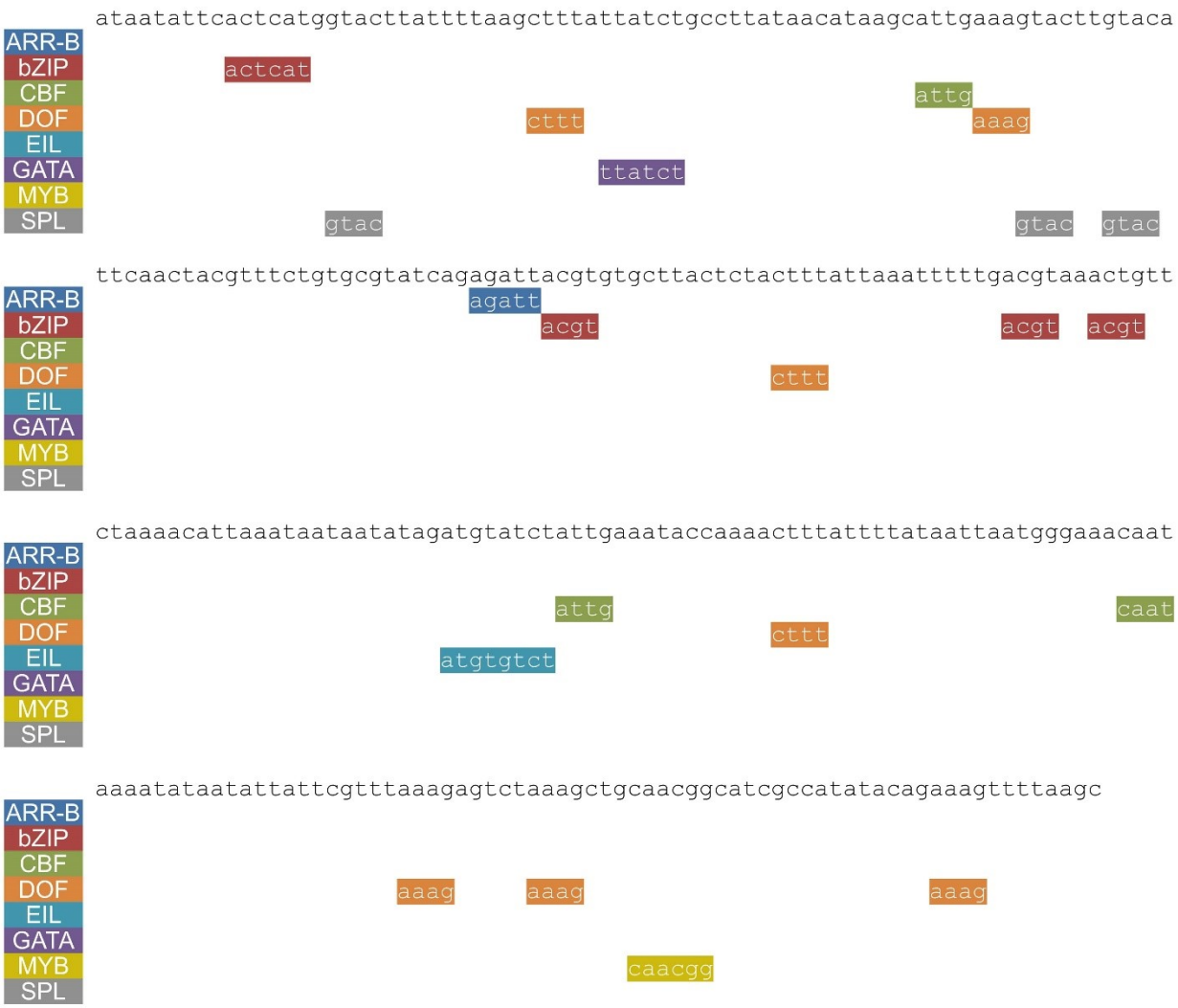

Figure 2.5. Putative transcription-factor binding sites in the 295-bp region of the *MP* promoter from nucleotide -972 to nucleotide -678.

Putative binding sites for transcription factors of the Type-B ARR (Hosoda et al., 2002), bZIP (Jakoby et al., 2002; Satoh et al., 2004), CBF (Bezhani et al., 2001), DOF (Yanagisawa, 2002), EIL (Kosugi and Ohashi, 2000), GATA (Reyes et al., 2004), MYB (Prouse and Campbell, 2012), and SPL (Birkenbihl et al., 2005) families are below sequence. Putative transcription-factor binding sites were identified as in (Donner and Scarpella, 2013). Presence of intact core sequence for each bioinformatically identified transcription-factor binding site was manually confirmed.

and the entire sequence encoding MP's CTD are present in *mp-G12*, and a similar *ARF* fragment has been shown to be sufficient to enhance auxin-responsive gene expression (Ulmasov et al., 1999a). Should the *mp-G12* allele be transcribed and translated, the resulting gene product might thus account for the weaker defects of *mp-G12* relative to those of *mp-13*. Alternatively, should the *mp-13* allele be transcribed and translated, the resulting protein—presumably lacking AD and CTD—might still be able to occupy MP binding sites in target promoters. Binding of such truncated protein might prevent binding of ARF proteins whose function is redundant to that of MP [e.g., (Hardtke et al., 2004)], and might thus account for the stronger defects of *mp-13* relative to those of *mp-G12*. However, these and other possibilities remain to be tested experimentally.

Unlike the defects of all the other *mp* alleles characterized here, the defects of *mp-14* appeared more or less severe depending on the phenotype feature used to assess strength: as weak alleles in other backgrounds (Berleth and Jürgens, 1993), *mp-14* seedlings occasionally form a short hypocotyl with a central vein; by contrast, cotyledon separation defects of *mp-14* are similar to those of *mp-13*, the strongest Col-0 allele; and vein pattern defects of *mp-14* are intermediate between those of *mp-13* and those of *mp-11*, the weakest allele described here. *mp-14* has an insertion at the beginning of the sequence encoding for MP's CTD, which mediates interaction with ARF proteins or AUX/IAA repressors (Guilfoyle and Hagen, 2012). The unusual behavior of *mp-14* might thus reflect the uneven contribution of these interactions to different developmental processes. This conclusion is consistent with the finding that *mp-S319*/*arf5-2*, which has an insertion only a few nucleotides downstream of the location of the *mp-14* insertion, has completely penetrant defects only in some of the developmental processes that depend on *MP* (Cole et al., 2009; Donner et al., 2009; Schlereth et al., 2010); it is also consistent with the finding that an MP protein lacking the entire CTD supplies semidominant functions only in a subset of *MP*-dependent developmental processes (Krogan et al., 2012).

In conclusion, by characterizing six mutant alleles of *MP* in the Col-0 background—including four new alleles, among which the first low-expression allele and the strongest Col-0 allele—we have provided the research community with new genetic resources to understand the role of *MP*-dependent auxin signaling in plant development.

2.3 Materials and Methods

2.3.1 Plants

Origin of lines is in Table 2.1. Unless otherwise stated, seeds were sterilized and germinated as in the work by (Sawchuk et al., 2008). Genotyping strategies are in Table 2.2. Oligonucleotide sequences are in Table 2.3.

2.3.2 Vectorette PCR

About 500 ng of *mp-G12* DNA were digested with *Csp*6I for two hours and ligated to a vectorette unit generated by annealing the "V-PCR FORWARD" and "V-PCR rev" oligonucleotides (Table 2.3). The sequences flanking the ligated vectorette unit were amplified with Phusion High-Fidelity DNA Polymerase (Thermo Fisher Scientific Inc., Waltham, MA) and the "V3" and "MP pro1 forw", or the "V3" and "MP vec1 Rev", oligonucleotides (Table 2.3). The resulting product was amplified with the "V4" and "MP pro3 forw", or the "V4" and "MP vec2 Rev", oligonucleotides (Table 2.3), and sequenced.

2.3.3 RT-PCR

Total RNA was extracted as in the work by (Chomczynski and Sacchi, 1987) from 4-day-old seedlings grown in half-strength Murashige and Skoog salts (Caisson Laboratories, North Logan, UT), 15 g l^{-1} sucrose (BioShop Canada Inc., Burlington, Canada), 0.5 g l^{-1} MES (BioShop Canada Inc.), pH 5.7, at 25°C under continuous light (~65 µmol m^{-2} sec^{-1}) on a rotary shaker at 50 rpm. RT-PCR was performed on 100 ng of total RNA with the "MP 1993 geno" and "WiscDsLoxHs148_12G/149_11H RP" oligonucleotides (Table 2.3), and with the "ROC1 F" and "ROC1 R" oligonucleotides (Beeckman et al., 2002) (Table 2.3), using the Access RT-PCR System (Promega, Fitchburg, WI).

Table 2.1. Origin and Nature of Lines

Line	**Origin/Nature**
mp-BS1354	(Hardtke and Berleth, 1998)
mp-B4149	(Weijers et al., 2005)
SALK_144183	ABRC; (Alonso et al., 2003)
WiscDsLoxHs148_12G	ABRC (CS914207); (Nishal et al., 2005; Woody et al., 2007; Zhang et al., 2003)
WiscDsLox489-492C10	ABRC (CS858306); (Woody et al., 2007)
mp-G12	(Hardtke and Berleth, 1998)
arf5-1	(Okushima et al., 2005)
mp-11/SAIL_1265_F06	ABRC (CS879048); (Sessions et al., 2002)
mp-12/SALK_149553	ABRC; (Alonso et al., 2003)
mp-13/WiscDsLoxHs148_11H	ABRC (CS914200); (Nishal et al., 2005; Woody et al., 2007; Zhang et al., 2003)
mp-14/SALK_001058	ABRC; (Alonso et al., 2003)

Table 2.2. Genotyping Strategies

Line	**Strategy**
SALK_144183	*MP*: 'SALK_144183 LP' and 'SALK_144183 RP'; *mp*: 'SALK_144183 RP' and 'LBb1.3'
WiscDsLoxHs148_12G	*MP*: 'WiscDsLoxHs148_12G/148_11H LP' and 'WiscDsLoxHs148_12G/149_11H RP'; *mp*: 'WiscDsLoxHs148_12G/149_11H RP' and 'L4'
WiscDsLox489-492C10	*MP*: 'WiscDsLox489-492C10 LP' and 'WiscDsLox489-492C10 RP'; *mp*: 'WiscDsLox489-492C10 RP' and 'p745'
mp-G12	*MP*: 'BS1354-F' and 'BS1354-R'; *mp*: 'G12 inst 2 forw' and 'MP vec2 Rev'
arf5-1	*MP*: 'SALK_023812 LP' and 'SALK_023812 RP' *mp*: 'MP2082-AS' and 'LBb1.3';
mp-11/SAIL_1265_F06	*MP*: 'SAIL_1265_F06LP' and 'SAIL_1265_F06RP'; *mp*: 'SAIL_1265_F06RP' and 'LB3'
mp-12/SALK_149553	*MP*: 'SALK_149553 LP' and 'SALK_149553 RP'; *mp*: 'SALK_149553 RP' and 'LBb1.3'
mp-13/WiscDsLoxHs148_11H	*MP*: 'WiscDsLoxHs148_12G/148_11H LP' and 'WiscDsLoxHs148_12G/149_11H RP'; *mp*: 'WiscDsLoxHs148_12G/149_11H RP' and 'L4'
mp-14/SALK_001058	*MP*: 'SALK_001058 LP' and 'SALK_001058 RP'; *mp* 'SALK_001058 RP' and 'LBb1.3'

Table 2.3. Oligonucleotide Sequences

Name	Sequence (5' to 3')
SALK_144183 LP	AGAAACCTCCATGTGTGCTTG
SALK_144183 RP	AATTCCTCTGGTTTGTCCTGG
LBb1.3	ATTTTGCCGATTTCGGAAC
WiscDsLoxHs148_12G/148_11H LP	TTTGTCCTTTGAAAATGTGCC
WiscDsLoxHs148_12G/149_11H RP	GTTAGCTTGTTTTGTGGCTGC
L4	TGATCCATGTAGATTTCCCGGACATGAAG
WiscDsLox489-492C10LP	GGCTCTTGCCTCTTCTCTTTC
WiscDsLox489-492C10RP	TTGGAAAGGAAAAGAACACCC
p745	AACGTCCGCAATGTGTTATTAAGTTGTC
BS1354-F	GAGATGGCCTGGTTCTAAGTGGC
BS1354-R	GCCAGTTCAACATCTCGGTTATCG
G12 inst 2 forw	GGATAAAGGTTTGATGCCAAGCGTG
MP vec2 Rev	CAAGAGACTGGAAGGAAGAGACTTGTG
SALK_023812 LP	GAGAGGAAGTAAGCACCCGAC
SALK_023812 RP	TCATTACATCCAGGCTCATCC
MP2082-AS	ATGGATGGAGCTGACGTTTGAGTTCGGACTCAAA CGTCAGCTCCATCCA
SAIL_1265_F06LP	GCTTCATCTCTTCAAGCAAGG
SAIL_1265_F06RP	TCCCAAAGTCTCACCACTCAC
LB3	TAGCATCTGAATTTCATAACCAATCTCGATACAC
SALK_149553 LP	AATTCCTCTGGTTTGTCCTGG
SALK_149553 RP	AGAAACCTCCATGTGTGCTTG
SALK_001058 LP	ATGGACTTGAGCAGTCAATGG
SALK_001058 RP	CCTTCTTCACTCATCTGCTGG

CIW11 Primer 1	CCCCGAGTTGAGGTATT
CIW11 Primer 2	GAAGAAATTCCTAAAGCATTC
CIW20 Primer 1	CATCGGCCTGAGTCAACT
CIW20 Primer 2	CACCATAGCTTCTTCCTTTCTT
NGA151 Primer 1	CAGTCTAAAAGCGAGAGTATGATG
NGA151 Primer 2	GTTTTGGGAAGTTTTGCTGG
NGA106 Primer 1	TGCCCCATTTTGTTCTTCTC
NGA106 Primer 2	GTTATGGAGTTTCTAGGGCACG
NGA249 Primer 1	GGATCCCTAACTGTAAAATCCC
NGA249 Primer 2	TACCGTCAATTTCATCGCC
V-PCR FORWARD	TACAGGAGAGGACGCTGTCTGTCGAAGGTAAGG AACGGACGAGAGAAGGGAGAG
V-PCR rev	CTCTCCCTTCTCGAATCGTAACCGTTCGTACGAG AATCGCTGTCCTCTCCTG
V3	ATCGTAACCGTTCGTACGAGAATCGC
MP pro1 forw	GAGAGAGAAAGAGAAGAGGCAAGAGC
MP vec1 Rev	CATCTTGAGCAAAGCTAGTGTTGTTG
V4	ACCGTTCGTACGAGAATCGCTGTC
MP pro3 forw	GCTAAAGCCTAGTTAGTGTTGAGTGTGG
MP 1993 geno	TCGGGTCAGTCCATGGGATATCG
ROC1 F	CAAACCTCTTCTTCAGTCTGATAGAGA
ROC1 R	GAGTGCTCATTCCTTATTTCTGGTAG

2.3.4 Imaging

Three-day-old seedlings were fixed, cleared, and mounted as in (Scarpella et al., 2004). Images were acquired with an Olympus SZ61TR (Olympus Corporation, Shinjuku, Japan) or an AxioImager.M1 (Carl Zeiss AG, Oberkochen, Germany) microscope equipped with an AxioCam HR camera (Carl Zeiss AG, Oberkochen, Germany) or a Hamamatsu ORCA-AG camera (Hamamatsu Photonics K.K., Hamamatsu, Japan), respectively. Brightness and contrast were adjusted by linear stretching of the histogram with ImageJ (Schneider et al., 2012). Images were cropped with Adobe Photoshop 7.0 (Adobe Systems Inc., San Jose, CA) and assembled into figures with Canvas 8.0 (ACD Systems Inc., Victoria, Canada).

CHAPTER 3: CONTROL OF LEAF VEIN FORMATION BY AUXIN SIGNALING

3.1 Introduction

How multicellular organisms activate gene expression in the correct cells at the correct time is a central question in biology. In animals, in which this question has been investigated extensively, gene expression is activated in narrow domains by broadly expressed transcription factors by a combination of (i) differential affinity of such transcription factors for their binding sites in target genes and (ii) combinatorial interactions between transcription factors [reviewed in (Ashe and Briscoe, 2006; Hironaka and Morishita, 2012; Rogers and Schier, 2011)]. For example, the transcription factor Dorsal forms a ventral-to-dorsal gradient in Drosophila embryos [reviewed in (Reeves and Stathopoulos, 2009)]. Expression of Dorsal target genes with high-affinity Dorsal-binding sites is activated already at low levels of Dorsal, whereas expression of Dorsal target genes with low-affinity Dorsal-binding sites is activated only at high levels of Dorsal. Though differential affinity of Dorsal-binding sites contributes to expression of Dorsal target genes, such expression is also controlled by additional transcription factors: Dorsal activates expression of *snail* (*sna*), which encodes a transcription factor that represses the expression of the Dorsal target gene *ventral nervous system defective* (*vnd*). Thus, expression of some Dorsal target genes such as *vnd* is repressed at high levels of Dorsal, at which *sna* is expressed, but activated at lower levels of Dorsal, at which *sna* is not expressed. In this way, interactions between transcription factors can contribute to define expression domains of target genes.

In plants too, gene expression is often activated in narrow domains by broadly expressed transcription factors [e.g., (Brady et al., 2011)]; however, how broadly expressed plant transcription factors activate expression of target genes in narrow domains is unclear. Here we

addressed this question for the *ARABIDOPSIS THALIANA HOMEOBOX8* (*ATHB8*)–*MONOPTEROS* (*MP*) pair of Arabidopsis genes.

ATHB8 expression is activated in files of isodiametric, polygonal, ground cells of the leaf; *ATHB8*-expressing ground cells will elongate into procambial cells—the precursors to all vascular cell-types—and are therefore referred to as "preprocambial cells" (Kang and Dengler, 2004; Sawchuk et al., 2007; Scarpella et al., 2004). Activation of *ATHB8* expression in files of preprocambial cells depends on binding of the broadly expressed MP transcription factor to a low-affinity MP-binding site in the *ATHB8* promoter (Donner et al., 2009). Here we tested the hypothesis that *ATHB8* preprocambial expression is restricted to narrow domains by binding of peak levels of the broadly expressed MP to a low-affinity MP-binding site in the *ATHB8* promoter; we found that *ATHB8* preprocambial expression is restricted to narrow domains by an MP-dependent incoherent feed-forward loop.

3.2 Results and Discussion

3.2.1 Relation Between *ATHB8* Expression Domains and MP Expression Levels

The hypothesis—that *ATHB8* preprocambial expression is activated in narrow domains by binding of peak levels of the broadly expressed MP to a low affinity site in the *ATHB8* promoter—predicts that narrow domains of *ATHB8* preprocambial expression correspond to peak levels of MP expression. To test this prediction, we simultaneously imaged expression of ATHB8::nCFP (nuclear CFP expressed by the *ATHB8* promoter) (Sawchuk et al., 2007) and MP::MP:YFP (MP:YFP fusion protein expressed by the *MP* promoter) in first leaves of the strong *mp-B4149* mutant (Weijers et al., 2005), the defects of which were rescued by MP::MP:YFP expression (Fig. 3.1A–C).

ATHB8 preprocambial expression can be reproducibly observed in midvein, first loops of veins ("first loops") and second loops of first leaves, respectively 2, 3, and 4 days after germination (DAG) (Donner and Scarpella, 2013; Donner et al., 2009; Gardiner et al., 2011)

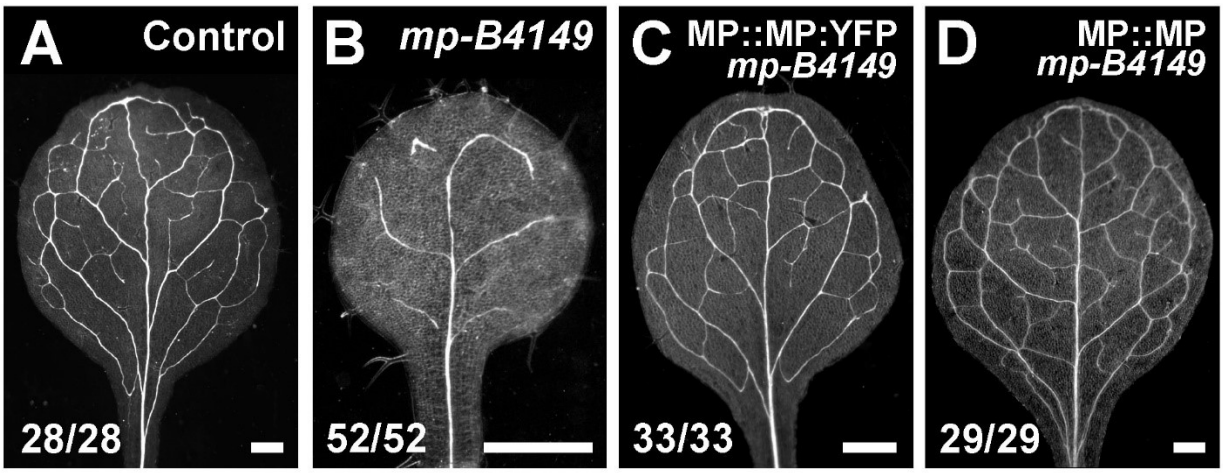

Figure 3.1. Functionality of MP::MP:YFP and MP::MP in Arabidopsis vein formation. Dark-field illumination of cleared first leaves 14 days after germination (DAG). Top right: genotype. Bottom left: reproducibility index. Scale bars: 0.5 mm.

(Chapter 4). At these stages, MP::MP:YFP was expressed in ATHB8::nCFP-expressing cells at higher levels than in cells flanking ATHB8::nCFP-expressing cells (Fig. 3.2; Fig. 3.3A,B).

To test whether the differential expression of MP::MP:YFP in ATHB8::nCFP-expressing cells and in cells flanking ATHB8::nCFP-expressing cells were an imaging artifact, we compared expression levels of nCFP driven by a ubiquitously active promoter (RIBO::nCFP) (Gordon et al., 2007) in cells expressing ATHB8::nYFP (Sawchuk et al., 2007) and in cells flanking ATHB8::nYFP-expressing cells; we focused our analysis on second loops of 4-DAG first leaves, in which *ATHB8* preprocambial expression can be reproducibly observed (Donner and Scarpella, 2013; Donner et al., 2009; Gardiner et al., 2011) (Chapter 4).

Because levels of RIBO::nCFP expression in ATHB8::nYFP-expressing cells were no higher than those in cells flanking ATHB8::nYFP-expressing cells (Fig. 3.3D,E; Fig. 3.4), we conclude that the differential expression of MP::MP:YFP in vein cells and in flanking cells is not an imaging artifact, and therefore that narrow domains of *ATHB8* preprocambial expression correspond to peak levels of MP expression.

3.2.2 Response of *ATHB8* Expression and Vein Network Formation to Manipulation of *MP* Levels

Loss of *MP* function—as in the strong *mp-U55* mutant (Donner et al., 2009)—leads to loss of *ATHB8* preprocambial expression—*ATHB8* preprocambial expression otherwise normally visible in second loops of 4-DAG first leaves (Donner and Scarpella, 2013; Donner et al., 2009; Gardiner et al., 2010, 2011) (Chapter 4) (Fig. 3.5A,B).

To characterize vein networks of *mp-U55* and all other genotypes in our study, we used four vein-network topology descriptors: a cardinality index (Verna et al., 2015), a continuity index (Verna et al., 2015) a connectivity index (Verna et al., 2015), and a cyclicity index. The cardinality index is a proxy for the number of "veins" (i.e. stretches of vascular elements that contact other stretches of vascular elements at least at one of their two ends) in a network. The continuity index quantifies how close a vein network is to a network with the same geometry but in which at least one end of each "vein fragment" (i.e. a stretch of vascular elements that is free of contact with other stretches of vascular elements) contacts a vein. The connectivity index

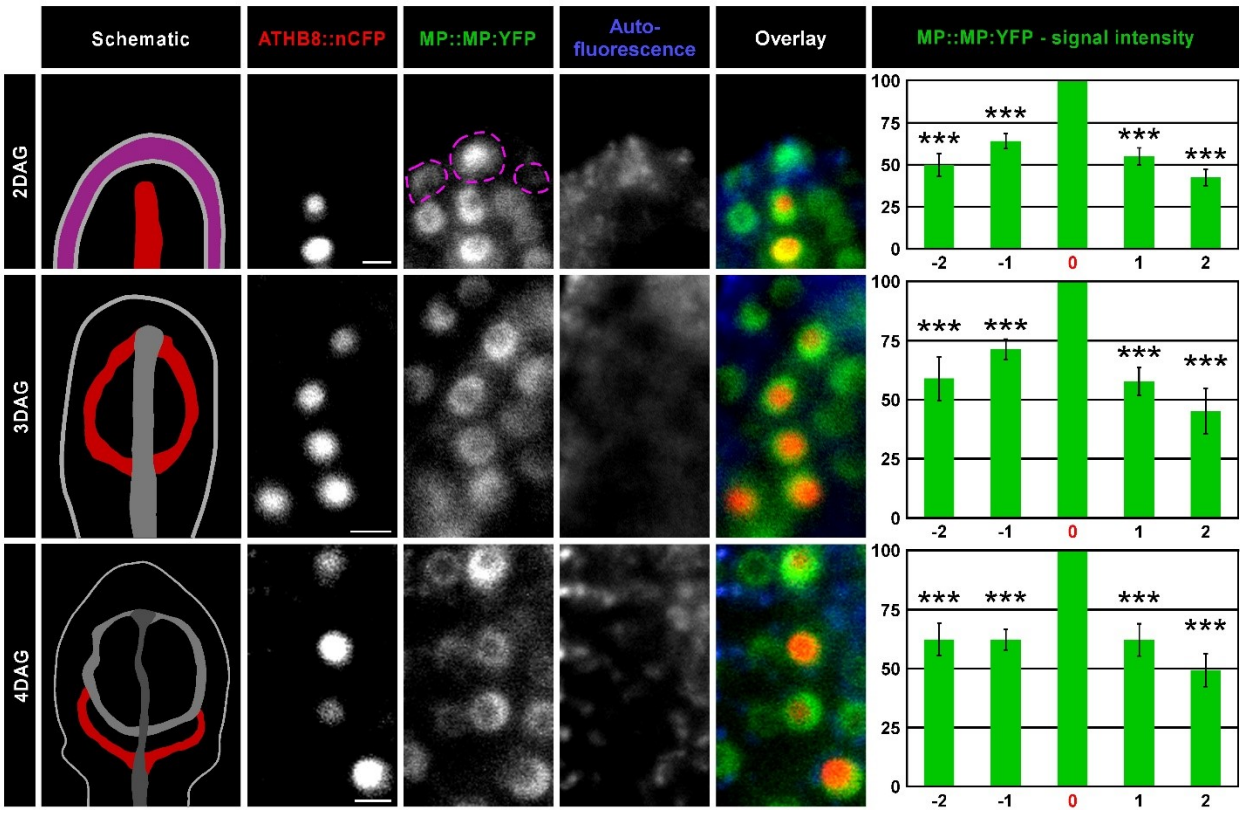

Figure 3.2. ***ATHB8*** **expression domains and MP expression levels in leaf development.** First leaves 2, 3, and 4 days after germination (DAG). Column 1: schematics of leaves—imaged in columns 2–5—illustrating onset of *ATHB8* expression (red)—imaged in column 2—associated with formation of midvein (2 DAG), first loop (3 DAG) or second loop (4 DAG) (Donner and Scarpella, 2013; Donner et al., 2009; Gardiner et al., 2010, 2011) (Chapter 4); magenta: epidermis; increasingly darker gray: progressively older *ATHB8* expression domains. Columns 2–5: confocal laser scanning microscopy. Column 2: ATHB8::nCFP expression. Column 3: MP::MP:YFP expression; dashed magenta outline: MP::MP:YFP-expressing epidermal nuclei. Column 4: autofluorescence. Column 5: overlays of images in columns 2–4; red: ATHB8::nCFP expression; green: MP::MP:YFP expression; blue: autofluorescence. Column 6: MP::MP:YFP expression levels (mean ± SE) in nuclei flanking ATHB8::nCFP-expressing nuclei (positions "-2", "-1", "1", and "2") relative to MP::MP:YFP expression levels in nuclei co-expressing ATHB8::nCFP (position "0") during formation of midvein (top), first loop (middle), or second loop (bottom). Difference between MP::MP:YFP expression levels in nuclei at position -2, -1, 1,

or 2 and MP::MP:YFP expression levels in nuclei at position 0 was significant at $P<0.001$ (***) by one-sample *t*-test with Bonferroni correction. Sample population sizes: 35 (2 DAG), 29 (3 DAG), or 31 (4 DAG) leaves; position -2: 30 (2 DAG), 45 (3 DAG), or 50 (4 DAG) nuclei; position -1: 63 (2 DAG), 72 (3 DAG), or 67 (4 DAG) nuclei; position 0: 70 (2 DAG), 75 (3 DAG), or 70 (4 DAG) nuclei; position 1: 58 (2 DAG), 47 (3 DAG), or 59 (4 DAG) nuclei; position 2: 24 (2 DAG), 19 (3 DAG), or 38 (4 DAG) nuclei. Scale bars (shown, for simplicity, only in column 2): 5 μm.

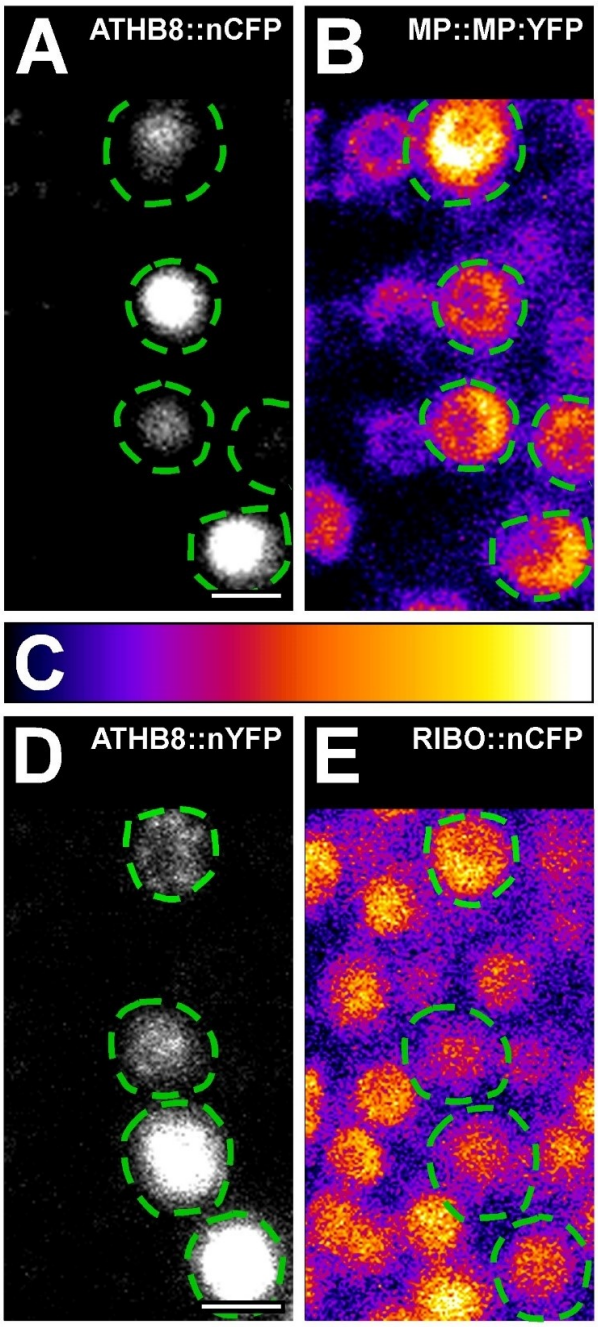

Figure 3.3. *ATHB8* expression domains and expression levels of MP and *RIBO*.

First leaves 4 days after germination (DAG). Confocal laser scanning microscopy. Top right: reporter. Dashed green outline: second-loop nuclei expressing ATHB8::nCFP (A,B) or ATHB8::nYFP (D,E). (B,E) Look-up table—ramp in C—visualizes expression levels. Scale bars (shown, for simplicity, only in A and D): 5 μm.

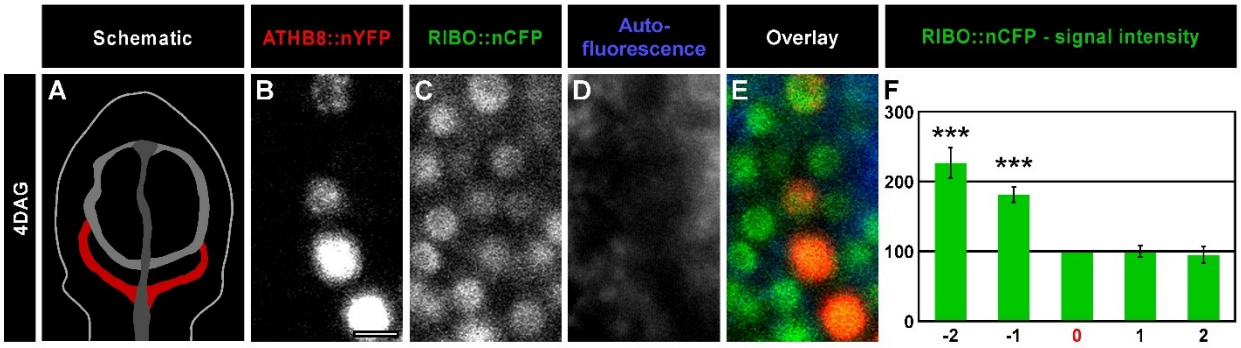

Figure 3.4. *ATHB8* expression domains and *RIBO* expression levels.

(A–F) First leaves 4 days after germination (DAG). (A) Schematic of 4-DAG leaf—imaged in B–E—illustrating onset of *ATHB8* expression (red)—imaged in B—associated with second loop formation (Donner and Scarpella, 2013; Donner et al., 2009; Gardiner et al., 2010, 2011) (Chapter 4); increasingly darker gray: progressively older *ATHB8* expression domains. (B–E) Confocal laser scanning microscopy. (B) ATHB8::nYFP expression. (C) RIBO::nCFP expression. (D) Autofluorescence. (E) Overlay of images in B–D; red: ATHB8::nYFP expression; green: RIBO::nCFP expression; blue: autofluorescence. (F) RIBO::nCFP expression levels (mean ± SE) in nuclei at positions -2, -1, 1, and 2—as defined in legend to Fig. 3.2—relative to RIBO::nCFP expression levels in nuclei at position 0—as defined in legend to Fig. 3.2—during second loop formation. Difference between RIBO::nCFP expression levels in nuclei at position -2 or -1 and RIBO::nCFP expression levels in nuclei at position 0 was significant at $P<0.001$ (***) by one-sample *t*-test with Bonferroni correction. Sample population sizes: 26 leaves; position -2, 42 nuclei; position -1, 64 nuclei; position 0, 69 nuclei; position 1, 50 nuclei; position 2, 28 nuclei. Scale bars (shown, for simplicity, only in column 2): 5 μm.

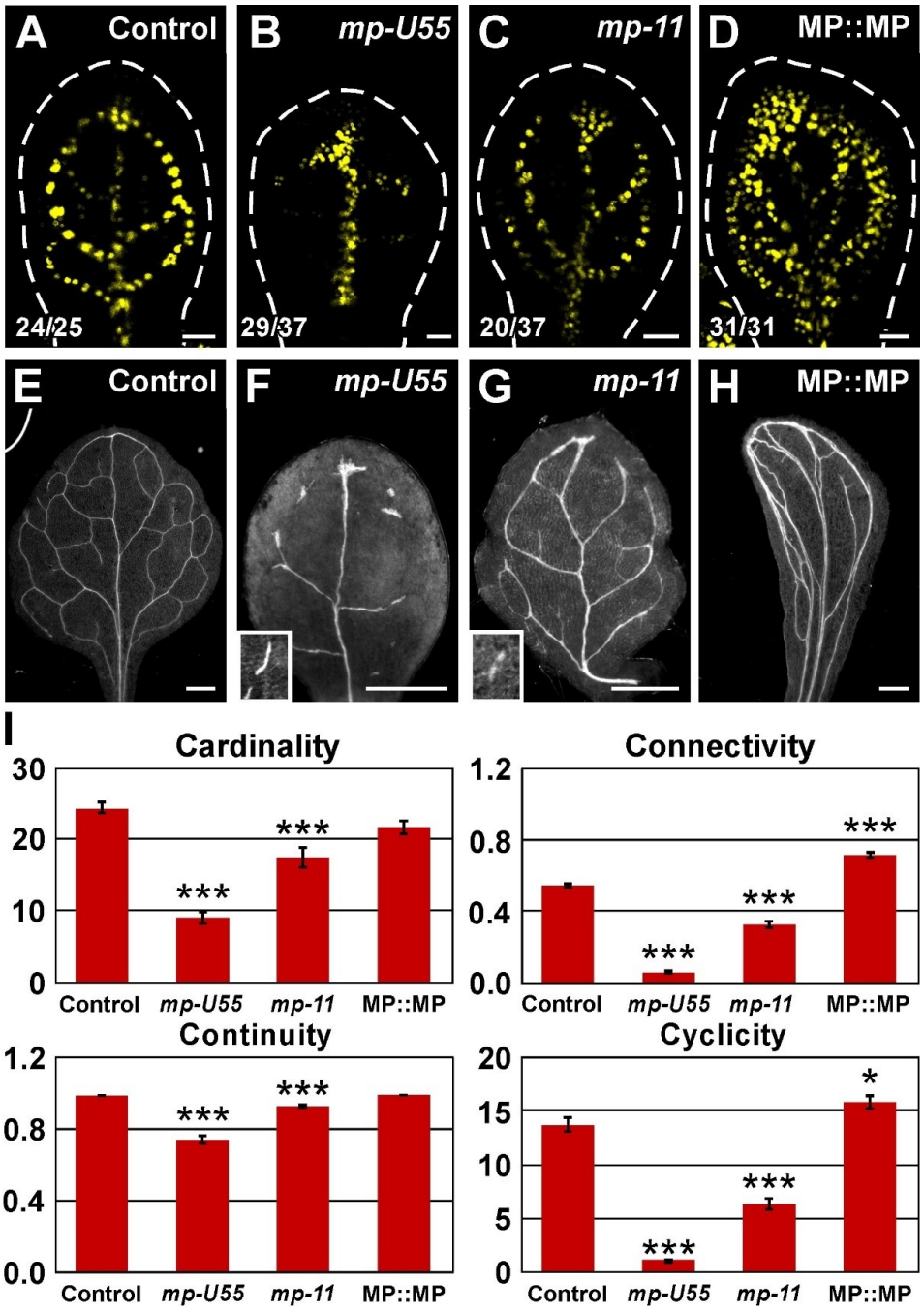

Figure 3.5. *MP* expression levels, *ATHB8* expression, and vein network formation.
Top right: genotype. Bottom left: reproducibility index. (A–D) First leaves 4 days after germination (DAG); confocal laser scanning microscopy; ATHB8::nYFP expression; dashed white line: leaf primordium outline. (E–H) Dark-field illumination of cleared 14-DAG first leaves. (I) Cardinality index, connectivity index, and continuity index (mean ± SE) as defined in

(Verna et al., 2015) and Materials and Methods; cyclicity index (mean ± SE) as defined in Materials and Methods. Difference between *mp-U55* and control cardinality indices, between *mp-11* and control cardinality indices, between *mp-U55* and control connectivity indices, between *mp-11* and control connectivity indices, between MP::MP and control connectivity indices, between *mp-U55* and control continuity indices, between *mp-11* and control continuity indices, between *mp-U55* and control cyclicity indices, between *mp-11* and control cyclicity indices, and between MP::MP and control cyclicity indices was significant at $P<0.05$ (*) or $P<0.001$ (***) by *F*-test and *t*-test with Bonferroni correction. Sample population sizes: Control, 39; *mp-U55*, 59; *mp-11*, 44; MP:MP, 41. Scale bars: (A–D) 25 μm; (E–H) 0.5 mm.

quantifies how close a vein network is to a network with the same geometry but in which both ends of each vein or vein fragment contact other veins. The cyclicity index is a proxy for the number of meshes in a vein network.

Consistent with previous observations (Donner et al., 2009; Przemeck et al., 1996), in *mp-U55* first leaves, loss of *ATHB8* preprocambial expression at 4 DAG was associated at maturity with networks of fewer, less frequently continuous and less frequently connected veins, and fewer meshes (Fig. 3.5E,F,I). We asked whether reduction in *MP* levels were sufficient to induce defects in *ATHB8* preprocambial expression and vein network formation. To address this question, we imaged ATHB8::nYFP expression and analyzed vein networks in first leaves of the weak *mp-11* mutant, in which an insertion in the *MP* promoter leads to ~30% reduction in levels of WT *MP* transcript (Odat et al., 2014) (Chapter 2).

In 4-DAG WT first leaves, cells at preprocambial stages of vein development—visible in second loops (Donner and Scarpella, 2013; Donner et al., 2009; Gardiner et al., 2010, 2011) (Chapter 4)—expressed ATHB8::nYFP strongly and homogeneously (Fig. 3.5A). By contrast, in 4-DAG *mp-11* first leaves, cells of second loops expressed ATHB8::nYFP weakly and heterogeneously, leading to seemingly fragmented expression domains (Fig. 3.5C). As in *mp-U55* first leaves, in *mp-11* first leaves, defects in ATHB8::nYFP expression at 4 DAG were associated at maturity with networks of fewer, less frequently continuous and less frequently connected veins, and fewer meshes; however, the vein network defects of *mp-11* were weaker than those of *mp-U55* (Fig. 3.5E–G,I).

We next asked whether MP expression levels in areas flanking domains of *ATHB8* preprocambial expression were suboptimal for activation of *ATHB8* expression. Were that so, increasing levels of MP in its native expression domain should lead to expansion of *ATHB8* expression domains. To test this prediction, we overexpressed *MP* by its own promoter (MP::MP)—overexpression which rescued defects of the strong *mp-B4149* mutant (Fig. 3.1A,B,D)—and imaged ATHB8::nYFP expression in first leaves of this background; we observed laterally expanded domains of ATHB8::nYFP expression in 4-DAG MP::MP first leaves (Fig. 3.5A,D). In MP::MP first leaves, expansion of ATHB8::nYFP expression domains at 4 DAG was associated at maturity with networks of thicker and more frequently connected veins, and more meshes (Fig. 3.5E–I).

In conclusion, our results suggest that *MP* expression levels are a limiting factor for *ATHB8* preprocambial expression and vein network formation.

3.2.3 Response of *ATHB8* Expression and Vein Network Formation to Manipulation of MP Activity

Levels of MP flanking domains of *ATHB8* preprocambial expression are insufficient for activation of *ATHB8* expression and vein network formation. We therefore asked whether increasing MP activity could overcome limiting MP levels. To address this question, we turned the unstable INDOLE-3-ACETIC ACID INDUCIBLE (IAA) 12/BODENLOS (BDL) repressor, which binds to MP and inhibits its transcriptional activity (Hamann et al., 2002; Hardtke et al., 2004; Weijers et al., 2005), into a stabilized transcriptional activator (VP16:bdl$^{\Delta I}$) (Li et al., 2011; Szemenyei et al., 2008) and expressed it by the *MP* promoter in the *iaa12-1* mutant (Overvoorde et al., 2005).

As in 4-DAG MP::MP first leaves, we observed laterally expanded domains of ATHB8::nYFP expression in 4-DAG MP::VP16:bdl$^{\Delta I}$;*iaa12-1* first leaves (Fig. 3.5A,D; Fig. 3.6A,B)—though the ATHB8::nYFP expression domains in MP::VP16:bdl$^{\Delta I}$;*iaa12-1* were not as wide as those in MP::MP (compare Fig. 3.5D with Fig. 3.6B). In MP::VP16:bdl$^{\Delta I}$;*iaa12-1* first leaves, defects in ATHB8::nYFP expression at 4 DAG were associated at maturity with networks of more veins, and—as in MP::MP—more meshes (Fig. 3.5E,H,I; Fig. 3.6D,E,G), suggesting that higher MP activity can compensate for lower MP levels.

If higher MP activity can compensate for lower MP levels in activation of *ATHB8* expression and vein network formation, decreased MP activity should mimic effects of low *MP* levels. To test this prediction, we imaged ATHB8::nYFP expression and analyzed vein networks in first leaves of the *bdl* mutant (Donner and Scarpella, 2009), which expresses a stabilized IAA12/BDL repressor (Dharmasiri et al., 2005).

As in 4-DAG *mp* first leaves, in 4-DAG *bdl* first leaves, cells of second loops either failed to activate ATHB8::nYFP expression or expressed ATHB8::nYFP weakly and heterogeneously, leading to seemingly fragmented ATHB8::nYFP expression domains (Fig. 3.5A–C; Fig. 3.6A,C). As in *mp* first leaves, in *bdl* first leaves defects in ATHB8::nYFP

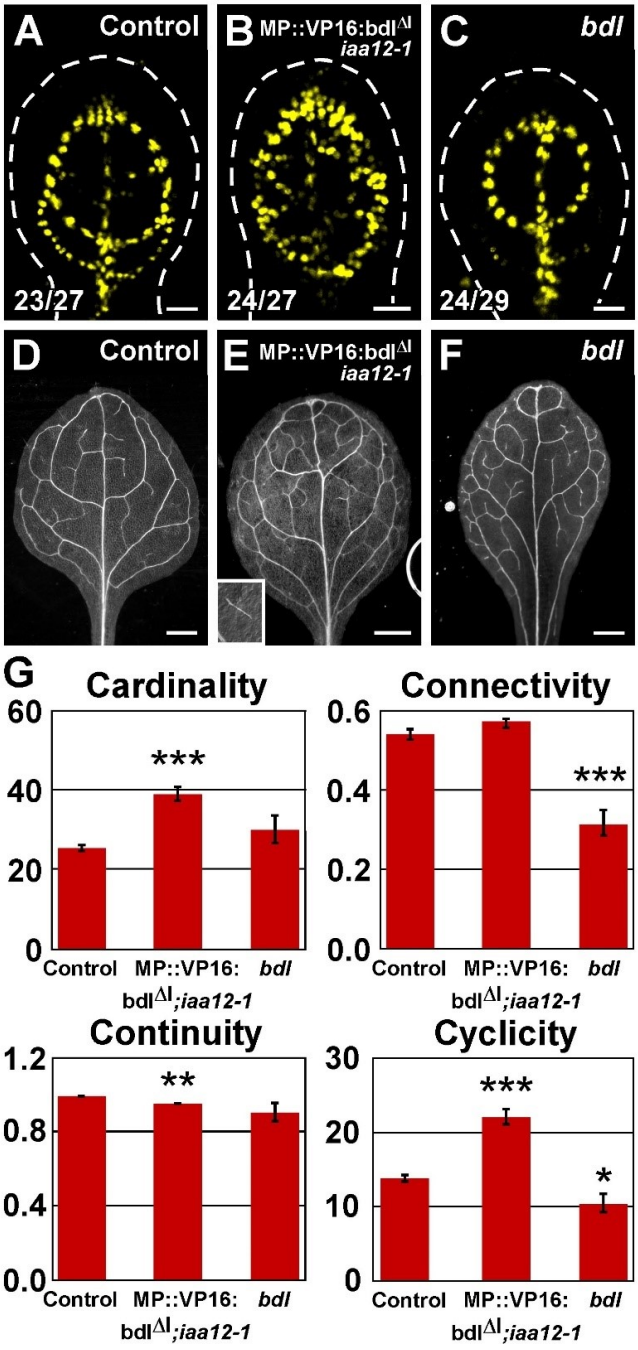

Figure 3.6. MP activity, *ATHB8* expression, and vein network formation.

Top right: genotype. Bottom left: reproducibility index. (A–C) First leaves 4 days after germination (DAG); confocal laser scanning microscopy; ATHB8::nYFP expression; dashed white line: leaf primordium outline. (D–F) Dark-field illumination of cleared 14-DAG first

leaves. (G) Cardinality index, connectivity index, and continuity index (mean ± SE) as defined in Verna et al., 2015 and Materials and Methods; cyclicity index (mean ± SE) as defined in Materials and Methods. Difference between MP::VP16:bdl$^{\Delta I}$;*iaa12-1* and control cardinality indices, between *bdl* and control connectivity indices, between MP::VP16:bdl$^{\Delta I}$;*iaa12-1* and control continuity indices, and between MP::VP16:bdl$^{\Delta I}$;*iaa12-1* and control cyclicity indices, and between *bdl* and control cyclicity indices, was significant at $P<0.05$ (*), $P<0.01$ (**) or $P<0.001$ (***) by *F*-test and *t*-test with Bonferroni correction. Sample population sizes: Control, 30; MP::VP16:bdl$^{\Delta I}$;*iaa12-1*, 72; *bdl*, 26. Scale bars: (A–C) 25 μm; (D–F) 0.5 mm.

expression at 4 DAG were associated at maturity with networks of less frequently connected veins and fewer meshes (Fig. 3.5E–G,I; Fig. 3.6D,F,G), suggesting that decreased MP activity mimics effects of low *MP* levels.

3.2.4 Relation Between *ATHB8* Expression Domains and Auxin Levels

The IAA12/BDL protein, as other AUX/IAA proteins (Gray et al., 2001; Zenser et al., 2001), is degraded in response to auxin (Dharmasiri et al., 2005; Weijers et al., 2005); auxin-dependent BDL degradation releases MP from inhibition, thus allowing MP to activate expression of its targets, which include *BDL* and *ATHB8* (Donner et al., 2009; Lau et al., 2011). Therefore, laterally expanded domains of ATHB8::nYFP expression in leaves of MP::MP and MP::VP16:bdl$^{\Delta I}$;*iaa12-1*, and weak or absent ATHB8::nYFP preprocambial expression in leaves of *mp* and *bdl,* suggests that narrow domains of *ATHB8* preprocambial expression correspond to peak levels of auxin. To test this prediction, we simultaneously imaged expression of ATHB8::nCFP and of the auxin reporter UBQ10::DII:nYFP or 35S::DII:nYFP (Vernoux et al., 2011)—the levels of which inversely correlate with those of auxin (Band et al., 2012, 2014; Brunoud et al., 2012; Santuari et al., 2011)—in midvein, first loops, and second loops of developing first leaves.

At all tested stages, UBQ10::DII:nYFP and 35S::DII:nYFP were expressed in ATHB8::nCFP-expressing cells at lower levels than in cells flanking ATHB8::nCFP-expressing cells (Fig. 3.7; Fig. 3.8A,B).

To control for possible deviations from ubiquitous and homogeneous activity of the *35S* promoter, we compared expression levels of the auxin-unresponsive 35S::mDII:nYFP (Vernoux et al., 2011) in cells expressing ATHB8::nCFP and in cells flanking ATHB8::nCFP-expressing cells; we focused our analysis on second loops of 4-DAG first leaves, in which *ATHB8* preprocambial expression can be reproducibly observed (Donner and Scarpella, 2013; Donner et al., 2009; Gardiner et al., 2010, 2011) (Chapter 4).

Because the levels of 35S::mDII:nYFP expression in ATHB8::nCFP-expressing cells were comparable to those in cells flanking ATHB8::nCFP-expressing cells (Fig. 3.8C,D;

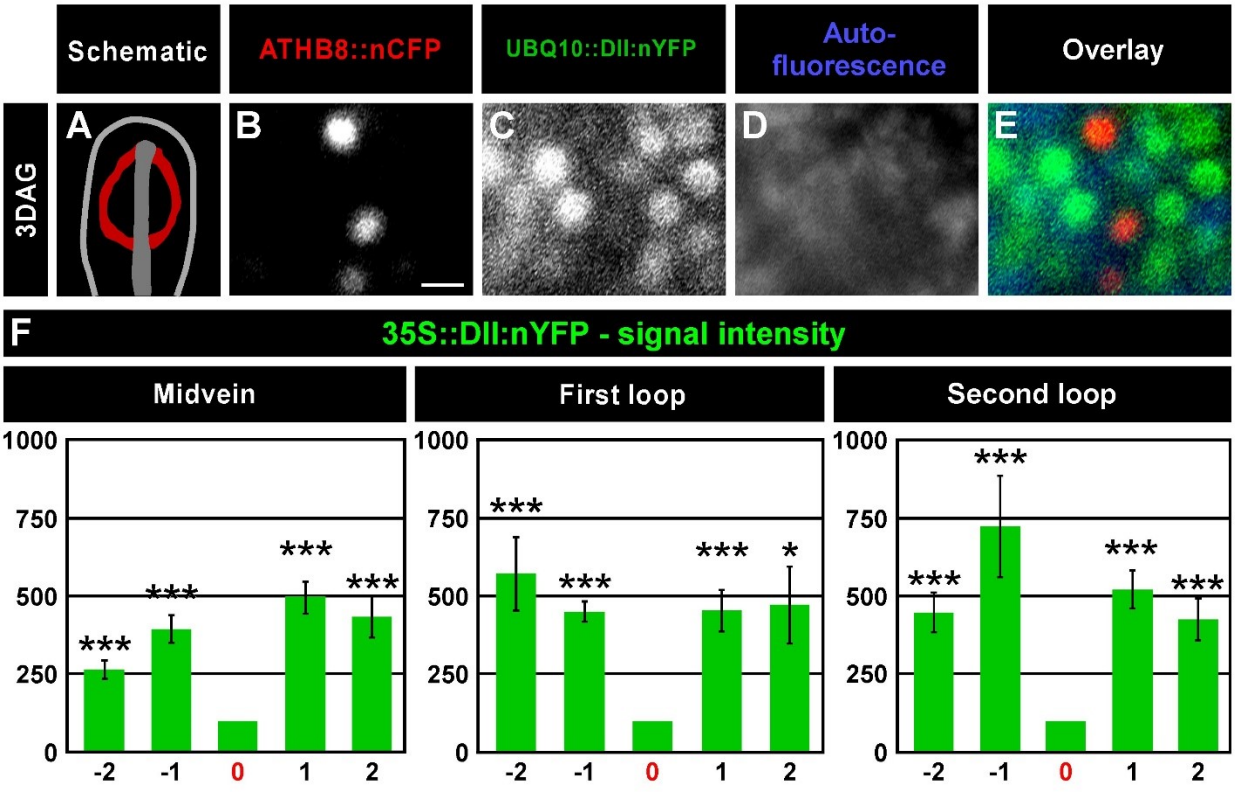

Figure 3.7. *ATHB8* expression domains and auxin levels.

(A–E) First leaves 3 days after germination (DAG). (A) Schematic of 3-DAG leaf—imaged in B–E—illustrating onset of *ATHB8* expression (red)—imaged in B—associated with first loop formation (Donner and Scarpella, 2013; Donner et al., 2009; Gardiner et al., 2010, 2011) (Chapter 4); gray: older *ATHB8* expression domain. (B–E) Confocal laser scanning microscopy. (B) ATHB8::nCFP expression. (C) UBQ10::DII:nYFP expression. (D) Autofluorescence. (E) Overlay of images in B–D; red: ATHB8::nCFP expression; green: UBQ10::DII:nYFP expression; blue: autofluorescence. (F) 35S::DII:nYFP expression levels (mean ± SE) in nuclei at positions -2, -1, 1, and 2—as defined in legend to Fig. 3.2—relative to 35S::DII:nYFP expression levels in nuclei at position 0—as defined in legend to Fig. 3.2—during formation of midvein (left), first loop (middle), or second loop (right). Difference between 35S::DII:nYFP expression levels in nuclei at position -2, -1, 1, or 2 and 35S::DII:nYFP expression levels in nuclei at position 0 was significant at $P<0.05$ (*) or $P<0.001$ (***) by one-sample *t*-test with Bonferroni correction. Sample population sizes: 52 leaves; position -2: 26 (midvein), 51 (first loop) or 62 (second loop) nuclei; position -1: 48 (midvein), 100 (first loop) or 91 (second loop) nuclei; position 0: 51

(midvein), 105 (first loop) or 99 (second loop) nuclei; position 1: 43 (midvein), 101 (first loop) or 92 (second loop) nuclei; position 2: 25 (midvein), 33 (first loop) or 50 (second loop) nuclei. Scale bars (shown, for simplicity, only in B): 5 μm.

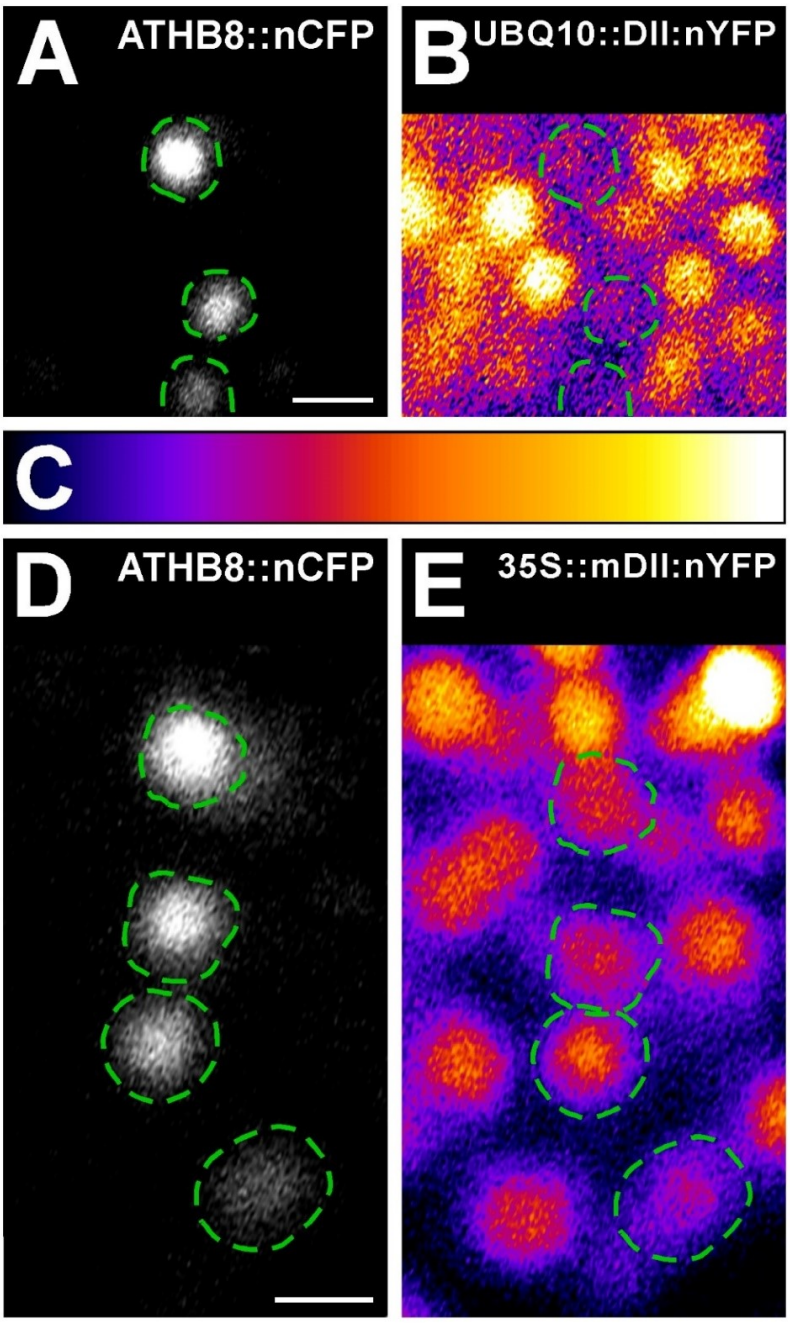

Figure 3.8. ***ATHB8*** **expression domains and auxin levels.**

First leaves 4 days after germination (DAG). Confocal laser scanning microscopy. Top right: reporter. Dashed green outline: second-loop nuclei expressing ATHB8::nCFP. (B,E) Look-up table—ramp in C—visualizes expression levels. Scale bars (shown, for simplicity, only in A and D): 5 μm**.**

Fig. 3.9), we conclude that—consistent with previous observations (Scarpella et al., 2004)—narrow domains of *ATHB8* preprocambial expression correspond to peak levels of auxin.

3.2.5 Response of *ATHB8* Expression to Manipulation of MP-Binding Site Affinity

The hypothesis predicts that activation of *ATHB8* preprocambial expression and width of *ATHB8* preprocambial-expression domains are directly proportional to the affinity of MP for its binding site in the *ATHB8* promoter. To test this prediction, we mutated the MP-binding site in the *ATHB8* promoter (TGTCTG) to variants with higher (TGTCTC), lower (TGTCAG), and negligible (TAGCTG) affinity for MP-binding (Donner et al., 2009; Ulmasov, 1997; Ulmasov et al., 1999b), and imaged nYFP expressed by the native or mutant promoters in second loops of 4-DAG first leaves, in which *ATHB8* preprocambial expression can be reproducibly observed (Donner and Scarpella, 2013; Donner et al., 2009; Gardiner et al., 2010, 2011) (Chapter 4).

Increasing the affinity of the MP-binding site in the *ATHB8* promoter for MP-binding led to expanded domains of nYFP expression in second loops of 4-DAG first leaves (Fig. 3.10A,B)—expanded domains of nYFP expression similar to those of ATHB8::nYFP expression in 4-DAG first leaves of MP::MP (Fig. 3.5D) and MP::VP16:bdl$^{\Delta I}$;*iaa12-1* (Fig. 3.6B). By contrast, decreasing the affinity of the MP-binding site in the *ATHB8* promoter for MP-binding led to weak and heterogeneous nYFP expression in second loops of 4-DAG first leaves, resulting in seemingly fragmented domains of nYFP expression (Fig. 3.10A,C), similar to those of ATHB8::nYFP expression in 4-DAG first leaves of *mp-11* (Fig. 3.5C) and *bdl* (Fig. 3.6C). Finally, reducing the affinity of the MP-binding site in the *ATHB8* promoter for MP-binding to negligible levels led to loss of nYFP expression in second loops of 4-DAG first leaves (Fig. 3.10A,D)—loss of nYFP expression similar to that of ATHB8::nYFP expression in 4-DAG first leaves of *mp-U55* (Donner et al., 2009) (Fig. 3.5B).

We conclude that the affinity of MP for its binding site in the *ATHB8* promoter determines activation of *ATHB8* preprocambial expression and width of *ATHB8* preprocambial-expression domains.

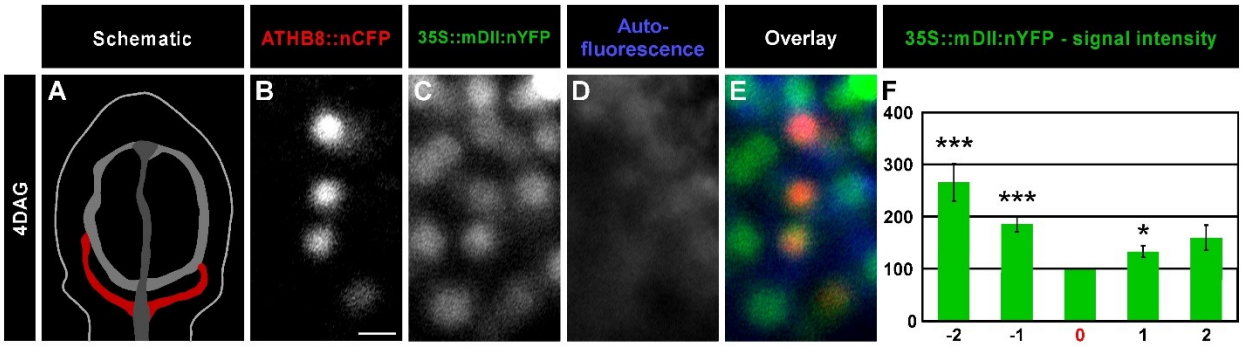

Figure 3.9. ***ATHB8* expression domains and 35S expression levels**.

(A–F) First leaves 4 days after germination (DAG). (A) Schematic of 4-DAG leaf—imaged in B–E—illustrating onset of *ATHB8* expression (red)—imaged in B—associated with second loop formation (Donner and Scarpella, 2013; Donner et al., 2009; Gardiner et al., 2010, 2011) (Chapter 4); increasingly darker gray: progressively older *ATHB8* expression domains. (B–E) Confocal laser scanning microscopy. (B) ATHB8::nCFP expression. (C) 35S::mDII:nYFP expression. (D) Autofluorescence. (E) Overlay of images in B–D; red: ATHB8::nCFP expression; green: 35S::mDII:nYFP expression; blue: autofluorescence. (F) 35S::mDII:nYFP expression levels (mean ± SE) in nuclei at positions -2, -1, 1, and 2—as defined in legend to Fig. 3.2—relative to 35S::mDII:nYFP expression levels in nuclei at position 0—as defined in legend to Fig. 3.2—during second loop formation. Difference between 35S::mDII:nYFP expression levels in nuclei at position -2 or -1 and 35S::mDII:nYFP expression levels in nuclei at position 0 was significant at $P<0.001$ (***) by one-sample *t*-test with Bonferroni correction. Sample population sizes: 24 leaves; position -2, 44 nuclei; position -1, 74 nuclei; position 0, 83 nuclei; position 1, 76 nuclei; position 2, 57 nuclei. Scale bars (shown, for simplicity, only in column 2): 5 μm.

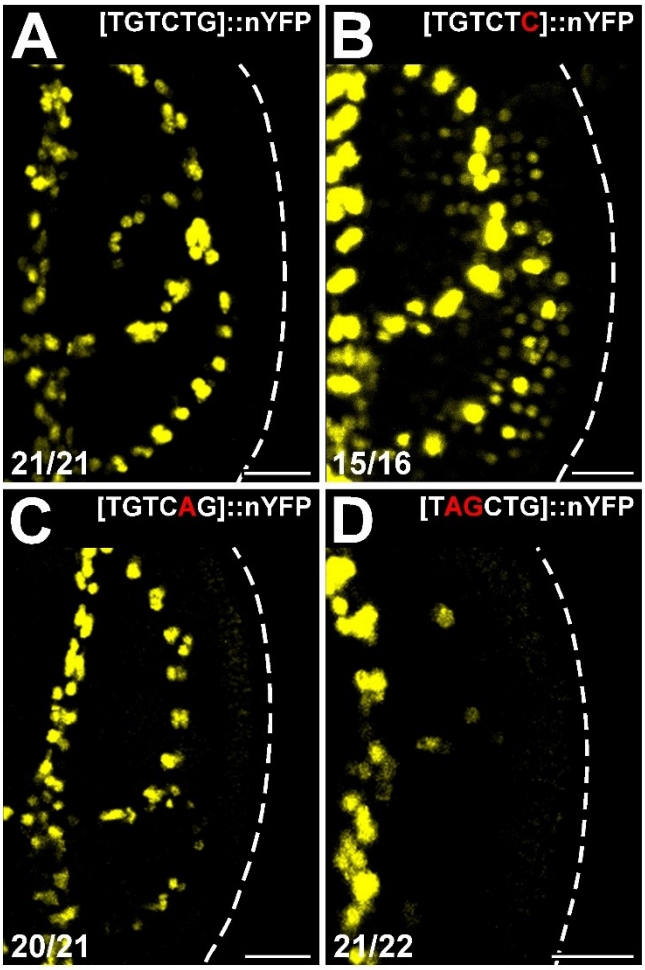

Figure 3.10. **Activity of *ATHB8* promoter variants.**

First leaves 4 days after germination (DAG). Confocal laser scanning microscopy. nYFP expression driven by promoter variants (top right) with native ([TGTCTG]::nYFP≡ATHB8::nYFP) (A), higher ([TGTCTC]::nYFP) (B), lower ([TGTCAG]::nYFP) (C) or negligible ([TAGCTG]::nYFP) (D) affinity for MP-binding. Dashed white line: leaf primordium outline; bottom left: reproducibility index. Scale bars: 25 μm.

3.2.6 Response of *MP* Expression and Vein Network Formation to Manipulation of ATHB8 Expression and Activity

Our results suggest that *ATHB8* preprocambial expression is activated in narrow domains by binding of peak levels of the broadly expressed MP to a low affinity site in the *ATHB8* promoter (Fig. 3.1–3.10). In animals, generation and interpretation of positional information are interdependent [reviewed in (Jaeger et al., 2008)]. We thus asked whether *ATHB8* fed back on *MP* expression and vein network formation.

To address this question, we first imaged expression of MP::nYFP (Sawchuk et al., 2013) in 4-DAG first leaves and networks of veins in mature first leaves of the *athb8-11* null allele (Prigge et al., 2005). MP::nYFP expression and vein networks in *athb8-11* were no different from those in WT (Fig. 3.11A,B,H,I,N,O).

The role of *ATHB8* in various developmental processes, including vascular differentiation, is obscured by functional redundancy within the *HD-ZIP III* family (Carlsbecker et al., 2010; Prigge et al., 2005); therefore, it is possible that such redundancy also masks *ATHB8* function in vein formation. We used two approaches to overcome *HD-ZIP III* redundancy in the *ATHB8* expression domain. First, we replaced the native ATHB8—a transcriptional activator (Baima et al., 2014)—with a transcriptional repressor variant by fusion to the EAR (for ETHYLENE-RESPONSIVE ELEMENT-BINDING FACTOR-associated amphiphilic repression) portable repressor domain (Hiratsu et al., 2003) (ATHB8::ATHB8:EAR;*athb8-11*). Second, we expressed *microRNA165a* (*miR165a*)—which targets all the *HD-ZIP III* genes (Zhou et al., 2007)—by the *SHORT-ROOT* (*SHR*) promoter—which drives expression in the *ATHB8* expression domain (Gardiner et al., 2011) (Chapter 4)—in the *athb8-11* background (SHR::miR165a;*athb8-11*). In first leaves of both ATHB8::ATHB8:EAR;*athb8-11* and SHR::miR165a;*athb8-11*, we observed weaker expression of MP::nYFP at 4 DAG and networks of fewer veins and meshes at maturity than in WT first leaves at those same stages (Fig. 3.11A,C,D,H,J,K,N,O). In addition, SHR::miR165a;*athb8-11* vein networks were less frequently continuous and less frequently connected (Fig. 3.11H,K,O). Therefore, our results suggest that *ATHB8* positively feeds back on *MP* expression and vein network formation.

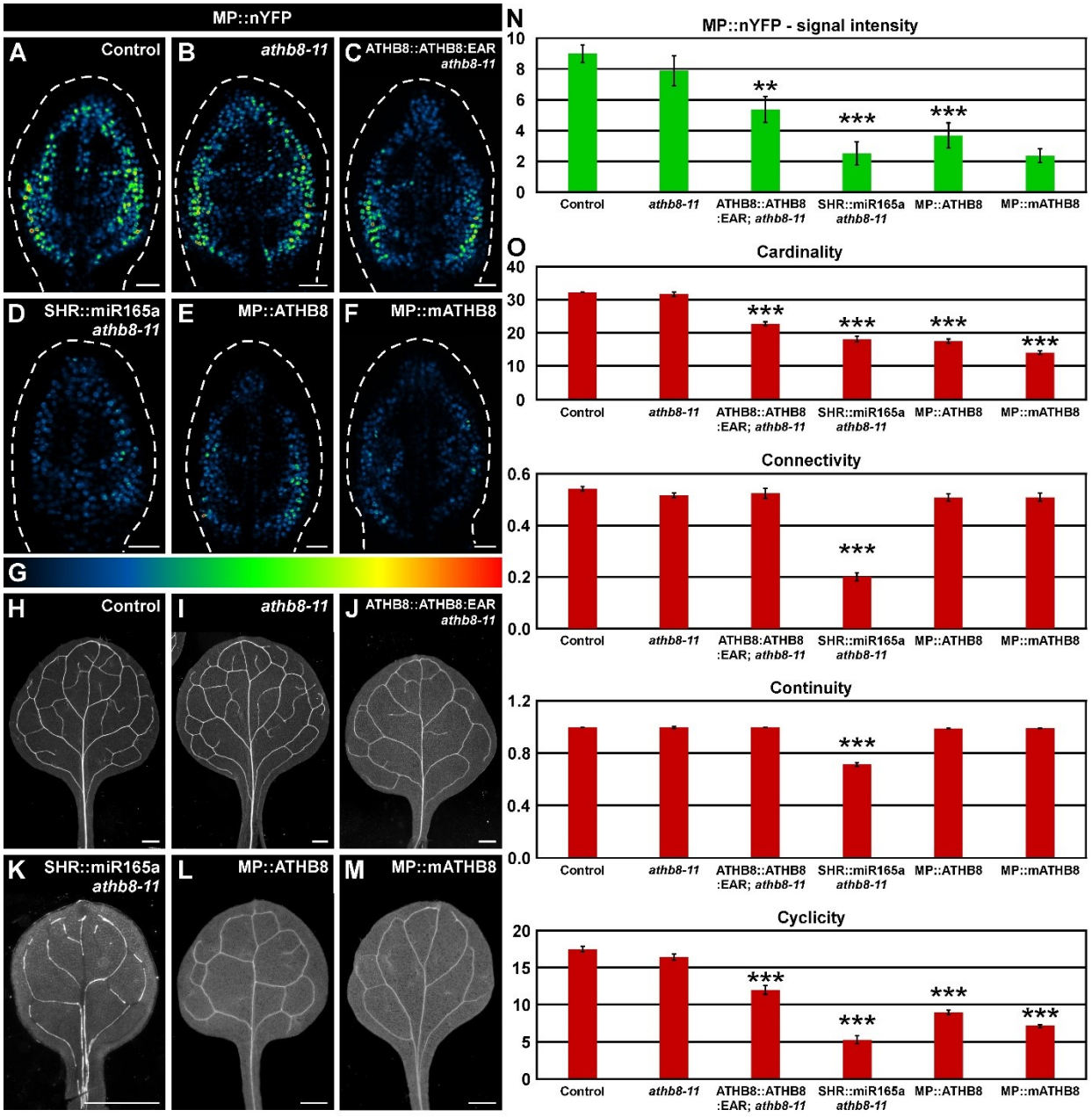

Figure 3.11. ***ATHB8*** **expression and activity,** ***MP*** **expression, and vein network formation.** (A–F,H–M) Top right: genotype. (A–F) First leaves 4 days after germination (DAG); confocal laser scanning microscopy; dashed white line: leaf primordium outline; MP::nYFP expression (look-up table—ramp in G—visualizes expression levels). (H–M) Dark-field illumination of cleared 14-DAG first leaves. (N) MP::nYFP expression levels expressed as mean percentage of pixels ± SE in the upper 75% of the pixel intensity-value histogram. Difference between

ATHB8::ATHB8:EAR;*athb8-11* and control, between SHR::miR165a;*athb8-11* and control, and between MP::ATHB8 and control was significant at $P<0.01$ (**) or $P<0.001$ (***) by *F*-test and *t*-test with Bonferroni correction. Sample population sizes: control, 25; *athb8-11*, 26; ATHB8::ATHB8:EAR;*athb8-11*, 24; SHR::miR165a;*athb8-11*, 19; MP::ATHB8, 24; MP::mATHB8, 24. (O) Cardinality index, connectivity index and continuity index (mean ± SE) as defined in (Verna et al., 2015) and Materials and Methods; cyclicity index (mean ± SE) as defined in Materials and Methods. Difference between ATHB8::ATHB8:EAR;*athb8-11* and control cardinality indices, between SHR::miR165a;*athb8-11* and control cardinality indices, between MP::ATHB8 and control cardinality indices, between MP::mATHB8 and MP::ATHB8 cardinality indices, between SHR::miR165a;*athb8-11* and control connectivity indices, between SHR::miR165a;*athb8-11* and control continuity indices, between ATHB8::ATHB8:EAR;*athb8-11* and control cyclicity indices, between SHR::miR165a;*athb8-11* and control cyclicity indices, between MP::ATHB8 and control cyclicity indices, and between MP::mATHB8 and MP::ATHB8 cyclicity indices was significant at $P<0.001$ (***) by *F*-test and *t*-test with Bonferroni correction. Sample population sizes: control, 69; *athb8-11*, 48; ATHB8::ATHB8:EAR;*athb8-11*, 25; SHR::miR165a;*athb8-11*, 35; MP::ATHB8, 74; MP::mATHB8, 68. Scale bars: (A–F) 25 μm; (H–M) 0.5 mm.

We next asked what effects had *ATHB8* ectopic expression in the *MP* expression domain on *MP* expression and vein network formation. To address this question, we imaged MP::nYFP expression and vein networks in MP::ATHB8 first leaves. MP::nYFP expression was weaker in MP::ATHB8 4-DAG leaves than in WT 4-DAG leaves, and networks had fewer veins and meshes in MP::ATHB8 mature leaves than in WT mature leaves (Fig. 3.11A,E,H,L,N,O), suggesting that *ATHB8* negatively feeds back on *MP* expression and vein network formation—a conclusion opposite, and therefore in apparent contrast to, what suggested by analysis of ATHB8::ATHB8:EAR;*athb8-11* and SHR::miR165a;*athb8-11* (Fig. 3.11A,C,D,H,J,K,N,O).

We finally reasoned that the negative effects of *ATHB8* ectopic expression in the *MP* expression domain on vein network formation would be stronger if *ATHB8* expression levels were also higher. To test this, we expressed by the *MP* promoter an *ATHB8* variant carrying a silent mutation that makes the derived transcript insensitive to *miR165*/*6*-mediated degradation (Ohashi-Ito et al., 2013) (mATHB8), and imaged vein networks in first leaves of MP::mATHB8. Networks had fewer veins and meshes in MP::mATHB8 mature leaves than in MP::ATHB8 mature leaves (Fig. 3.11L,M,O), supporting that *ATHB8* negatively feeds back on *MP* expression and vein network formation.

3.2.7 Conclusions

Our results suggest that an incoherent feed-forward loop regulates *ATHB8* expression: MP activates *ATHB8* expression; MP also activates *IAA12*/*BDL* expression (Krogan et al., 2014; Lau et al., 2011), which inhibits MP-mediated activation of *ATHB8* expression (Fig. 3.12). By contrast, it seems more challenging to account for the repression of *MP* expression by both gain and loss of *ATHB8* function. One possibility is that expression of *MP*, as that of *ATHB8*, is regulated by an incoherent feed-forward loop: ATHB8 would simultaneously activate, directly or indirectly, expression of *MP* and of an inhibitor of MP (Fig. 3.12). Direct activation of root expression of *MP* has been suggested for the ATHB8-related PHABULOSA transcription factor (Müller et al., 2016), and it is tempting to speculate that the MP inhibitor the expression of which would be regulated by ATHB8 might be IAA12/BDL; if this were so, the incoherent feed-forward loop regulating *ATHB8* expression and that regulating *MP* expression would be coincident—though opposite. Resolution of this scenario will likely have to await computer

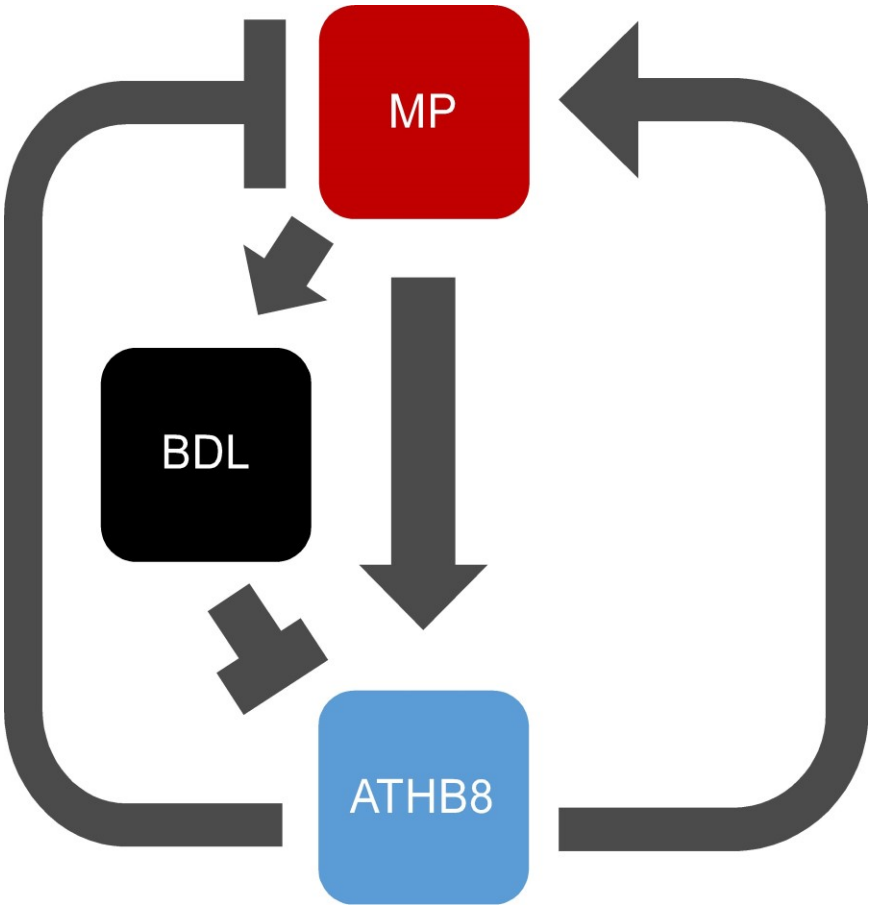

Figure 3.12 Genetic interaction network of *MP*, *BDL,* and *ATHB8.*

Arrows indicate positive effects; blunt-ended lines indicate negative effects.

simulation of mathematical models; however, our results already suggest a mechanism by which expression of a plant gene is activated in narrow domains by a broadly expressed transcription factor; the very same regulatory mechanism is most frequently used in animals to generate narrow domains of gene expression (Cotterell and Sharpe, 2010), suggesting conservation of regulatory logic of striped gene expression in multicellular organisms.

3.3 Materials and Methods

3.3.1 Plants

Origin and nature of lines, genotyping strategies, and oligonucleotide sequences are in Tables 3.1–3.3, respectively. Seeds were sterilized and germinated, seedlings and plants were grown (seedlings: ~90 μmol m^{-2} s^{-1}; plants: ~110 μmol m^{-2} s^{-1}), and plants were transformed as described in (Sawchuk et al., 2008).

3.3.2 Imaging

Developing leaves were mounted and imaged as in (Sawchuk et al., 2013), except that emission was collected from ~2.5–5.0-μm-thick optical slices. Marker-line-specific imaging parameters are in Tables 3.4. Signal levels in 8-bit, grayscale images acquired at identical settings were quantified in ImageJ (Schneider et al., 2012). Mature leaves were fixed, cleared, and mounted as in (Verna et al., 2015), and imaged as in Chapter 2. Image brightness and contrast were adjusted by linear stretching of the histogram with ImageJ (Schneider et al., 2012). Images were cropped with Photoshop (Adobe Systems Inc., San Jose, CA) and assembled into figures with Canvas (ACD Systems Inc., Victoria, Canada).

3.3.3 Vein Network Analysis

The cardinality index, the continuity index, and the connectivity index of vein networks were calculated as in (Verna et al., 2015). Briefly, number of "touch points" (TPs; TP defined as the point where a vein end contacts another vein or a vein fragment), "end points" (EPs; EP defined as the point where an "open" vein—a vein that contacts another vein only at one end—terminates free of contact with another vein or a vein fragment), "break points" (KPs; KP defined as each of the two points where a vein fragment terminates free of contact with veins or other vein fragments), and "exit points" (XPs; XP defined as the point where a vein exits leaf blade and enters leaf petiole) in dark-field images of cleared mature leaves was calculated with the Cell Counter plugin of ImageJ (Schneider et al., 2012).

Because a vein network can be understood as an undirected graph in which TPs, EPs, KPs, and XPs are vertices, and veins and vein fragments are edges, and because each vein is incident to two TPs, a TP and an XP, a TP and an EP, or an XP and an EP, the cardinality index—a measure of the size (i.e. the number of edges) of a graph—is a proxy for the number of veins and is calculated as: $[(TPs+XPs-EPs)/2]+EPs$, or: $(TPs+XPs+EPs)/2$.

The continuity index quantifies how close a vein network is to a network with the same number of veins but in which at least one end of each vein fragment contacts a vein, and is therefore calculated as the ratio of the cardinality index of the first network to the cardinality index of the second network: $[(TP + XP + EP)/2]/[(TP + XP + EP + KP)/2]$, or: $(TP + XP + EP)/(TP + XP + EP + KP)$.

The connectivity index quantifies how close a vein network is to a network with the same number of veins but in which both ends of each vein or vein fragment contact other veins, and is therefore calculated as the ratio of the number of "closed" veins—those veins which contact vein fragments or other veins at both ends—in the first network to the number of closed veins in the second network (i.e. the cardinality index of the second network): $[(TP + XP - EP)/2]/[(TP + XP + EP + KP)/2]$, or: $(TP + XP - EP)/(TP + XP + EP + KP)$.

Finally, because the number of meshes in a vein network equals the number of closed veins, the cyclicity index—a proxy for the number of meshes in a vein network—is calculated as: $(TP+XP-EP)/2$.

Table 3.1. Origin and Nature of Lines

Line	Origin/Nature
ATHB8::nCFP	(Sawchuk et al., 2007)
MP::MP:YFP	Translational fusion of *MP* (AT1G19850; -3281 to +3815; primers: 'MP Prom SalI Fwd' and 'MP KpnI Rev-2'; 'MP 3 kb SalI Fwd' and 'MP 3 kb XhoI Rev') to the sequence encoding EYFP (primers: 'ECFP AflII F' and 'ECFP AflII R'); rescues the root (240/240 seedlings), vein (Fig. 3.1) and inflorescence (160/160 plants) defects of *mp-B4149*
mp-B4149	(Weijers et al., 2005)
RIBO::nCFP	ABRC (CS23898); (Gordon et al., 2007); WT at the *ER* (AT2G26330) locus
ATHB8::nYFP	(Sawchuk et al., 2007)
mp-U55	ABRC (CS8147); (Mayer et al., 1993)
mp-11	(Odat et al., 2014) (Chapter 2)
MP::MP	*MP* (AT1G19850; -3281 to +3830; primers: 'MP Prom SalI Fwd' and 'MP KpnI Rev-2'; 'MP 3KB SalI Fwd' and 'MP 3kb XhoI Rev'); rescues the root (169/176 seedlings), vein (Fig. 3.1) and inflorescence (6/6 plants) defects of *mp-B4149*
MP::VP16:bdl$^{\Delta I}$	Transcriptional fusion of *MP* (AT1G19850; -3281 to -1; primers: 'MP BamHI Fwd' and 'MP KpnI Rev-1') to a translational fusion of the sequence encoding the VP16 activation domain (Triezenberg et al., 1988) (primers: 'VP16 NcoIF2' and 'VP16 PstIR') to an 5'-terminally deleted *bdl* (Hamann et al., 2002) (+94 and +1229; primers: 'BDL PstIF' and 'BDL BamHIR'; 'BDL mut F1', 'BDL mut F2', 'BDL mut F3', 'BDL mut F4', 'BDL PstIF' and 'BDL MfeI mut R'; 'BDLd1 PstI F' and 'BDL BAMHI R')
iaa12-1	ABRC (CS25213); (Overvoorde et al., 2005)

bdl	(Hamann et al., 1999); introgressed in Col
35S::DII:nYFP	ABRC (CS799173); (Vernoux et al., 2011)
35S::mDII:nYFP	ABRC (CS799174); (Vernoux et al., 2011)
[TGTCTG]::nYFP	(Donner et al., 2009)
[TGTCTC]::nYFP	Transcriptional fusion of *ATHB8* (AT4G32880; -953 to -1; primers: '1NcARE' and 'Athb8 R-5'') to the sequence encoding HTA6:EYFP (Zhang et al., 2005).
[TGTCAG]::nYFP	Transcriptional fusion of *ATHB8* (AT4G32880; -953 to -1; primers: '1NagARE' and 'Athb8 R-5'') to the sequence encoding HTA6:EYFP (Zhang et al., 2005)
[TAGCTG]::nYFP	(Donner et al., 2009)
MP::nYFP	(Sawchuk et al., 2013)
athb8-11	ABRC (CS6969); (Prigge et al., 2005); WT at the *ER* (AT2G26330) locus
ATHB8::ATHB8:EAR	Translational fusion of *ATHB8* (AT4G32880; -1997 to +4233; primers: 'Athb8 SalI Fwd' and 'ATHB8 gORF KpnI Rev') to the sequence encoding the EAR portable repressor domain (Hiratsu et al., 2003) (oligonucleotides: 'EAR KpnI SmaI PstI F' and 'EAR KpnI SmaI PstI R')
SHR::miR165a	Transcriptional fusion of *SHR* (AT4G37650; -2505 to -10; primers: 'SHR HindIII F' and 'SHR SalI R') to *miRNA165a* (AT1G01183; -138 to +323 relative to the transcriptional start-site; primers: 'SalI FWD – MiRNA 165' and 'KpnI REV – MiRNA 165')
MP::ATHB8	Transcriptional fusion of *MP* (AT1G19850; -3281 to -1; primers: 'MP BamHI Fwd' and 'MP KpnI Rev') to the *ATHB8* (AT4G32880) cDNA (GeneBank accession: BT008798; ABRC U24724; +1 to +2502; primers: 'ATHB8 cDNA KpnI FWD' and 'ATHB8 cDNA SmaI Rev')
MP::mATHB8	Transcriptional fusion of *MP* (AT1G19850; -3281 to -1; primers:

	'MP BamHI Fwd' and 'MP KpnI Rev') to the *ATHB8* (AT4G32880) cDNA (GeneBank accession: BT008798; ABRC U24724; +1 to +2502; primers: 'ATHB8 cDNA KpnI FWD' and 'ATHB8 cDNA SmaI Rev'; 'ATHB8mut165FWD' and 'ATHB8mut165REV')

[1]Unless otherwise indicated, all coordinates are relative to the translational start-site.

Table 3.2. Genotyping Strategies

Line	Strategy
mp-B4149	'MP 1498-s' and 'MP2082-AS'; *Mse*I
mp-U55	'MP Seq 2061' and 'U55 Geno Rev'; *Sml*I
mp-11	*MP:* 'Sail_1265_F06LP' and 'Sail_1265_F06RP'; *mp*: 'LB3' and 'Sail_1265_F06RP'
iaa12-1	*IAA12:* 'SALK_138684 LP' and 'SALK_138684 RP'; *iaa12*: 'LBb1.3' and 'SALK_138684 RP'
bdl	'bdl geno F' and 'bdl geno R'; *Hae*III
athb8-11	*ATHB8:* 'Athb8 0.5' and 'athb8attB2R'; *athb8*: 'athb8 -5944' and 'PD991-RB'

Table 3.3. Oligonucleotide Sequences

Name	Sequence (5' to 3')
MP Prom SalI Fwd	CCCGTCGACGTATATATAAACAATACCACCTTATAAC
MP KpnI Rev-2	CATGGTACCTGCAGAATTAGCATACCACAC
MP 3 kb SalI Fwd	TCTGTCGACTCCGGGTTAATCAGTATTATTAC
MP 3 Kb XhoI Rev	ATTCTCGAGTTAAGAGTTAAGACCACCTCC
ECFP AflII F	TTACTTAAGGTGAGCAAGGGCGACGAGC
ECFP AflII R	AGACTTAAGATTGTACAGCTCGTCCATGCC
MP 1498-s	CTCTCAGCGGATAGTATGCACATCGG
MP2082-AS	ATGGATGGAGCTGACGTTTGAGTTC
MP Seq 2061	CATAATGTTACTCTTCATGTACGCC
U55 Geno Rev	GTGCTGTTTGTTGGCGATTGG
Sail_1265_F06LP	GCTTCATCTCTTCAAGCAAGG
Sail_1265_F06RP	TCCCAAAGTCTCACCACTCAC
LB3	TAGCATCTGAATTTCATAACCAATCTCGATACAC
MP BamHI Fwd	AAGGGATCCTCCGGGTTAATCAGTATTATTAC
MP KpnI Rev-1	ACAGGTACCACAGAGAGATTTTTCAATGTTCTG
VP16 NcoIF2	TTACCATGGCCCCCCCGACCGATGTC
VP16 PstIR	TTTCTGCAGCCCCACCGTACTCGTCAATTC
BDL PstIF	ATACTGCAGCTCGTGGTGTGTCAGAATTGGAC
BDL BamHIR	TACGGATCCACTAAACTGGGTTGTTTCTTTGTC
BDL mut F1	AATCTTCCGGCGGAGAGTGTTAGAGAATTGGG
BDL mut F2	GTGGGTAAAAGTAATCTTCCGGCGGAGAGTG
BDL mut F3	GTGTCAGAATTGGAGGTGGGTAAAAGTAATCTTCCG
BDL mut F4	CGTGGTGTGTCAGAATTGGAGGTGGGGAAGAGTAATC
BDL MfeI mut R	TAACAATTGGTGACCATCCTACCACTTGAC
BDLdI PstI F	AAACTGCAGCGTGGAAAGAGCGTGGG
SALK_138684 LP	GTGGGGAAGAGTAATCTTCCG

SALK_138684 RP	CTTCTGCTCTTGACGTCTTGG
LBb1.3	ATTTTGCCGATTTCGGAAC
bdl geno F	GCTCAAATCTTGTGATGTGAGTG
bdl geno R	AGTCCACTAGCTTCTGAGGTTCCC
1NcARE	GGGGACAAGTTTGTACAAAAAAGCAGGCTTGGTTACCTGGTATTAAGGG
Athb8 R-5'	GGGGACCACTTTGTACAAGAAAGCTGGGTCTTTGATCCTCTCCGATCTCTC
1NagARE	GGGGACAAGTTTGTACAAAAAAGCAGGCTTGGTTGTCTCGTATTAAGGG
MP prom Gateway F	GGGGACAAGTTTGTACAAAAAAGCAGGCTCCGGCTTAATCAGTATTATTAC
MP prom Gateway R	GGGGACCACTTTGTACAAGAAAGCTGGGTACAGAGAGATTTTTCAATGTTCTG
Athb8 0.5	GGGGACAAGTTTGTACAAAAAAGCAGGCTTCCTTTGCTTCCAGAGACCAGCG
athb8attB2R	GGGGACCACTTTGTACAAGAAAGCTGGGTCTTTGATCCTCTCCGATCTCTC
athb8 -5944	GGTTTGGCATAAAAGTGCGG
PD991-RB	AAAACCTGGCGTTACCCAACT
Athb8 SalI Fwd	AGTGTCGACGACGATAATGATGATAACTAC
ATHB8 gORF KpnI Rev	CTCGGTACCTATAAAAGACCAGTTGAGGAAC
EAR KpnI SmaI PstI F	CCTAGATCTGGATCTAGAACTCCGTTTGGGTTTCGCTTAACCCGGGCTGCA
EAR KpnI SmaI PstI R	GCCCGGGTTAAGCGAAACCCAAACGGAGTTCTAGATCCAGATCTAGGGTAC
SHR HindIII F	GAGAAGCTTGACAAAGAAGCAGAGCGTGG
SHR SalI R	TGGGTCGACTTAATGAATAAGAAAATGAATAGAAGAAAGGG

SalI FWD – MiRNA 165	ATTGTCGACCCACTCATCATTCCCTCATC
KpnI REV – MiRNA 165	AGCGGTACCCTTATAGAAAATACTTCGTTAGCTTG
ATHB8 cDNA KpnI FWD	GTCGGTACCATGGGAGGAGGAAGCAATAATAG
ATHB8 cDNA SmaI Rev	ATGCCCGGGATCATATAAAAGACCAGTTGAGG
ATHB8mut165FWD	ATAGGAATCGTTGCTATTTCTC
ATHB8mut165REV	GGAATCTGGTCCAGGCTTCATC

Table 3.4. Imaging Parameters

A. Single-fluorophore lines

Line	Laser	Wavelength (nm)	Main dichroic beam splitter	First secondary dichroic beam splitter	Second secondary dichroic beam splitter	Emission filter (detector)
ATHB8::nYFP	Ar	514	HFT 405/514/594	NFT 595	NFT 515	BP 520-555 IR (PMT3)
35S::DII:nYFP	Ar	514	HFT 405/514/594	NFT 595	NFT 515	BP 520-555 IR (PMT3)
[TGTCTG]::nYFP	Ar	514	HFT 405/514/594	NFT 595	NFT 515	BP 520-555 IR (PMT3)
[TGTCTC]::nYFP	Ar	514	HFT 405/514/594	NFT 595	NFT 515	BP 520-555 IR (PMT3)
[TGTCAG]::nYFP	Ar	514	HFT 405/514/594	NFT 595	NFT 515	BP 520-555 IR (PMT3)
[TAGCTG]::nYFP	Ar	514	HFT 405/514/594	NFT 595	NFT 515	BP 520-555 IR (PMT3)
MP::nYFP	Ar	514	HFT 405/514/594	NFT 595	NFT 515	BP 520-555 IR (PMT3)

B. Multi-fluorophore lines

Multi-marker lines	Single-marker lines	Laser	Wavelength (nm)	Main dichroic beam	First secondary dichroic beam splitter	Second secondary dichroic beam	Emission filter (detector)

				splitter		**splitter**	
ATHB8::nCFP Autofluorescence MP::MP:YFP	ATHB8::nCFP	Ar	458	HFT 458/543	NFT 595	NFT 545	BP 475-525 (PMT2)
	Autofluorescence	Ar	458	Plate			604-700 (META)
	MP::MP:YFP	Ar	514	HFT 458/514	NFT 595	NFT 515	BP 520-555 IR (PMT3)
RIBO::nCFP Autofluorescence ATHB8::nYFP	RIBO::nCFP	Ar	458	HFT 458/514	NFT 595	NFT 515	BP 470-500 (PMT2)
	Autofluorescence	Ar	458	Plate			604-700 (META)
	ATHB8::nYFP	Ar	514	HFT 458/514	NFT 595	NFT 515	BP 520-555 IR (PMT3)
ATHB8::nCFP Autofluorescence 35S::DII:nYFP	ATHB8::nCFP	Ar	458	HFT 458/514	NFT 595	NFT 515	BP 470-500 (PMT2)
	Autofluorescence	Ar	458	Plate			604-700 (META)
	35S::DII:nYFP	Ar	514	HFT 458/514	NFT 595	NFT 515	BP 520-555 IR (PMT3)
ATHB8::nCFP Autofluorescence	ATHB8::nCFP	Ar	458	HFT 458/514	NFT 595	NFT 515	BP 470-500 (PMT2)

35S::mDII:nYFP	Autofluorescence	Ar	458	Plate			604-700 (META)
	35S::mDII:nYFP	Ar	514	HFT 458/514	NFT 595	NFT 515	BP 520-555 IR (PMT3)

CHAPTER 4: SIMULTANEOUS ACTIVATION OF *SHR* AND *ATHB8* EXPRESSION DEFINES SWITCH TO PREPROCAMBIAL CELL STATE IN ARABIDOPSIS LEAF DEVELOPMENT

4.1 Introduction

The vascular system of plants is a network of veins that extends throughout all organs (Esau, 1965). Veins transport water and nutrients, and are a source of signals that act locally, to assign identity to surrounding cells, and systemically, to coordinate initiation of new shoot organs with that of new roots (Berleth and Sachs, 2001). Sites of vein formation are foreshadowed by the appearance of files of elongated procambial cells, which in leaf development seem to emerge de novo from within a homogeneous population of isodiametric ground cells (Esau, 1943; Foster, 1952; Louis, 1935).

The molecular events that lead to acquisition of procambial cell identity during leaf development are not entirely clear, but available evidence supports a decisive role for transport and transduction of the plant signaling molecule auxin in specifying paths of leaf vein formation. Auxin application to leaf primordia induces formation of new veins (Sachs, 1975, 1989; Scarpella et al., 2006), and chemical inhibition of auxin transport during leaf development severely disturbs vein patterning (Mattsson et al., 1999; Sieburth, 1999). Consistent with these observations, mutants impaired in auxin biosynthesis, response, or transport display diagnostic alterations in leaf vein patterns (Alonso-Peral et al., 2006; Cheng et al., 2006; Mattsson et al., 1999; Przemeck et al., 1996). During leaf development, ground cells are directed toward procambial fate through induction of wide domains of expression of the PIN-FORMED1 (PIN1) auxin exporter and of the auxin response transcription factor MONOPTEROS (MP) (Donner et

al., 2009; Hardtke and Berleth, 1998; Sawchuk et al., 2007; Scarpella et al., 2006; Wenzel et al., 2007). Cessation of PIN1 and MP expression occurs in some of the cells, as fields of PIN1 and MP expression become restricted to individual lines of elongating procambial cells (Donner et al., 2009; Scarpella et al., 2006; Wenzel et al., 2007).

While initiation of PIN1 and MP expression identifies a reversible state in leaf vein formation, files of PIN1- and MP-expressing ground cells that are stabilized toward procambial fate activate expression of the Class III *HOMEODOMAIN-LEUCINE ZIPPER* (*HD-ZIP III*) gene *ARABIDOPSIS THALIANA HOMEOBOX8* (*ATHB8*) (Baima et al., 1995; Donner et al., 2009; Kang and Dengler, 2004; Sawchuk et al., 2007; Scarpella et al., 2004). Onset of *ATHB8* expression is directly controlled by MP (Donner et al., 2009), and identifies the transition to a typically irreversible ‘‘preprocambial’’ cell state that accurately predicts sites of leaf vein formation [e.g., (Alonso-Peral et al., 2006; Carland and Nelson, 2004; Carland et al., 2010; Cnops et al., 2006; Donner et al., 2009; Kang and Dengler, 2004; Koizumi et al., 2000; Petricka and Nelson, 2007; Pineau et al., 2005; Sawchuk et al., 2008, 2007, Scarpella et al., 2004, 2006)]. Therefore, characterization of the transcriptional profile of ground cells that have switched to preprocambial state would be particularly desirable, as it may provide insight into the molecular pathways controlling vein formation. However, as of yet, no genes have been identified whose expression in vein development is initiated simultaneously with that of *ATHB8*.

In this study, we searched for gene expression patterns associated with early stages of vein development in Arabidopsis leaves. We found that onset of expression of *SHORT-ROOT* (*SHR*), which encodes a transcription factor of the GRAS family (after GIBBERELLIC ACID INSENSITIVE, REPRESSOR OF *gibberellic acid1-3,* AND SCARECROW) (Helariutta et al., 2000; Di Laurenzio et al., 1996; Peng et al., 1997; Pysh et al., 1999; Silverstone et al., 1998), coincides with that of *ATHB8* during undisturbed leaf development. Parallel initiation of expression of *SHR* and *ATHB8* persisted under conditions of experimentally manipulated leaf vascular patterning, suggesting that synchronous activation of expression of *SHR* and *ATHB8* operationally defines a reproducible cell state that presages vein appearance. While the *ATHB8* protein remained confined to leaf vascular cells, however, the SHR protein additionally localized to adjacent, periveinal positions, suggesting functions of preprocambial cells beyond vein

formation. Our observations assist in the molecular characterization of cell state at morphologically indistinguishable, preprocambial stages of leaf vein formation.

4.2 Results

In Arabidopsis leaves, veins are arranged in a ramified pattern that largely reflects the shape of the leaf (Candela et al., 1999; Dengler and Kang, 2001; Nelson and Dengler, 1997) (Fig. 4.1A). Lateral veins depart from either side of a conspicuous central vein (midvein), extend along the leaf margin, and connect to distal veins to form prominent closed loops. A series of higher-order veins branch from midvein and loops, and can either terminate in the lamina or join two veins. Veins of succeeding orders become recognizable progressively later in the same area of the developing leaf primordium, and veins of the same order appear in a tip-to-base sequence during leaf development (Candela et al., 1999; Kang and Dengler, 2002, 2004; Kinsman and Pyke, 1998; Mattsson et al., 1999; Scarpella et al., 2004; Sieburth, 1999; Steynen and Schultz, 2003; Telfer and Poethig, RS., 1994) (Fig. 4.1B–D). The illustrations in Fig. 4.1A–D schematically depict the temporal sequence of vein formation events in Arabidopsis leaf development, and define stages and terminology to which we refer throughout this study.

4.2.1 Leaf Expression of Root Vascular Markers

All the genes whose expression has previously been assigned to early stages of leaf vein development have also been reported to be expressed in the root procambium [e.g., (Alonso-Peral et al., 2006; Baima et al., 1995; Carland and Nelson, 2009; Gardiner et al., 2010; Hardtke and Berleth, 1998; Kang and Dengler, 2004; Konishi and Yanagisawa, 2007; Scarpella et al., 2004, 2006; Steinmann et al., 1999; Wenzel et al., 2007)], and identification of leaf vascular gene expression profiles based on root procambial expression has proved to be an effective strategy (Gardiner et al., 2010). Reporter gene expression in the J2501 and Q0990::erGFP enhancer-trap lines, and in transcriptional fusions to *SHR* or to *ARABIDOPSIS HISTIDINE KINASE4*/*CYTOKININ RESPONSE1*/*WOODEN LEG* (*WOL* hereafter) (Inoue et al., 2001; Mahonen et al., 2000; Suzuki et al., 2001) has consistently been used as reliable markers of root

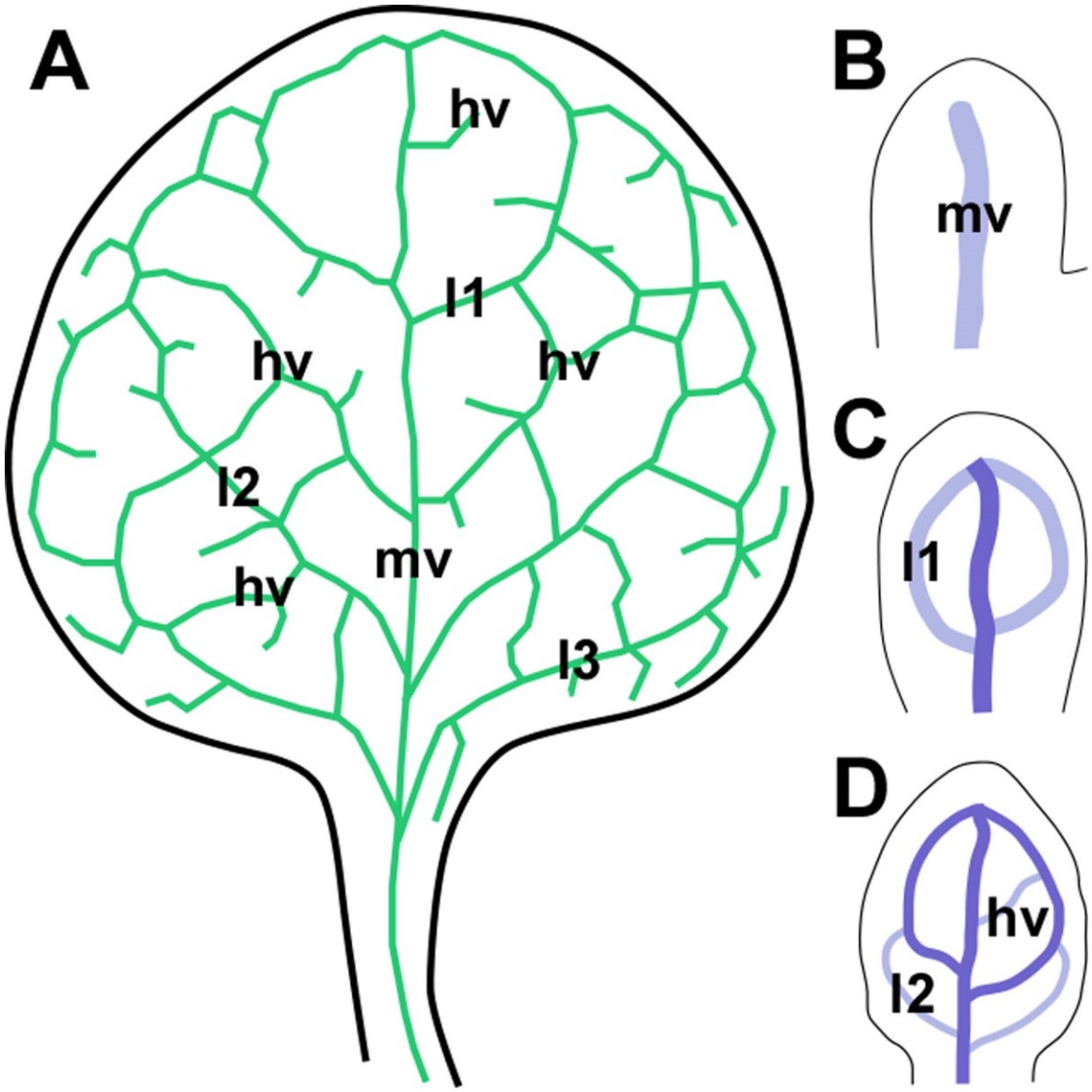

Figure 4.1. Vein development in the Arabidopsis first leaf.

(A,C,D) Abaxial (i.e. ventral) view. (B) Lateral view (abaxial side to the left). (A–D): Illustrations depicting the vein pattern of the mature first leaf (A) and the spatiotemporal course of vein formation in first leaf development (B–D) as inferred from published works (see text for references), and definition of terms used in this study. (B) Two days after germination (DAG). (C) Three DAG. (D) Four DAG. Green, mature veins; indigo, procambial stages; lavender, preprocambial stages; hv, higher-order vein; l1, l2, and l3, first, second, and third loop, respectively; mv, midvein.

procambial cells [e.g., (Benková et al., 2003; Birnbaum et al., 2003; Hirota et al., 2007; Dello Ioio et al., 2007; Mustroph et al., 2009; Wang et al., 2005; Zhang et al., 2005)] (Fig. 4.2A–D). Activation of Q0990::erGFP expression in the leaf coincides with acquisition of procambial cell identity (Sawchuk et al., 2007) (Fig. 4.2E), further supporting the value of root-procambial-expression-filtering for discovery of leaf vascular expression patterns. Therefore, to identify new preprocambial expression profiles, we asked whether reporter gene expression in the J2501::erGFP enhancer-trap line and in transcriptional fusions to *SHR* or *WOL* retained, like Q0990::erGFP, vascular specificity in the leaf. To address this question, we visualized fluorescence protein activity in J2501::erGFP and in transcriptional fusions of *SHR* or *WOL* to nuclear YFP or GFP [nYFP or nGFP (Zhang et al., 2005)], and compared it with that of Q0990::erGFP, in first leaves of seedlings 4 days after germination (DAG) as their venation is predominantly preprocambial and procambial (Donner et al., 2009; Sawchuk et al., 2007) (Fig. 4.1D).

While, in agreement with previous observations (Donner et al., 2009; Sawchuk et al., 2007), Q0990::erGFP signals in 4-DAG leaves were restricted to procambial midvein and first loops (Fig. 4.2E), expression of J2501::erGFP was not detected (Fig. 4.2F), and weak WOL::nGFP fluorescence was observed in nearly all cells (Fig. 4.2G). However, territories of SHR::nYFP activity were associated with sites of formation of midvein, first and second loops, and higher-order veins (Fig. 4.2H). Because neither expression of J2501:::erGFP nor that of WOL::nGFP displayed leaf vascular bias, successive characterization focused on SHR::nYFP.

4.2.2 Expression of *SHR* During Leaf Development

Expression of *SHR* in second loops of 4-DAG leaves (Fig. 4.2H; compare with Fig. 4.1D and Fig. 4.2E), suggests that, like *ATHB8* (Kang and Dengler, 2004; Scarpella et al., 2004), *SHR* is expressed in ground cells that have shifted to preprocambial state. However, patterns of initiation, progression and termination of *SHR* expression could be dramatically different from those of *ATHB8*, even if the two genes are expressed similarly at a single stage of leaf development. Therefore, to visualize dynamics of *SHR* expression in leaf vein formation, we monitored activity of SHR::nYFP and of the reference preprocambial marker ATHB8::nYFP (Donner et al., 2009; Sawchuk et al., 2007) in first leaf primordia at 2, 3, 4, and 5 DAG.

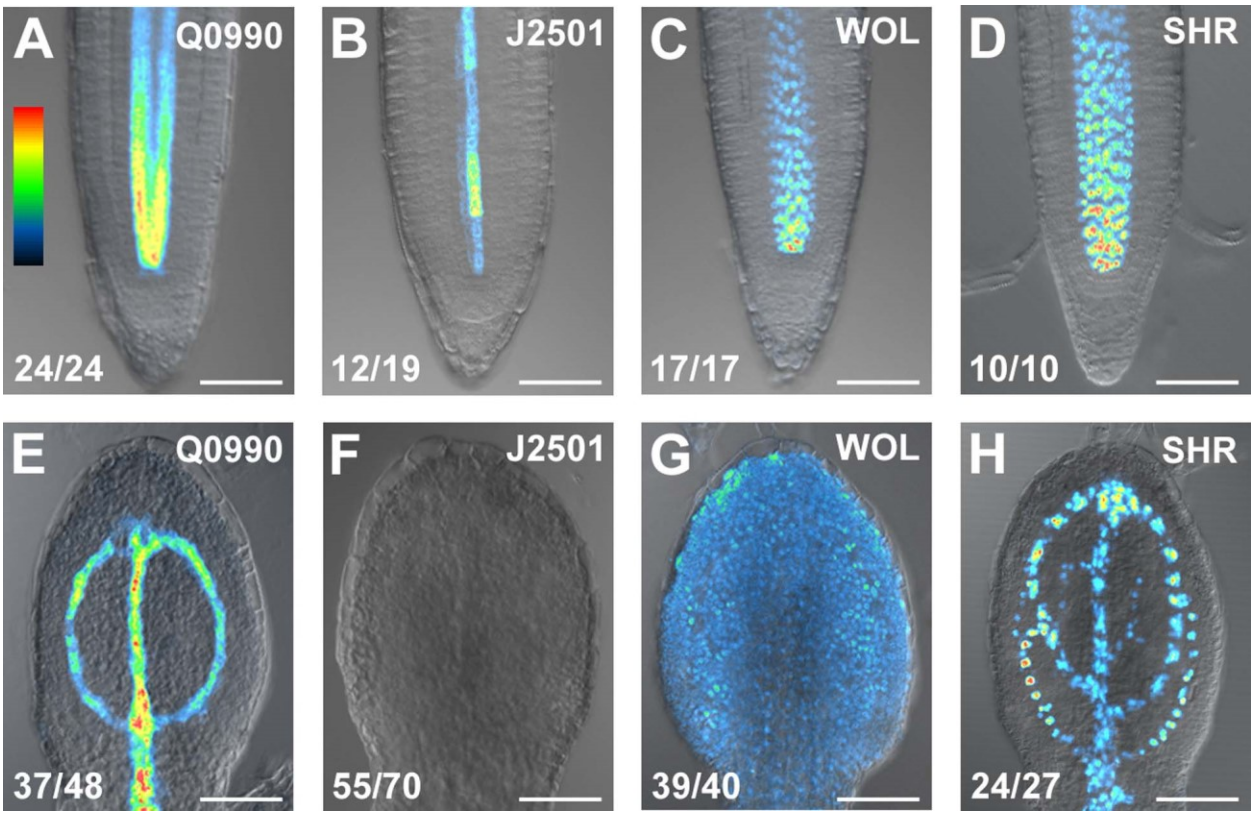

Figure 4.2. Marker expression in seedling organs.

(A–H) Overlay of confocal-laser-scanning and differential-interference-contrast microscopy, subepidermal focal plane. A look-up-table (LUT) (displayed in A), in which black was used to encode background, and cyan, green, yellow, orange, and red to encode increasing signal intensities (Sawchuk et al., 2008), was applied to eight-bit gray scaled images to generate color-coded images. Top right, marker identity. Bottom left, fraction of samples showing the displayed features. (A–D) Four-DAG root tips. (E–H) Four-DAG first leaves, abaxial view. (F) See Fig. 4.3 for additional expression patterns and their frequencies. Scale bars: 50 μm.

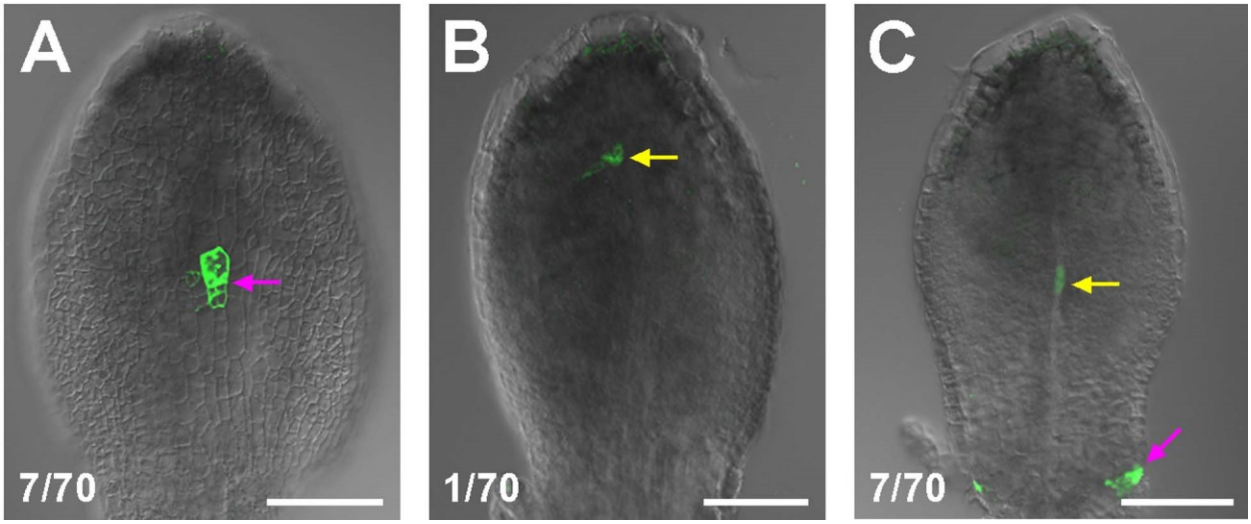

Figure 4.3. Additional expression patterns of J2501 in leaves.

(A–C) Four-DAG first leaves, abaxial view. Overlay of confocal-laser-scanning and differential-interference-contrast microscopy. Green, J2501::erGFP expression. Bottom left, fraction of samples showing the displayed features. (A) Epidermal focal plane. (B,C) Subepidermal focal plane. Note erratic expression in epidermal cells (A, magenta arrow), in subepidermal cells (B, yellow arrow), or in both positions (C). Scale bars: 50 µm.

At 2 DAG, SHR::nYFP and ATHB8::nYFP signals were confined to a single cell file along the midline of the leaf primordium (Fig. 4.4A,E). At 3 DAG, *SHR* and *ATHB8* transcriptional fusions were expressed in narrow domains at sites of midvein and first loop formation (Fig. 4.4B,F). At 4 DAG, slender zones of SHR::nYFP and ATHB8::nYFP activity marked appearance of midvein, first and second loops, and higher-order veins (Fig. 4.4C,G). Finally, at 5 DAG, *SHR* and *ATHB8* promoters directed expression in developing midvein, first, second, and third loops, and higher-order veins (Fig. 4.4D,H). However, while ATHB8::nYFP expression had subsided from the apical portion of midvein and first loops (Fig. 4.4D), the *SHR* transcriptional fusion was evenly active throughout the leaf vasculature (Fig. 4.4H).

In summary, expression of *SHR* seemed to be tightly associated with regions of *ATHB8*-labeled vein formation throughout leaf development.

4.2.3 Stage-Specific *SHR* Expression in Leaf Vein Formation

Comparison between *SHR* and *ATHB8* expression profiles during leaf development (Fig. 4.4) suggests that expression of *SHR* is initiated as early as that of *ATHB8*, and that therefore *SHR* expression could be assigned to ground cells that have switched to preprocambial state. We adopted two criteria to test such a hypothesis: (1) visualization of shape of cells expressing *SHR*; (2) detection of *SHR* and *ATHB8* expression within the same sample. Simultaneous imaging of activity of *SHR* transcriptional fusions and plasma-membrane-localized GFP (Sawchuk et al., 2008) in basal regions of 4-DAG first leaves showed that, like *ATHB8* (Kang and Dengler, 2004; Scarpella et al., 2004) (Fig. 4.5A), *SHR* is expressed in isodiametric cells (Fig. 4.5B,C), suggesting that *SHR* expression is initiated in ground cells. Covisualization of signals of SHR::nYFP and ATHB::nCFP (Sawchuk et al., 2007) in second loops of 4-DAG first leaves showed matching expression of fluorescent reporters (Fig. 4.5G–I), suggesting that expression of *SHR* is initiated simultaneously with that *ATHB8*. To test for possible artifacts induced by fluorophore intrinsic properties (e.g., different maturation times and stabilities of nYFP and nCFP) or detection parameters (e.g., suboptimal excitation wavelengths and emission intervals), we visualized extent of coexpression between SHR::nRFP and ATHB8::nYFP signals. The reproducible coincidence of fluorescence in reciprocal permutations of *SHR* and *ATHB8*

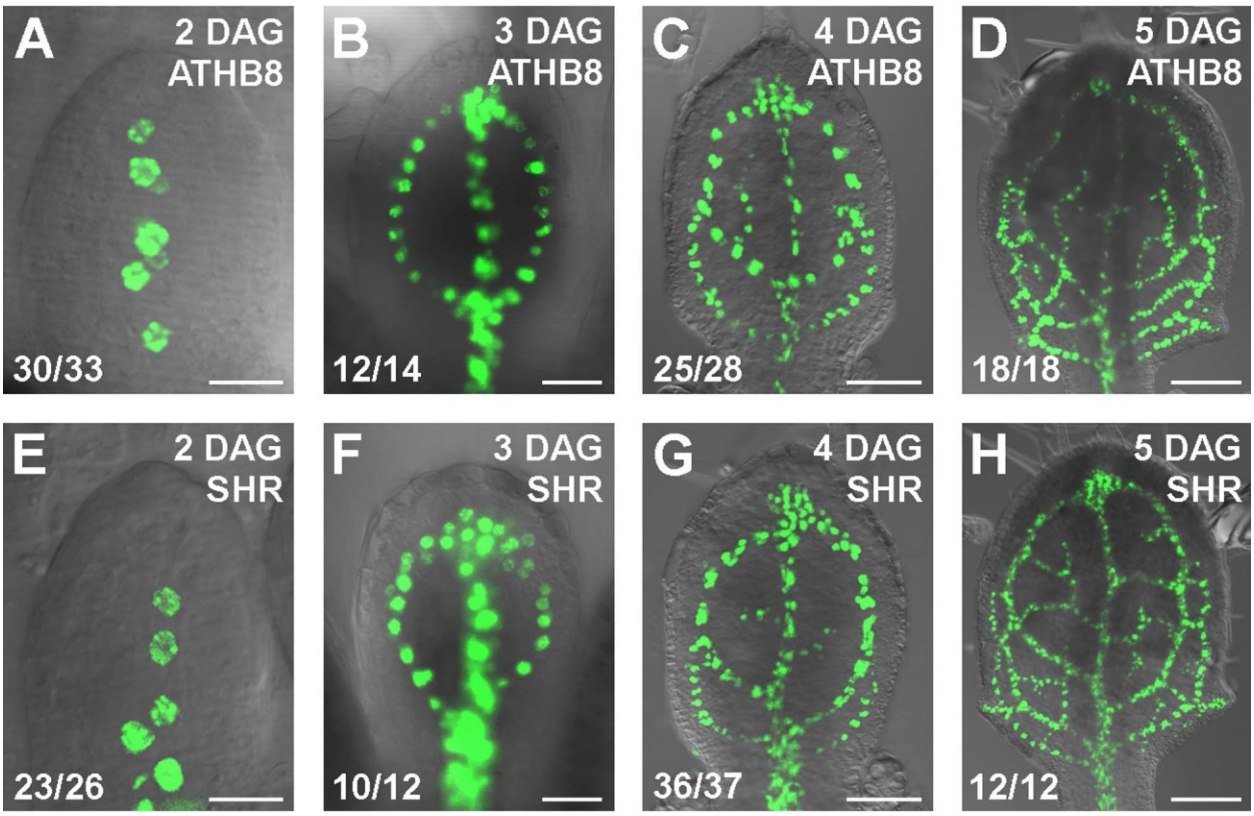

Figure 4.4. *ATHB8* and *SHR* expression in first leaf development.

(A–H) Overlay of confocal-laser-scanning and differential-interference-contrast microscopy, subepidermal focal plane. Top right, leaf primordium age and gene identity. Bottom left, fraction of samples showing the displayed features. (A,E) Lateral view (abaxial side to the left). (B–D,F–H) Abaxial view. (A–D) Green, ATHB8::nYFP expression. (E–H) Green, SHR::nYFP expression. Scale bars: (A,E) 10 µm; (B,F) 20 µm; (C,G) 50 µm; (D,H) 75 µm.

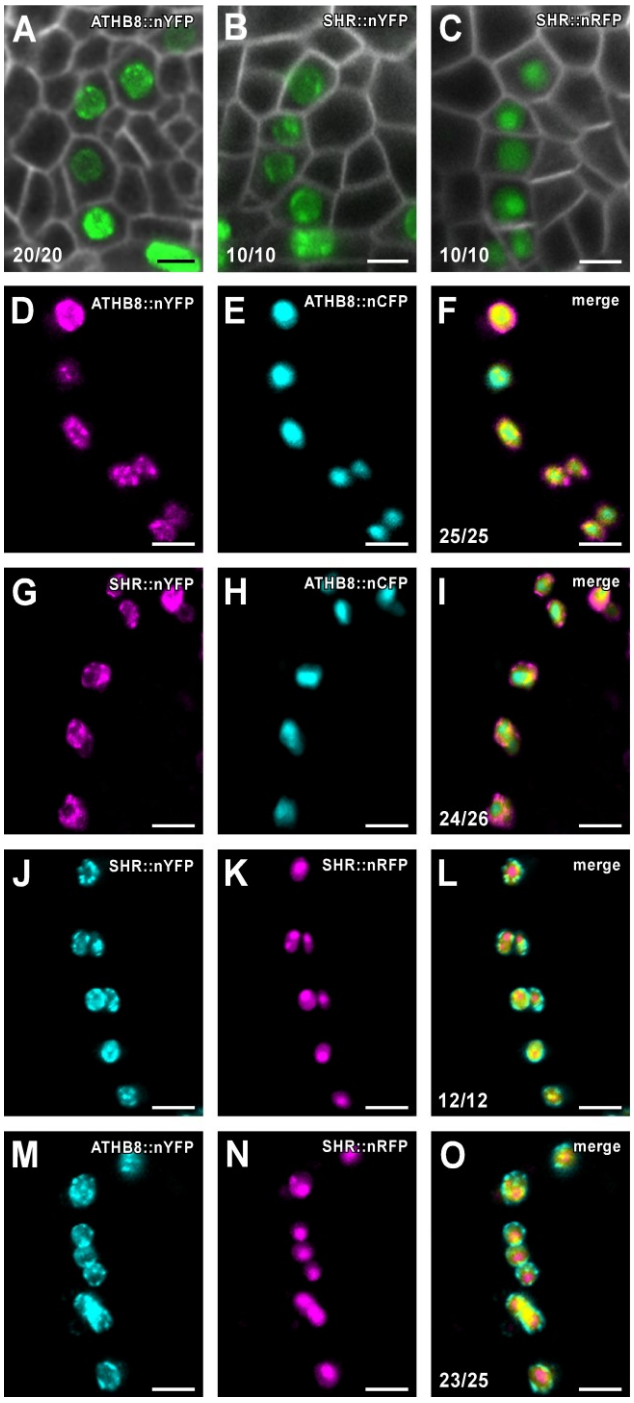

Figure 4.5. Stage-specific *SHR* expression in leaf vein development.

(A–O) Details of basal regions (A–C) or second loops (D–O) of 4-DAG first leaves, abaxial view. Confocal-laser-scanning microscopy, subepidermal focal plane. Top right, marker identity. Bottom left, fraction of samples showing the displayed features. (A–C) White,

UBQ10::GFP:LTI6B expression. (A) Green, ATHB8::nYFP expression. (B) Green, SHR::nYFP expression. (C) Green, SHR::nRFP expression. (D,F) Magenta, ATHB8::nYFP expression. (E,F,H,I) Cyan, ATHB8::nCFP expression. (G,I) Magenta, SHR::nYFP expression. (J,L) Cyan, SHR::nYFP expression. (K,L,N,O) Magenta, SHR::nRFP expression. (M,O) Cyan, ATHB8::nYFP expression. (F,I,L,O) Merge of images in D and E, G and H, J and K, and M and N, respectively. Images are color-coded with a dual-channel LUT from cyan to magenta through green, yellow and red (Demandolx and Davoust, 1997). Fluorescence in each detection channel was displayed in either magenta or cyan. Single-fluorophore images were then merged using a differential operator. As a result, preponderance of cyan signal over colocalized magenta signal is encoded in green, opposite in red, and colocalized cyan and magenta signals of equal intensity in yellow. Scale bars: (A–C) 5 μm; (D–O) 10 μm.

regulatory regions with YFP and CFP, or RFP (compare Fig. 4.5M–O to Fig. 4.5G–I), suggests that our covisualization data are fluorophore independent, further supporting that expression of *SHR* and *ATHB8* is simultaneously activated in ground cells that have transitioned to preprocambial state.

4.2.4 *SHR* Expression in Auxin Transport-Inhibited Leaves

Domains of *SHR* expression may be rigidly specified in leaf development and only incidentally matching with zones of vein appearance. Therefore, we asked whether fields of *SHR* expression remained associated with areas of leaf vein formation upon experimental interference with vascular patterning. Auxin transport has been shown to define sites of vein appearance in developing leaf primordia (Mattsson et al., 1999; Sieburth, 1999). Therefore, we grew seedlings harboring the *SHR* and *ATHB8* transcriptional fusions in the presence of the auxin transport inhibitor 1-N-naphthylphthalamic acid (NPA) and imaged fluorescent protein expression in first leaves at 3, 4, and 5 DAG.

Leaves of plants germinated and grown in the presence of auxin transport inhibitors are characterized by several reproducible, distinct abnormalities in vein network configuration; most conspicuously, great numbers of broad-vein loops that fuse along the entire edge of the leaf, to give rise to a wide marginal zone of vascular differentiation, and that extend parallel to one another at the center of the leaf, to give rise to a laterally expanded midvein (Mattsson et al., 1999; Sieburth, 1999). As shown in Fig. 4.5, domains of SHR::nRFP and ATHB8::nYFP expression retained their tight relation to sites of vein formation throughout development of auxin transport-inhibited leaves (Fig. 4.6A–F). Furthermore, strict congruence between regions of *SHR* and *ATHB8* promoter activity was preserved under conditions of reduced auxin transport (Fig. 4.6G–I). However, as observed in undisturbed leaf development, SHR::nRFP signals persisted at later stages of vein differentiation, while expression of the *ATHB8* transcriptional fusion had declined (Fig. 4.6H,I).

In conclusion, association between *SHR* expression domains with areas of *ATHB8*-marked vein formation observed under undisturbed conditions persisted in auxin-transport-inhibited leaves, suggesting non-circumstantial correlation between *SHR* expression and leaf vein emergence.

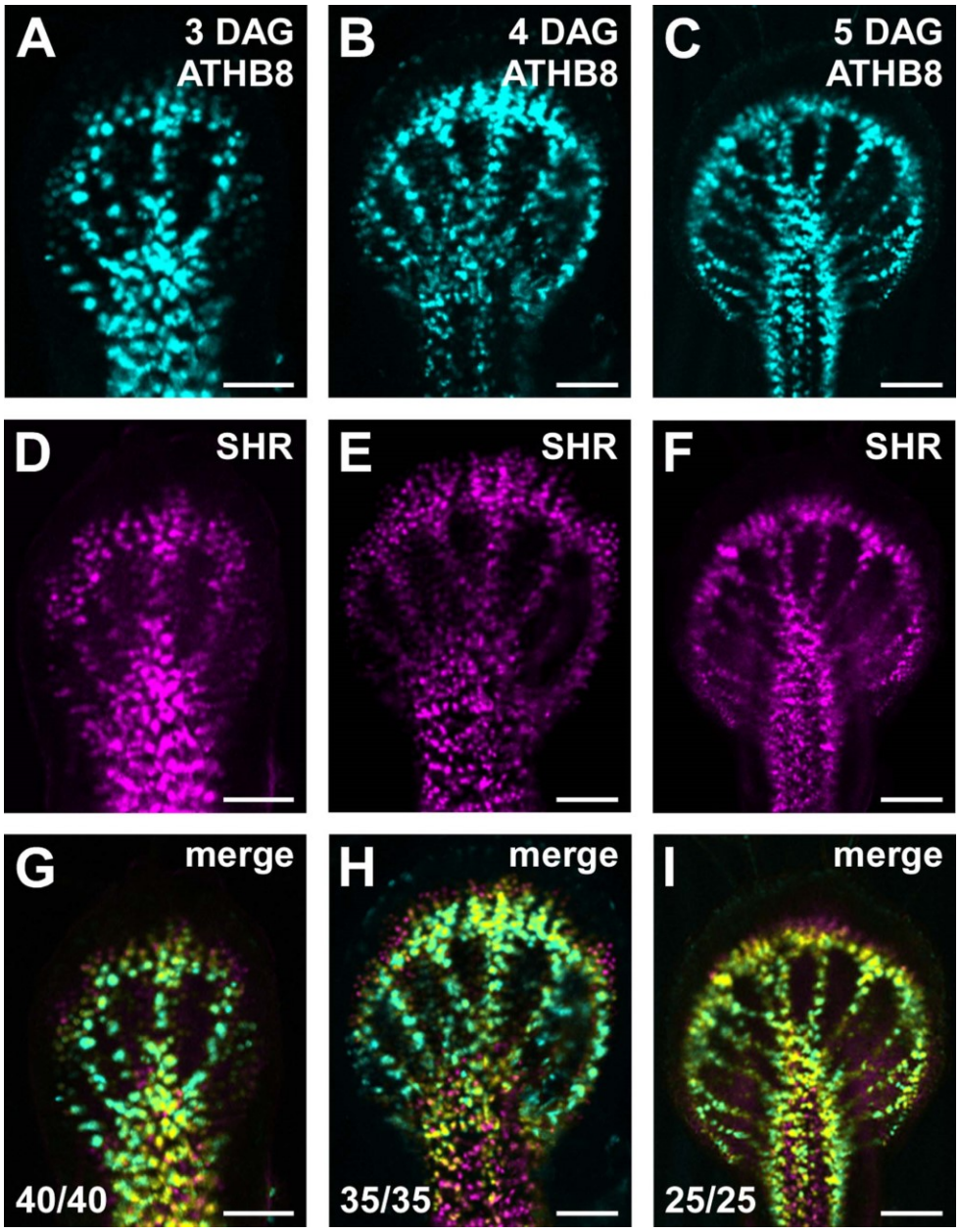

Figure 4.6. *SHR* and *ATHB8* expression in auxin-transport-inhibited leaves.
(A–I) First leaves, abaxial view, developing in the presence of 2.5 µM 1-N-naphthylphthalamic acid (NPA). Confocal-laser-scanning microscopy, subepidermal focal plane. Top right, leaf primordium age and gene identity. Bottom left, fraction of samples showing the displayed features. (A–C) Cyan, ATHB8::nYFP expression. (D–F) Magenta, SHR::nRFP expression. (G–I) Merge of images in A and D, B and E, and C and F, respectively. Images color-coded with a dual-channel LUT as described for Fig. 4.5. Scale bars: 50 µm.

4.2.5 SHR Expression in Leaf Vein Development

In the root, *SHR* transcription is restricted to the procambium, but SHR protein is additionally localized to the cell layer surrounding the root vasculature (Helariutta et al., 2000; Nakajima et al., 2001). We therefore asked whether SHR displayed similar behavior in the leaf. To address this question, we visualized expression of a translational fusion of *SHR* to YFP in 4-DAG first leaves, and compared it to expression of the non-mobile ATHB8::ATHB8:RFP translational fusion (Donner et al., 2009).

In agreement with previous observations (Donner et al., 2009), expression of the fluorescently tagged ATHB8 protein mimicked *ATHB8* promoter activity in leaf vascular cells (Fig. 4.7A–C). In contrast, SHR::SHR:YFP signals were further detected in cells adjacent the preprocambial and procambial domains of expression of the *SHR* transcriptional fusion (Fig. 4.7D–I). However, while SHR::SHR:YFP fluorescence was distributed in both nucleus and cytoplasm of cells within the vascular expression territory, fusion protein localization in the periveinal cell layer was markedly nuclear (Fig. 4.7D–I).

4.2.6 Leaf Expression of *SHR*-Related Genes

SHR belongs to a small clade of GRAS genes that includes *SCARECROW-LIKE29* (*SCL29*) and *SCL32* (Bolle, 2004; Lee et al., 2008). Therefore, we asked whether *SCL29* and *SCL32* were expressed in the leaf in a pattern similar to that of *SHR*. To address this question, we visualized expression of transcriptional and translational fusions of *SCL29* or *SCL32* to YFP in 4-DAG first leaves.

While expression of *SCL29* fusions was confined to epidermal cells (Fig. 4.8A,D), activity of *SCL32* fusions was detected at nearly all subepidermal positions (Fig. 4.8B,E). We therefore asked whether the expression domain of *SCL32* in the leaf comprised vascular cells. To address this question, we imaged degree of signal overlap in leaves simultaneously expressing SHR::nRFP and transcriptional or translational fusions of *SCL32*. We observed separate activity of *SCL32* fusions and of SHR::nRFP (Fig. 4.8C,F), suggesting non-vascular expression of *SCL32* in the leaf.

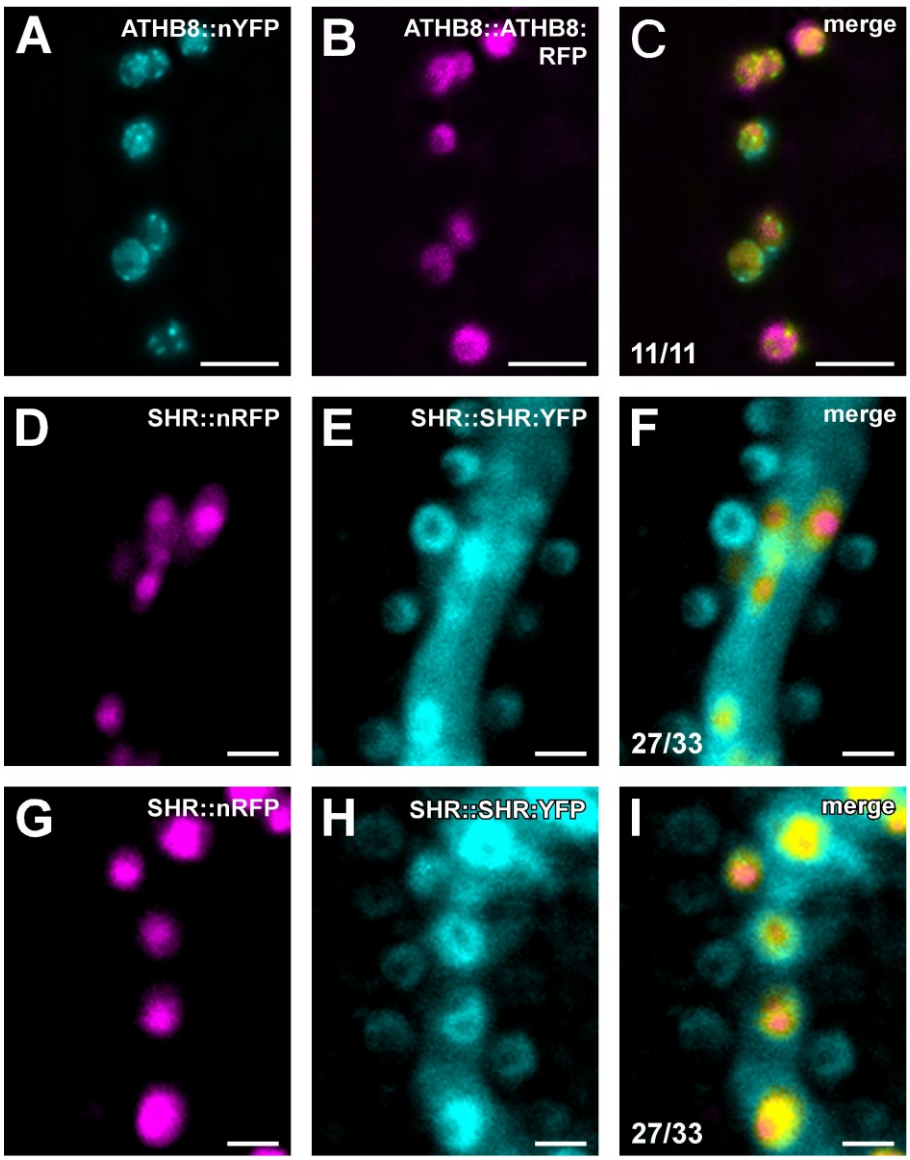

Figure 4.7. SHR expression in first leaves.

(A–I) Four-DAG first leaves, abaxial view. Confocal laser scanning microscopy, subepidermal focal plane. Top right, marker identity. Bottom left, fraction of samples showing the displayed features. (A–C,G–I) Details of second loops. (D–F) Details of first loops. (A,C) Cyan, ATHB8::nYFP expression. (B,C) Magenta, ATHB8::ATHB8:RFP expression. (D,F,G,I) Magenta, SHR::nRFP expression. (E,F,H,I) Cyan, SHR::SHR:YFP expression. (C,F,I) Merge of images in A and B, D and E, and G and H, respectively. Images color-coded with a dual-channel LUT as described for Fig. 4.5. Scale bars: (A–C) 10 µm; (D–F) 50 µm; (G–L) 5 µm.

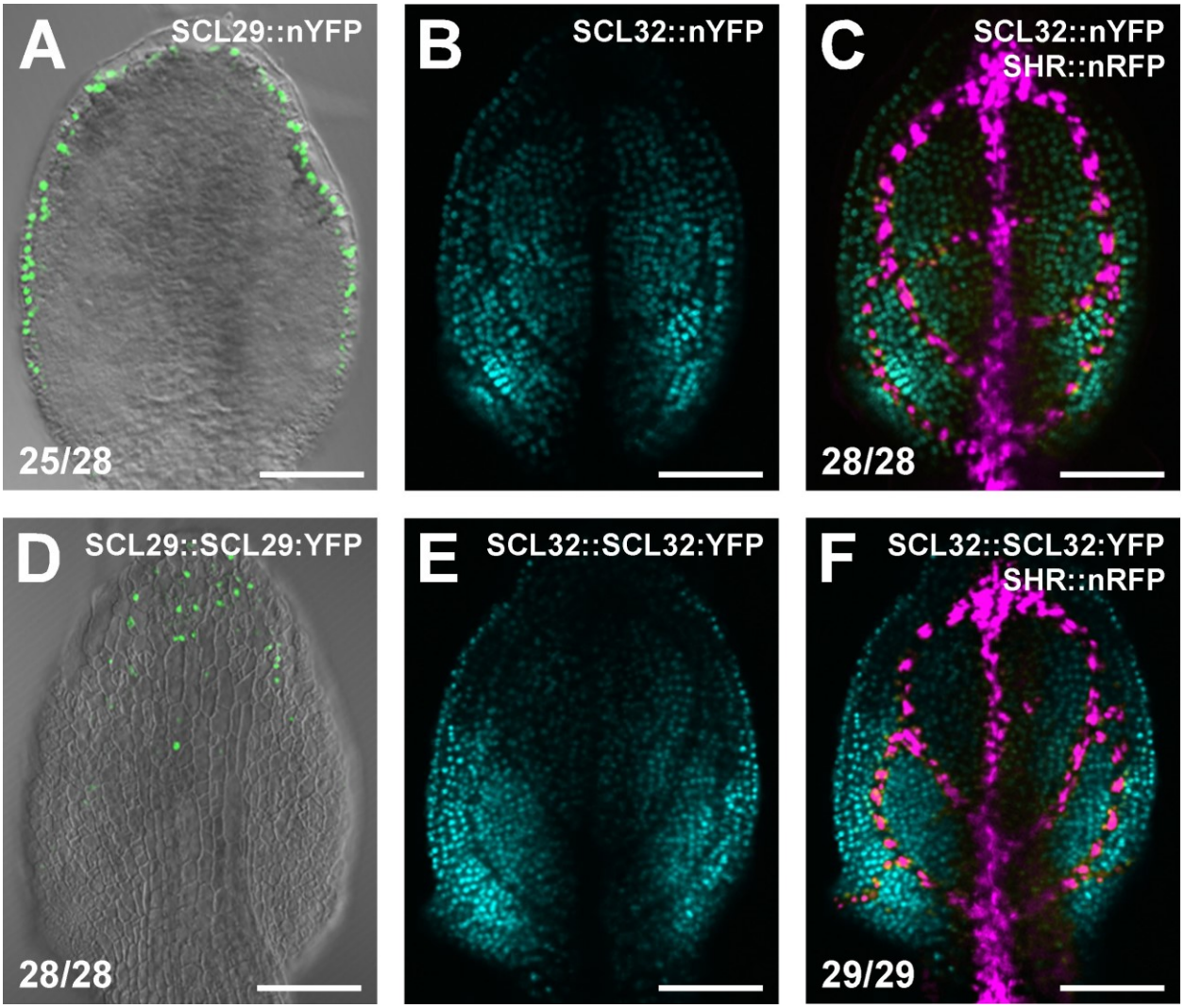

Figure 4.8. SCL29 and SCL32 expression in first leaves.

(A–F) Four-DAG, first leaves, abaxial view. Top right, marker identity. Bottom left, fraction of samples showing the displayed features. (A,D) Overlay of confocal-laser-scanning and differential-interference-contrast microscopy. (B,C,E,F) Confocal-laser-scanning microscopy. (A–C,E,F) Subepidermal focal plane. (D) Epidermal focal plane. (A) Green, SCL29::nYFP expression. (B,C) Cyan, SCL32::nYFP expression. (C,F) Magenta, SHR::nRFP expression. Images color-coded with a dual-channel LUT as described for Fig. 4.5. (D) Green, SCL29::SCL29:YFP expression. (E,F) Cyan, SCL32::SCL32:YFP expression. Scale bars: 50 µm.

4.3 Discussion

While the molecular events that control recruitment of ground cells toward procambium formation in leaf development are largely unknown, available evidence suggests that the selection process culminates with initiation of expression of the *HD-ZIP III* gene *ATHB8* (Alonso-Peral et al., 2006; Carland and Nelson, 2004; Carland et al., 2010; Cnops et al., 2006; Donner et al., 2009; Kang and Dengler, 2004; Koizumi et al., 2000; Petricka and Nelson, 2007; Pineau et al., 2005; Sawchuk et al., 2008, 2007, Scarpella et al., 2004, 2006). Activation of *ATHB8* expression defines transition to a morphologically inconspicuous preprocambial cell state that preludes to procambium appearance. Therefore, characterization of the molecular identity of ground cells that have switched to preprocambial state would be particularly informative as it may provide insight into the molecular circuits controlling vein formation.

In this study, we searched for gene expression profiles associated with preprocambial stages of vein development in Arabidopsis leaves. We found that expression of *SHR*, which encodes a member of the GRAS family of plant-specific transcription factors (Helariutta et al., 2000; Di Laurenzio et al., 1996; Pysh et al., 1999), emerges in synchrony with that of *ATHB8* in leaf development, suggesting that parallel activation of expression of *SHR* and *ATHB8* identifies a preprocambial cell state that announces vein formation. However, while ATHB8 protein expression remained confined to developing veins, the SHR protein expression domain further included a contiguous, perivascular cell layer, suggestive of activities of procambium-precursor cells beyond vein formation.

4.3.1 Transition to Preprocambial Cell State

During leaf development, *SHR* and *ATHB8* were expressed in seemingly overlapping subepidermal domains and with amazingly comparable dynamics. Expression of both *SHR* and *ATHB8* was initiated in narrow domains that became associated with sites of vein formation. Further, vein-associated expression fields of *SHR* and *ATHB8* emerged in the same temporal sequence: midvein, first loops, second loops, and higher-order veins, third loops. Finally, vein

order-specific expression domains of *SHR* and *ATHB8* became apparent at the same stage of leaf development. However, expression of *SHR* was sustained at all stages of vein formation, while that of *ATHB8* became dissipated at later stages of vascular differentiation, in agreement with previous reports (Kang and Dengler, 2002, 2004; Scarpella et al., 2004). Expression of both *SHR* and *ATHB8* was initiated in files of polygonal, isodiametric ground cells, and positions of activation of *SHR* expression overlapped with sites of initiation of *ATHB8* expression, suggesting that *SHR* is expressed at preprocambial stages of vein development. Moreover, that *SHR* and *ATHB8* preprocambial expression domains reproducibly coincided with one another suggests that expression of *SHR* is initiated concurrently with transition to *ATHB8* preprocambial cell state.

If coincidence between expression of *SHR* and *ATHB8* were merely circumstantial, one would not expect such association to endure under conditions of manipulated *ATHB8* expression. Behavior of *SHR* expression in leaves developing under conditions of reduced auxin transport, which dramatically changes the architecture of *ATHB8* expression domains and of vein networks (Gardiner et al., 2010; Mattsson et al., 1999; Sieburth, 1999), was comparable to that observed under undisturbed vein patterning. All aspects of *SHR* expression, including relation to *ATHB8* expression and association with positions of vein formation, proved to be highly reproducible under all experimental conditions. We therefore suggest that, together with *ATHB8*, activation of expression of *SHR* defines switch to a morphologically inconspicuous transcriptional state that foreshadows procambial development.

Unlike ATHB8, the SHR protein is additionally localized to a layer of non-vascular cells that surrounds leaf veins. This observation is consistent with events occurring in root development, where SHR movement from vascular to neighboring cells is required for the formation of the cell sheath that envelops the single vein (Gallagher et al., 2004; Helariutta et al., 2000; Nakajima et al., 2001). Leaf veins have long been suspected to provide positional cues that control differentiation of adjoining photosynthetic cell types (Langdale and Nelson, 1991), and the pattern of SHR expression in the leaf suggests that such organizing influence may arise simultaneously with transition to preprocambial cell state.

Correct initiation of *ATHB8* expression at preprocambial stages of leaf vein development strictly depends on the presence of a TGTCTG regulatory element in the *ATHB8* promoter

(Donner et al., 2009). The *SHR* promoter does not contain any TGTCTG element, suggesting an independent mechanism controlling onset of *SHR* expression. It will be interesting to understand the molecular basis of *SHR* preprocambial expression; nevertheless, our findings already contribute to molecularly define cells at incipient stages of leaf vascular development.

4.3.2 Complementary Leaf Expression Profiles of *SHR*-Related Genes

Members of gene families frequently display overlapping expression profiles [e.g., (Mason et al., 2004; Sawchuk et al., 2008; Tsuchisaka and Theologis, 2004)]. In contrast, the expression of the related *SHR*, *SCL29*, and *SCL32* genes defines complementary territories of cells in the leaf.

Epidermal domains of *SCL29* promoter activity become further compartmentalized by presence of the intronless *SCL29* coding sequence. Reports of regulatory elements within the coding region are not unprecedented [e.g., (Ito et al., 2003)], and various post-transcriptional control mechanisms have been described that could account for the differential behavior of *SCL29* transcriptional and translational fusions, including regulated nuclear export (Bailey-Serres et al., 2009), mRNA decay (Belostotsky and Sieburth, 2009), and intercellular mRNA trafficking (Ueki and Citovskytle, 2000).

Subepidermal cells that express either type of *SCL32* fusion lack expression of the preprocambial marker gene *SHR*, and mutual exclusivity of *SCL32* and *SHR* expression domains is consistent with the view that photosynthetic and vascular cell identity acquisition represent antagonistic pathways in leaf subepidermal tissue ontogeny (Kang et al., 2007; Sawchuk et al., 2008; Scarpella et al., 2004).

Tissue-specific expression data are available for 21 of the 32 *GRAS* genes in *Arabidopsis*, but function is only known for 10 of them (Bolle et al., 2000; Dill and Sun, 2001; Fode et al., 2008; Fu et al., 2004; Greb et al., 2003; Di Laurenzio et al., 1996; Lee et al., 2008, 2002; Peng et al., 1997; Pysh et al., 1999; Silverstone et al., 1998; Torres-Galea et al., 2006; Tyler et al., 2004; Wen and Chang, 2002). While it will be interesting to learn whether the non-overlapping expression patterns of *SHR*, *SCL29*, and *SCL32* are associated with equally distinct functions,

our results already assist in the characterization of a family of plant-specific transcription factors in leaf development.

4.4 Materials and Methods

4.4.1 Vector Construction

All amplifications were performed on Arabidopsis (*Arabidopsis thaliana*) ecotype Col-0 genomic DNA using Finnzymes Phusion high-fidelity DNA polymerase (New England Biolabs Inc., Ipswich, MA) and gene-specific primers (Table 4.1). To generate the SHR::nYFP construct, the 2490-bp region from -2505 to -16 of the *SHR* gene (AT4G37650) was recombined into the pFYTAG vector (Zhang et al., 2005). To generate the SHR::nRFP construct, the 2495-bp region of the *SHR* gene from -2504 to -10 was cloned upstream of a translational fusion of the RFP coding sequence (Shaner et al., 2004) to the 3xSV40 nuclear localization signal from pEYFP-Nuc (Clontech Laboratories, Mountain View, CA). To generate the SHR::SHR:YFP construct, the 4107-bp region of the *SHR* gene from -2514 to +1593 was cloned upstream of the YFP coding sequence (Clontech) using an Asp-Pro-Gly linker as described in (Gallagher et al., 2004). To generate the SCL29::nYFP construct, the 1679-bp region from -1686 to -7 of the *SCARECROW-LIKE29* (*SCL29*) gene (AT3G13840) was recombined into the pFYTAG vector (Zhang et al., 2005). To generate the SCL29::SCL29:YFP construct, the 3227-bp region of the *SCL29* gene from -1697 to +1530 was cloned upstream of the YFP coding sequence (Clontech) using a Pro-Asp-Pro-Gly linker. To generate the SCL32::nYFP construct, the 2886-bp region from -2888 to -2 of the *SCL32* gene (AT3G49950) was recombined into the pFYTAG vector (Zhang et al., 2005). To generate the SCL32::SCL32:YFP construct, the 4169-bp of the *SCL32* gene from -2940 to +1229 was cloned upstream of the YFP coding sequence (Clontech) using an Asp-Pro-Gly linker.

Table 4.1. Oligonucleotide Sequences

Name	Sequence (5' to 3')
SHR-2.5	GGGGACAAGTTTGTACAAAAAAGCAGGCTGGACAAAGAAGCAG AGCGTGG
SHR-R	GGGGACCACTTTGTACAAGAAAGCTGGGTAATAAGAAAATGAAT AGAAGAAAGGGAGACC
SHR HindIII F	GAGAAGCTTGACAAAGAAGCAGAGCGTGG
SHR SalI R	TGGGTCGACTTAATGAATAAGAAAATGAATAGA AGAAAGGG
SHR prom SalI Forw2	AAAGTCGACCGAAGAAAGGGACAAAGAAGC
SHR gDNA BamHI Rev2	ATAGGATCCGTAGGTCGCCACGCACTAG
SCL32 Transcriptional FWD	GGGGACAAGTTTGTACAAAAAAGCAGGCTTAGAATCACGTTCCT ATCGG
SCL32 Transcriptional REV	GGGGACCACTTTGTACAAGAAAGCTGGGTGAGTCTGGTTTTAGA GAGAAATG
SCL32 Translational FWD	AGAGTCGACATCTTAGTAGAAATAAGCGAAC
SCL32 Translational REV	TGCGGATCCAAGGGAACCCAAACGGTAGC
SCL29 Transcriptional FWD	GGGGACAAGTTTGTACAAAAAAGCAGGCTGAACAAGCGCATTGA CGGTGAG
SCL29	GGGGACCACTTTGTACAAGAAAGCTGGGTATGATG

Transcriptional REV	AAAAAGGTATAATTTGTGAGTAGG
SCL29 Translational FWD	ACCGTCGACTACCAAGAGAGGAACAAGCG
SCL29 Translational REV	ACTGATATCCTTCCACAATGAACAAAAGGAAACTG

4.4.2 Plant Material and Growth Conditions

The J2501 and Q0990::erGFP enhancer-trap lines of the Haseloff collection (Haseloff, 1999) were obtained from the Arabidopsis Biological Resource Center. The WOL::nGFP line was a generous gift of David Galbraith. The origins of the ATHB8::nYFP, UBQ10::GFP:LTI6B, ATHB8::nCFP, and ATHB8::ATHB8:RFP lines have been described (Donner et al., 2009; Sawchuk et al., 2007, 2008). Seeds were sterilized and germinated, and seedlings and plants were grown, transformed, and selected as described in (Donner et al., 2009). For SHR::nYFP, SHR::nRFP, SCL29::nYFP, SCL32::nYFP, SHR::SHR:YFP, SCL29::SCL29:YFP, and SCL32::SCL32:YFP, the progeny of 10 to 26 independent transgenic lines were inspected to identify the most representative expression pattern. Successive expression analysis was performed on the progeny of at least three lines per construct, which were selected because of strong fluorescent protein expression that was emblematic of the expression profile observed across the entire series of transgenic lines and that resulted from single insertion of the transgene. In genetic crosses, the progeny of at least two independent lines per construct were examined. For auxin transport inhibition, seeds were germinated on growth medium supplemented with 2.5 µM 1-N-naphthylphthalamic acid (NPA) (Chem Service Inc., West Chester, PA). We define ‘‘days after germination’’ (DAG) as days following exposure of imbibed seeds to light.

4.4.3 Microscopy and Image Analysis

Dissected seedling organs were mounted and imaged as described in (Donner et al., 2009). Brightness and contrast were adjusted through linear stretching of the histogram in ImageJ (Schneider et al., 2012). Signal levels and colocalization were visualized as described in (Donner et al., 2009). Images were cropped and figures were assembled as described in (Donner et al., 2009).

CHAPTER 5: TRANSCRIPTIONAL CONTROL OF VEIN-DERIVED POSITIONAL SIGNALS

5.1 Introduction

The development of multicellular organisms requires that not only do cells differentiate correctly but that they do so at the correct position. The correct differentiation of cells at the correct position depends on communication between cells; therefore, how cells communicate with one another is a key question in biology.

In animals, such cell-cell communication often relies on direct interaction between cells; for example, during Drosophila eye development, interaction between the Bride of sevenless ligand in the plasma membrane of the R8 photoreceptor and the Sevenless receptor in the plasma membrane of the adjacent cell induces this latter to differentiate into R7 photoreceptor (Krämer et al., 1991).

Direct cell-cell interactions such as these are precluded in plants by a wall that surrounds each cell; yet, precisely because a cell wall holds plant cells in place and prevents their migration, positional signals, rather than lineage, specify cell fate in plants (van den Berg et al., 1995, 1997; Kidner et al., 2000). For example, positional signals from leaf veins have long been known to control the differentiation of the adjacent bundle-sheath cells (Jankovsky et al., 2001; Langdale et al., 1987, 1988a, 1988b); however, the nature of such vein-derived signal had remained unclear.

Available evidence now suggests that the SHORT-ROOT (SHR) transcription factor is such signal. In the root, the *SHR* gene is expressed in the vascular cylinder, but the SHR protein moves to the adjacent cell layer to control its correct differentiation into endodermis (Helariutta et al., 2000; Nakajima et al., 2001). As in the root, in the leaf, the *SHR* gene is expressed in veins (Cui et al., 2014; Gardiner et al., 2011) (Chapter 4), but the SHR protein is additionally localized

to the adjacent layer of bundle-sheath cell precursors (Gardiner et al., 2011) (Chapter 4), and *shr* mutants fail to differentiate bundle-sheath cells (Cui et al., 2014).

Root vascular cells are unable to respond to the SHR signal that induces endodermis differentiation, but they support SHR movement to the cell layer adjacent to the vascular cylinder—cell layer which, by contrast, is able to respond to such signal (Helariutta et al., 2000; Nakajima et al., 2001). However, ectopic expression of *SHR* in the cell layer adjacent to the vascular cylinder leads to supernumerary layers of endodermis (Nakajima et al., 2001), just as supernumerary layers of endodermis are the result of ectopic expression of *SHR* in the epidermis (Sena et al., 2004). Therefore, that *SHR* expression is restricted to vascular cells is critical to SHR-mediated endodermis differentiation; yet what controls *SHR* vascular expression is poorly understood (Gong et al., 2016).

Here we address this question for the Arabidopsis leaf. We show that *SHR* expression at early stages of vein development is required for SHR-mediated bundle-sheath differentiation, and that both *SHR* expression at early stages of vein development and *SHR* function in bundle-sheath cell differentiation are directly and positively controlled by a group of previously functionally uncharacterized transcription factors of the DNA-BINDING WITH ONE FINGER (DOF) family.

5.2 Results and Discussion

5.2.1 Expression and Function of *SHR* in the Arabidopsis Leaf

Veins form sequentially during Arabidopsis leaf development: the formation of the midvein is followed by that of the first loops of veins (“first loops”), which in turn is followed by that of second loops and minor veins (Donner and Scarpella, 2013; Donner et al., 2009; Gardiner et al., 2010, 2011; Kang and Dengler, 2004; Mattsson et al., 1999; Sawchuk et al., 2007; Scarpella et al., 2004; Sieburth, 1999) (Chapter 4) (Fig. 5.1A–C). In first leaves 4 days after germination (DAG), the midvein and first loops are composed of files of elongated, procambial cells, which are the precursors to all mature vascular cell types (Esau, 1965), and are labeled by onset of

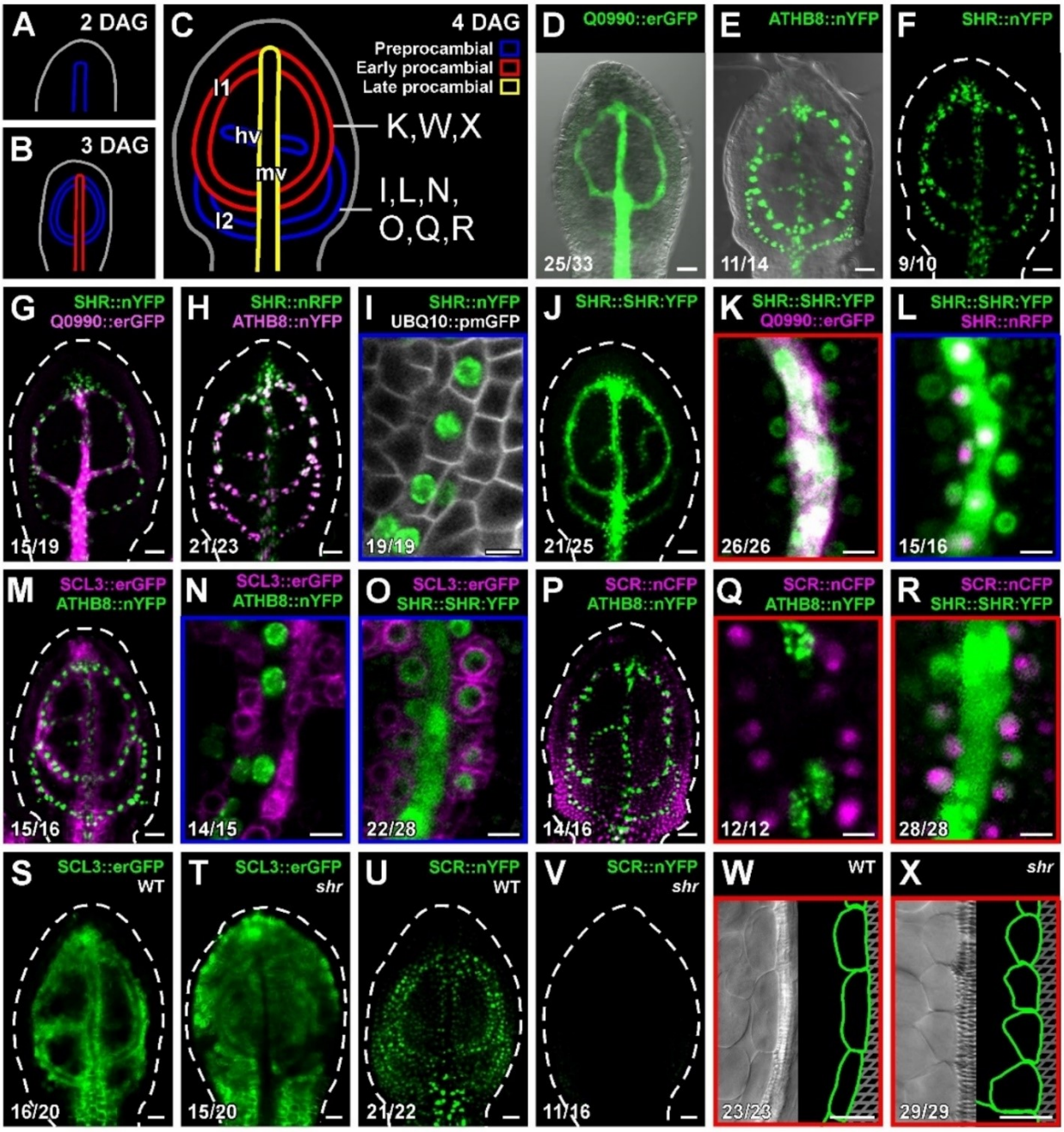

Figure 5.1. Expression and function of *SHR* in the Arabidopsis leaf.

Top right: leaf age in days after germination (DAG) (A–C), or marker identity and genotype (D–X); bottom left: reproducibility index. (A–C) Midvein (mv), first loops (l1), second loops (l2), and minor veins (hv) form sequentially during leaf development (Donner and Scarpella, 2013; Donner et al., 2009; Gardiner et al., 2010, 2011; Kang and Dengler, 2004; Mattsson et al., 1999;

Scarpella et al., 2004; Sieburth, 1999) (Chapter 4); blue, red, and yellow outlines depict successive stages of vein development. Panel identifiers illustrate positions of close-ups in K, Q, R, W, and X (boxed in red), and in I, L, N, and O (boxed in blue). (D–V). Confocal laser scanning microscopy, with (D,E) or without (F–V) transmitted light, of 4-DAG first leaves. White dashed line delineates leaf outline. (W,X) Differential interference contrast microscopy of mature first leaves (left); outline (green) of cells flanking first loops (right). Scale bars: (D–H,J,M,P,S–X) 25 μm; (I,K,L,N,O,Q,R) 5 μm.

expression of endoplasmic-reticulum-localized GFP in the Q0990 enhancer-trap line (Q0990::erGFP hereafter) (Donner et al., 2009; Gardiner et al., 2011; Haseloff, 1999; Sawchuk et al., 2007) (Chapter 4) (Fig. 5.1D). By contrast, at this stage of first-leaf development, second loops and minor veins are composed of files of isodiametric, polygonal, ground cells that have activated expression of ATHB8::nYFP (*ARABIDOPSIS THALIANA HOMEOBOX8* promoter driving expression of nuclear YFP) (Donner and Scarpella, 2013; Donner et al., 2009; Gardiner et al., 2010, 2011; Sawchuk et al., 2007) (Chapter 4) (Fig. 5.1E). During leaf development, ATHB8::nYFP-expressing ground cells will elongate into procambial cells and are therefore referred to as "preprocambial cells" (Kang and Dengler, 2004; Sawchuk et al., 2007; Scarpella et al., 2004). ATHB8::nYFP expression is sustained in procambial cells—for example, in the midvein and first loops of 4-DAG first leaves (Fig. 5.1E)—and subsides at later stages of vein development (Donner and Scarpella, 2013; Donner et al., 2009; Gardiner et al., 2010, 2011; Sawchuk et al., 2007) (Chapter 4).

In agreement with previous observations (Gardiner et al., 2011) (Chapter 4), in 4-DAG first leaves, expression domains of *SHR* transcriptional fusions (2490-bp region from -2505 to -16 relative to the start codon of the *SHR* start codon—*SHR* promoter hereafter—driving expression of nYFP—SHR::nYFP—or 2496-bp region from -2504 to -10 driving expression of nRFP—SHR::nRFP) (Fig. 5.1F) overlapped with those of QO990::erGFP (Fig. 5.1G), and coincided with those of ATHB8::nYFP (Fig. 5.1H), including isodiametric, polygonal, ground cells of second loops (Fig. 5.1I), confirming that *SHR* expression is initiated in preprocambial cells and sustained in procambial cells.

In further agreement with previous observations (Gardiner et al., 2011) (Chapter 4), a functional (see below) SHR::SHR:YFP translational fusion (*SHR* promoter driving expression of a SHR:YFP fusion protein) (Fig. 5.1J) was expressed in procambial and preprocambial cells—labeled by expression of QO990::erGFP and SHR::nRFP, respectively—(Fig. 5.1K,L); however, SHR::SHR:YFP was additionally expressed in isodiametric, polygonal, ground cells that surround procambial and preprocambial veins (Fig. 5.1K,L), and that are the precursors to the elongated, bundle-sheath cells (Kinsman and Pyke, 1998). Bundle-sheath cell precursors specifically expressed SCL3::erGFP (*SCARECROW-LIKE3* promoter driving expression of erGFP) (Fig. 5.1M–O) (Ckurshumova et al., 2009), and—in agreement with previous

observations (Wysocka-Diller et al., 2000)—ubiquitous expression of SCR::nCFP (*SCARECROW* promoter driving expression of nCFP) in ground cells (visible in basal, younger areas of the leaf) (Fig. 5.1P) became restricted to bundle-sheath cell precursors (visible in apical, older areas of the leaf) (Fig. 5.1P–R).

In the root and stem, *SHR* function is required for the formation of the precursors to the endodermis (Benfey et al., 1993; Fukaki et al., 1998; Helariutta et al., 2000)—the cell layer that surrounds the veins in the root and stem and which is therefore equivalent to the bundle-sheath in the leaf. As a result, *shr* roots and stems lack the endodermis (Kang and Dengler, 2004; Scarpella et al., 2004; Sieburth, 1999). We asked whether *SHR* had a similar function in the leaf. To address this question, we compared expression of SCL3::erGFP and SCR::nYFP (*SCARECROW* promoter driving expression of nYFP) (Heidstra et al., 2004) in 4-DAG first leaves of WT and *shr*. In *shr*, SCL3::erGFP expression was no longer restricted to bundle-sheath cell precursors but had expanded to include nearly all ground cells (Fig. 5.1S,T), and SCR::nYFP expression was almost entirely absent, except for extremely weak expression in ground cells at the base of the leaf (Fig. 5.1U,V). Consistent with these observations and in agreement with a previous report (Cui et al., 2014), in mature *shr* leaves, veins were surrounded by cells that lacked the elongated shape characteristic of bundle-sheath cells (Fig. 5.1W,X). We conclude that *SHR* function is required for the formation of bundle-sheath cells and their precursors; therefore, *SHR* has a similar function in the root, stem and leaf.

5.2.2 Cis-Regulation of Functional *SHR* Expression at Early Stages of Vein Development

We next asked what regulatory elements were required for preprocambial *SHR* expression. To address this question, we first successively deleted 483, 507, 460, and 602 bp from the 5'-end of the 2490-bp *SHR* promoter (Fig. 5.2A), and tested the ability of the resulting four *SHR* promoter fragments to drive nYFP expression in second loops of 4-DAG first leaves, as these veins are composed of files of preprocambial cells at this stage of first-leaf development (Fig. 5.1) [12,19-22]. The *SHR* promoter fragment from -2022 to -16 relative to the start codon—[-2022,-16] hereafter—was the shortest fragment that drove expression in second loops, as the [-1515,-16]

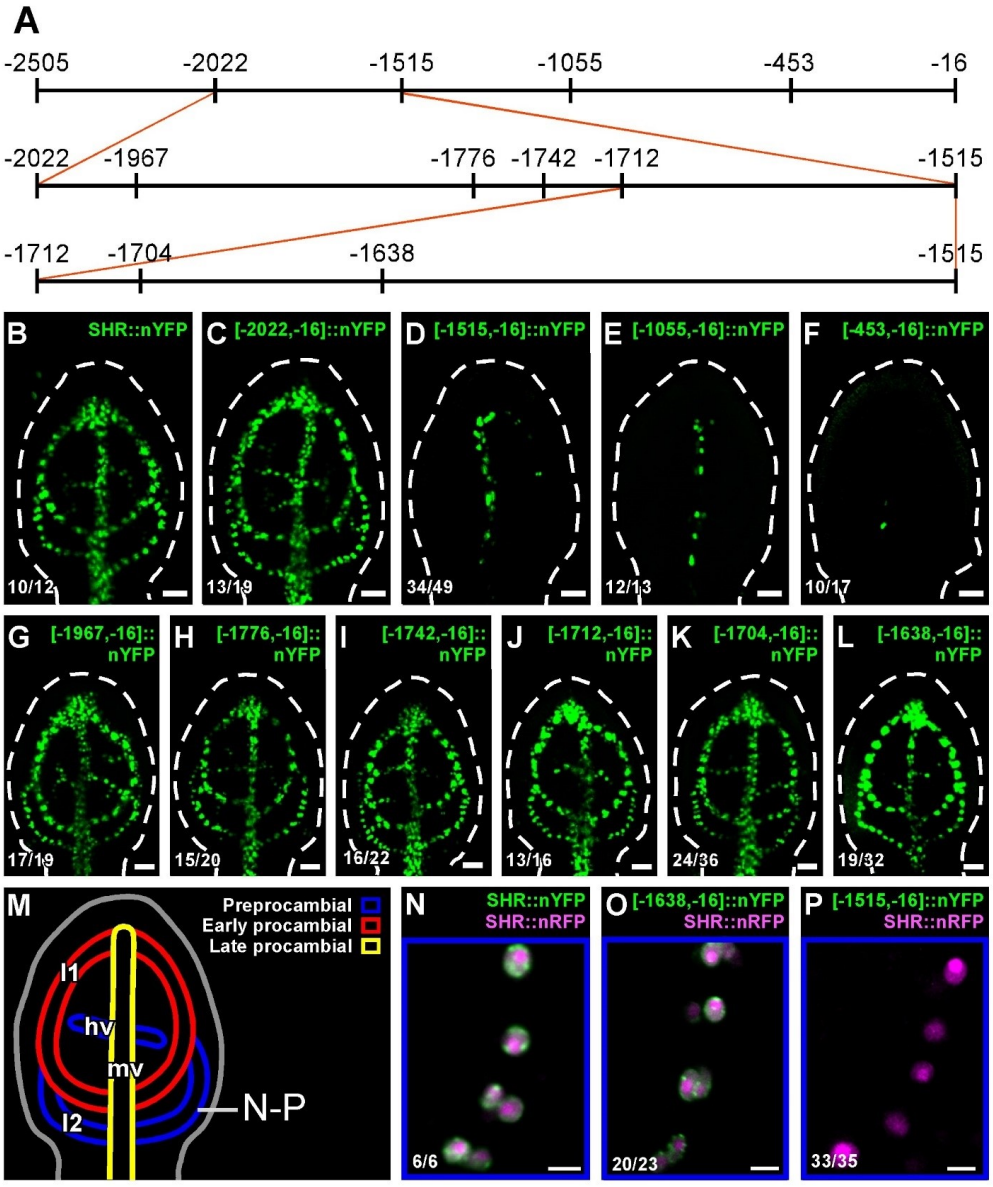

Figure 5.2. **Leaf activity of *SHR* promoter fragments.**

(A) *SHR* promoter fragments. Coordinates relative to start-codon's first nucleotide. (B–L,N–P) Confocal laser scanning microscopy of 4-DAG first leaves. White dashed line delineates leaf outline. Top right: marker identity; bottom left: reproducibility index. (M) 4-DAG first leaf. Blue, red, and yellow outlines depict successive stages of vein development. mv, midvein; l1, first loops; l2, second loops; hv, minor veins. Panel identifiers illustrate positions of close-ups in N–P (boxed in blue). Scale bars: (B–L) 25 µm; (N–P) 5 µm.

fragment drove nYFP expression only in the midvein and first loops (Fig. 5.2B–F). These observations suggest that the [-2022,-1516] region of the *SHR* promoter is required for preprocambial *SHR* expression. We thus successively deleted 55, 191, 34, and 30 bp within the [-2022,-1516] region from the 5'-end of the [-2022,-16] fragment (Fig. 5.2A), and tested the ability of the resulting four promoter fragments to drive nYFP expression in second loops of 4-DAG first leaves. Because all four fragments, including the shortest one—[-1712,-16]—drove nYFP expression in second loops (Fig. 5.2G–J), we successively deleted 8 and 66 bp within the [-1712,-1516] region from the 5'-end of the [-1712,-16] fragment (Fig. 5.2A), and tested the ability of the resulting two promoter fragments to drive nYFP expression in second loops of 4-DAG first leaves. Both the [-1704,-16] and the [-1638,-16] fragments drove nYFP expression in second loops (Fig. 5.2K,L), suggesting that the [-1638,-1516] region of the *SHR* promoter is required for preprocambial *SHR* expression. To test further the ability of the [-1638,-16] fragment to drive preprocambial nYFP expression and the inability of the [-1515,-16] fragment to do so, we assessed coexpression of [-1638,-16]::nYFP and SHR::nRFP, and of [-1515,-16]::nYFP and SHR::nRFP, and compared it with that of SHR::nYFP and SHR::nRFP in second loops of 4-DAG first leaves. In agreement with previous observations (Gardiner et al., 2011) (Chapter 4), expression of SHR::nYFP coincided with that of SHR::nRFP (Fig. 5.2N). As SHR::nYFP expression, [-1638,-16]::nYFP expression coincided with that of SHR::nRFP (Fig. 5.2O); by contrast, [-1515,-16]::nYFP failed to be expressed in SHR::nRFP-expressing, second loops (Fig. 5.2P), supporting that the [-1638,-1516] region of the *SHR* promoter is required for preprocambial *SHR* expression.

A SHR:YFP fusion protein expressed by the 2490-bp *SHR* promoter (SHR::SHR:YFP) (Gardiner et al., 2011) (Chapter 4) (Fig. 5.1J–L,O,R; Fig. 5.3D) rescues *shr* defects in bundle-sheath cell differentiation (Fig. 5.3B,C,E). We asked whether SHR:YFP expression by the [-1638,-16] fragment of the *SHR* promoter—fragment which is sufficient to drive preprocambial nYFP expression (Fig. 5.2)—were sufficient to rescue *shr* defects in bundle-sheath cell differentiation. Expression of [-1638,-1]::SHR:YFP (Fig. 5.3F,G) rescued *shr* defects in bundle-sheath cell differentiation (Fig. 5.3B,C,H), suggesting that the [-1638,-16] fragment of the *SHR* promoter is sufficient for both preprocambial *SHR* expression and *SHR* function in bundle-sheath cell differentiation. We next asked whether SHR:YFP expression by the [-1515,-16] fragment of

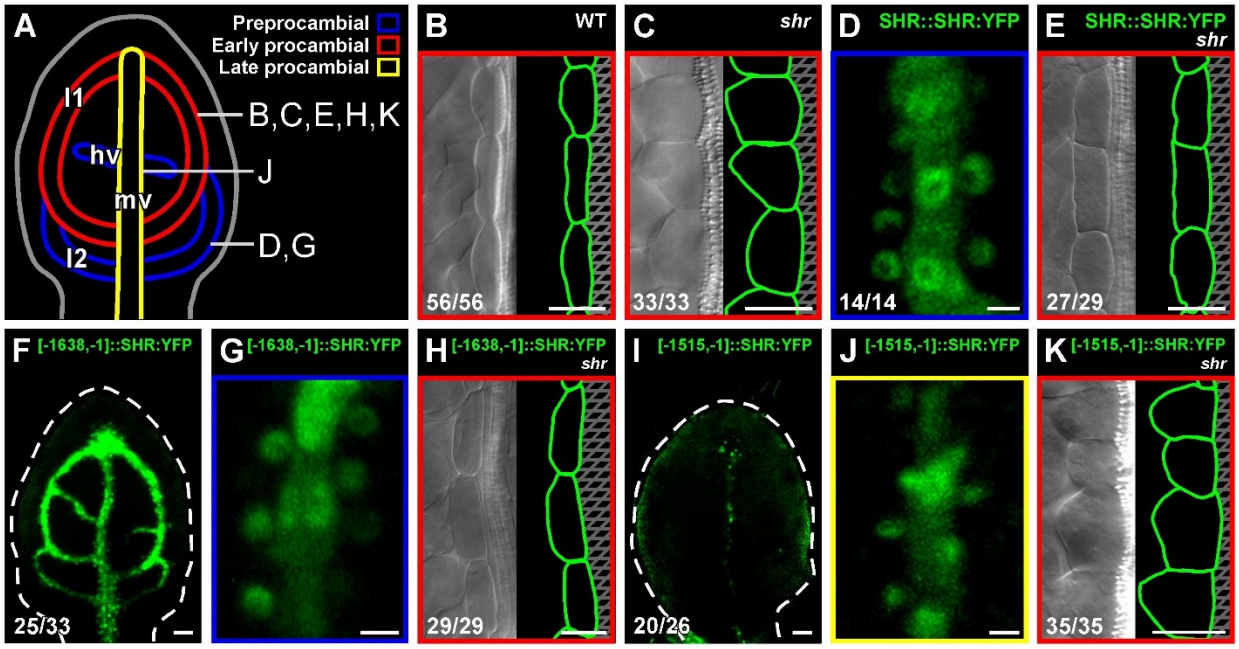

Figure 5.3. Functional *SHR* expression in the leaf.

(A) 4-DAG first leaf. Blue, red, and yellow outlines depict successive stages of vein development. mv, midvein; l1, first loops; l2, second loops; hv, minor veins. Panel identifiers illustrate positions of close-ups in B, C, E, H, and K (boxed in red), in D and G (boxed in blue), and in J (boxed in yellow). (B–K) Top right: marker identity and genotype; bottom left: reproducibility index. (B,C,E,H,K) Differential interference contrast microscopy of mature first leaves (left); outline (green) of cells flanking first loops (right). (D,F,G,I,J) Confocal laser scanning microscopy of 4-DAG first leaves. White dashed line delineates leaf outline. Scale bars: (B,C,E,F,H,I,K) 25 µm; (D,G,J) 5 µm.

the *SHR* promoter—fragment which is insufficient to drive preprocambial nYFP expression (Fig. 5.2)—were sufficient to rescue *shr* defects in bundle-sheath cell differentiation. Expression of [-1515,-1]::SHR:YFP (Fig. 5.3I,J) failed to rescue *shr* defects in bundle-sheath cell differentiation (Fig. 5.3B,C,K), suggesting that the [-1638,-1516] region of the *SHR* promoter is required for both preprocambial *SHR* expression and *SHR* function in bundle-sheath cell differentiation. These observations also suggest that cells surrounding veins at late procambial stages of development are no longer able to respond to the vein-derived SHR signal that induces bundle-sheath cell differentiation.

The [-1638,-1516] region of the *SHR* promoter contains four putative binding sites for transcription factors of the DNA-BINDING WITH ONE ZINC FINGER (DOF) family (Yanagisawa, 2002) (Fig. 5.4A). We asked whether such putative DOF-binding sites were required for preprocambial *SHR* expression. To address this question, we deleted the first putative DOF-binding site, or the first, second, and third putative DOF-binding sites, and tested the ability of the resulting two promoter fragments ([-1588,-16] and [-1552,-16], respectively) (Fig. 5.4A) to drive preprocambial nYFP expression, as assessed by coexpression with SHR::nRFP in second loops of 4-DAG first leaves. The ability to drive preprocambial nYFP expression was only partially lost by the [-1588,-16] fragment (Fig. 5.4C,H), but was almost completely lost by the [-1552,-16] fragment (Fig. 5.4E,J). Next, we mutated the first putative DOF-binding site to a sequence that is unable to bind DOF transcription factors in vitro (Yanagisawa and Schmidt, 1999); deleted the first putative DOF-binding site and mutated the second and third; or deleted the first, second, and third putative DOF-binding-sites and mutated the fourth; and tested the ability of the resulting three promoter fragments (mDBS1, mDBS2,3, and mDBS4, respectively) (Fig. 5.4A) to drive preprocambial nYFP expression, as assessed by coexpression with SHR::nRFP in second loops of 4-DAG first leaves. The preprocambial activity of the promoter fragments in which the putative DOF-binding sites had been mutated was similar to that of the promoter fragments in which the same sites had been deleted (compare Fig. 5.4D,I with Fig. 4C,H; Fig. 4F,K with Fig. 4E,J; Fig. 4G with Fig. 2D; and Fig. 4L with Fig. 2P), suggesting that the four putative DOF-binding sites in the [-1638,-1516] region of the *SHR* promoter are required for preprocambial *SHR* expression.

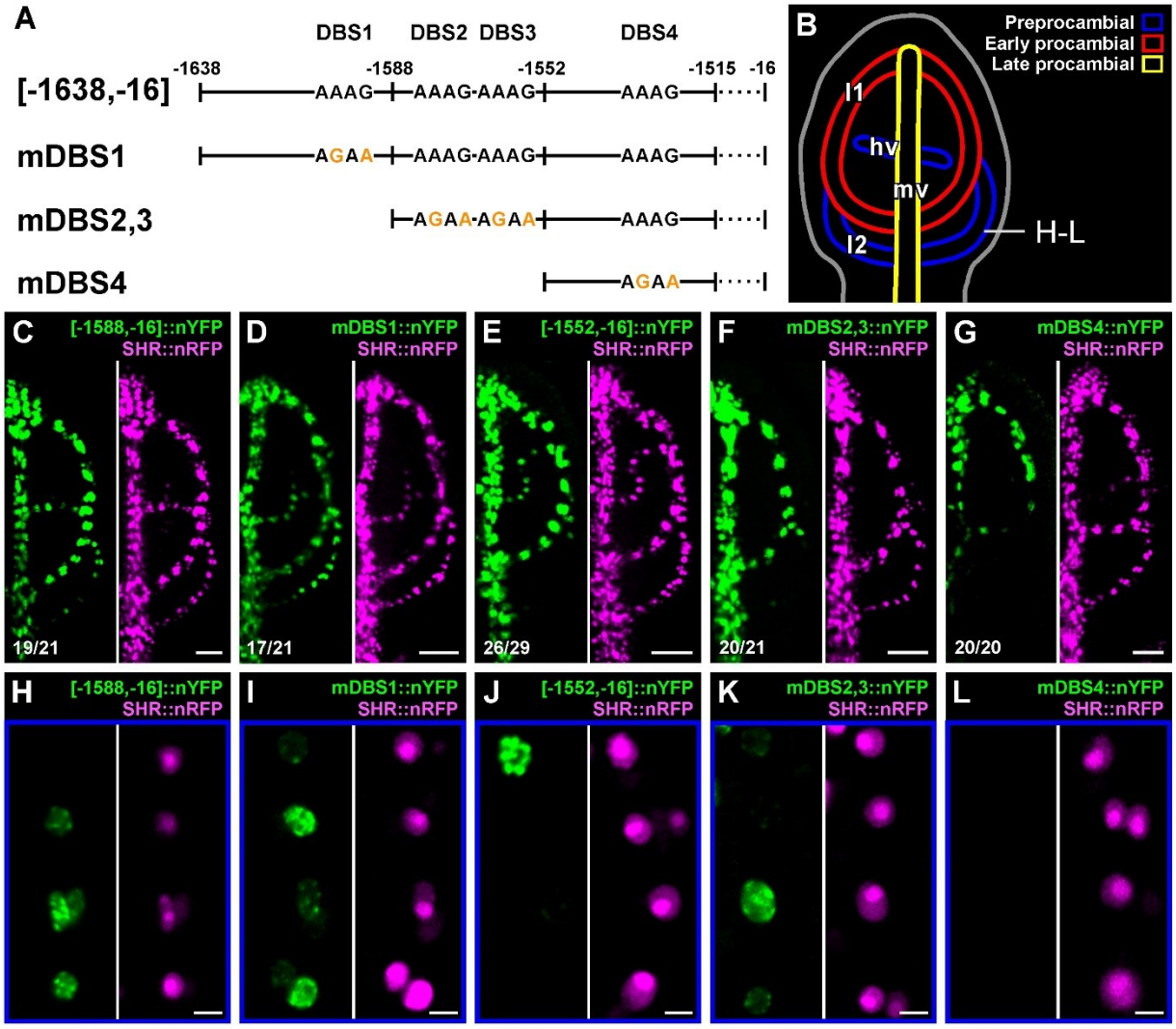

Figure 5.4. Leaf activity of *SHR* promoter fragments and mutations.

(A) *SHR* promoter fragments and mutations. Coordinates relative to start-codon's first nucleotide. Black font, putative DOF binding sites (AAAG); orange font, introduced mutations. (B) 4-DAG first leaf. Blue, red, and yellow outlines depict successive stages of vein development. mv, midvein; l1, first loops; l2, second loops; hv, minor veins. Panel identifiers illustrate positions of close-ups in H–L (boxed in blue). (C–L) Confocal laser scanning microscopy of 4-DAG first leaves. Activity of promoter fragments or mutations (green; left), and of full-length promoter (magenta; right) in the same leaves. Scale bars: (C–G) 25 µm; (H–L) 5 µm.

5.2.3 Trans-Regulation of Functional *SHR* Expression at Early Stages of Vein Development

Functional *SHR* expression in preprocambial cells depends on four putative DOF-binding sites in the [-1638,-1516] region of the *SHR* promoter (Figs. 5.2–5.4). If functional *SHR* expression in preprocambial cells indeed depended on the activity of one or more DOF transcription factors, lowering the expression levels of *DOF* genes might lead to lower levels of preprocambial *SHR* expression and defects in bundle-sheath cell differentiation. To test this prediction, we expressed by the ubiquitously active *UBIQUITIN10* (*UBQ10*) promoter (Norris et al., 1993) an RNA interference construct targeting the sequence encoding the highly conserved DOF DNA-binding domain (Yanagisawa, 2002) (UBQ10::DOFi), and compared levels of SHR::nYFP expression and shape of cells surrounding veins in, respectively, 4-DAG and mature first leaves of WT and UBQ10::DOFi. SHR::nYFP expression was weaker in UBQ10::DOFi than in WT (Fig. 5.5B,C), and in UBQ10::DOFi, veins were surrounded by cells that had begun to lose the elongated shape characteristic of bundle-sheath cells (Fig. 5.5D–F), suggesting that functional *SHR* expression at early stages of vein development depends on the activity of one or more DOF transcription factors.

We next reasoned that the expression of *SHR* and that of the one or more *DOF* genes the products of which activate preprocambial *SHR* expression might be regulated similarly. By means of the Expression Angler tool (Toufighi et al., 2005), we found that *DOF5.3* (Yanagisawa, 2002) is the *DOF* gene the expression of which is regulated most similarly to that of *SHR*. Preprocambial *SHR* expression is required for bundle-sheath cell differentiation (Fig. 5.3); therefore, if DOF5.3 were a non-redundant activator of preprocambial *SHR* expression, mutation of *DOF5.3* should lead to defects in bundle-sheath cell differentiation. To test this prediction, we compared the shape of the cells surrounding the veins in mature first leaves of WT and *dof5.3*. The shape of cells surrounding veins in mature leaves of *dof5.3* was no different from that of WT (Fig. 5.6), suggesting that DOF5.3 is not an activator of functional *SHR* expression in preprocambial cells or that DOF5.3 function in this process is redundant.

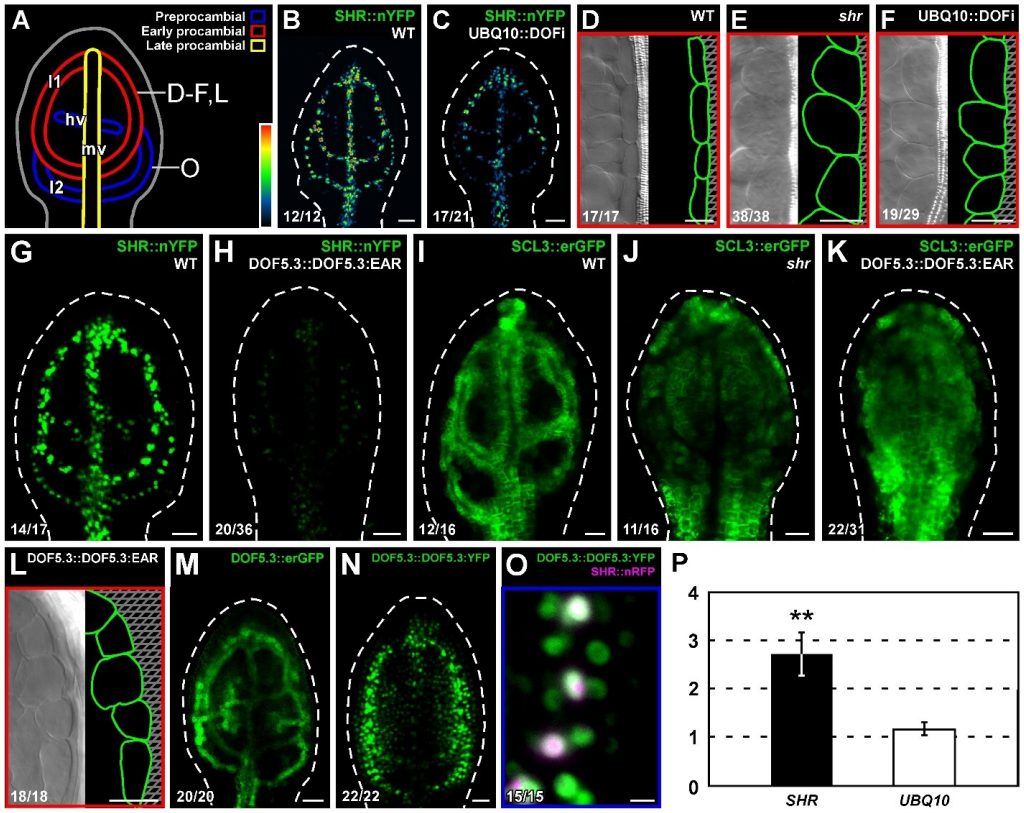

Figure 5.5. Trans-regulation of functional *SHR* expression in the leaf.

(A) 4-DAG first leaf. Blue, red, and yellow outlines depict successive stages of vein development. mv, midvein; l1, first loops; l2, second loops; hv, minor veins. Panel identifiers illustrate positions of close-ups in D–F, and L (boxed in red). (B–O) Top right: marker identity and genotype; bottom left: reproducibility index. (B,C,G–K,M–O) Confocal laser scanning microscopy of 4-DAG first leaves. White dashed line delineates leaf outline. (B,C) Look-up table (ramp in A) visualizes expression levels. (D–F,L) Differential interference contrast microscopy of mature first leaves (left); outline (green) of cells flanking first loops (right). (P) Levels of [-1707,-1493] *SHR* (black bar) and [-799,-610] *UBQ10* (white bar) promoter regions co-immunoprecipitated with YFP from 4-DAG DOF5.3::DOF5.3:YFP seedling lysates, normalized to those from MP::nYFP lysates to control for binding of nuclear YFP to chromatin. Mean ± SE of five technical replicates for each of two biological replicates. Difference between *SHR* and *UBQ10* was significant at $P < 0.01$ (**) by *F*-test and two-tailed, unpaired, unequal-variance *t*-test. Scale bars: (B–N) 25 μm; (O) 5 μm.

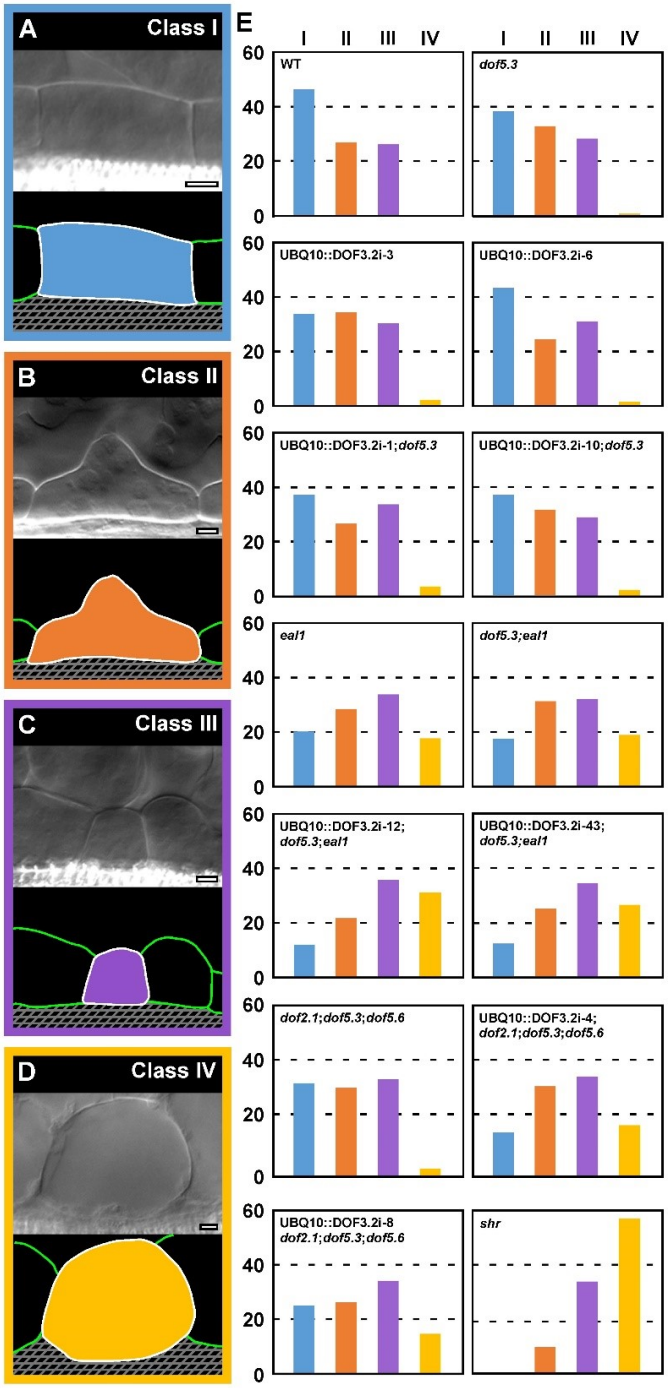

Figure 5.6. Genetic analysis of *SHR* and *DOF* genes.

(A–D) Differential interference contrast microscopy of mature first leaves (top) and outline (green or white) of cells flanking first loops (bottom) illustrating phenotype classes: elongated, polygonal cell (A; blue); elongated, irregularly shaped cell (B; orange); isodiametric cell smaller

than surrounding mesophyll cells (C; violet); rounded cell indistinguishable from surrounding mesophyll cells (D; yellow). (E) Percentages of first-loop-flanking cells in phenotype classes, assessed for each whole first loop in 349-µm by 266-µm, nonoverlapping regions. Difference between *eal1* and WT, between UBQ10::DOF3.2i;*dof5.3*;*eal1* and *eal1*, between UBQ10::DOF3.2i;*dof2.1*;*dof5.3*;*dof5.6* and UBQ10::DOF3.2i;*dof5.3*, and between *shr* and UBQ10::DOF3.2i;*dof2.1*;*dof5.3*;*dof5.6* was significant at $P < 0.05$ (*) or $P < 0.001$ (***) by Kruskal-Wallis and Mann–Whitney test with Bonferroni correction. Sample population sizes (number of leaves): WT, 20; *dof5.3*, 20; UBQ10::DOF3.2i-3, 16; UBQ10::DOF3.2i-6, 16; UBQ10::DOF3.2i-1;*dof5.3*, 13; UBQ10::DOF3.2i-10;*dof5.3*, 15; *eal1*, 19; *dof5.3*;*eal1*, 25; UBQ10::DOF3.2i-12;*dof5.3*;*eal1*, 18; UBQ10::DOF3.2i-43;*dof5.3*;*eal1*, 18; *dof2.1*;*dof5.3*;*dof5.6*, 20; UBQ10::DOF3.2i-4;*dof2.1*;*dof5.3*;*dof5.6*, 17; UBQ10::DOF3.2i-8;*dof2.1*;*dof5.3*;*dof5.6*, 20; *shr*, 20. Scale bars: (A–D) 5 µm.

To distinguish between these possibilities, we turned DOF5.3 into a transcriptional repressor by fusing it to the EAR (for ETHYLENE-RESPONSIVE ELEMENT-BINDING FACTOR-associated amphiphilic repression) portable repressor domain (Hiratsu et al., 2003); we expressed the resulting DOF5.3:EAR by the *DOF5.3* promoter (DOF5.3::DOF5.3:EAR), and compared expression of SHR::nYFP and of the bundle-sheath-cell precursor marker SCL3:erGFP in 4-DAG first leaves of WT and DOF5.3::DOF5.3:EAR, and shape of cells surrounding veins in mature first leaves of WT and DOF5.3::DOF5.3:EAR. SHR::nYFP expression was weaker in DOF5.3::DOF5.3:EAR than in WT (Fig. 5.5G,H). As in *shr*, in DOF5.3::DOF5.3:EAR, SCL3::erGFP expression was no longer restricted to bundle-sheath cell precursors but had expanded to include nearly all ground cells (Fig. 5.5I–K). And in mature DOF5.3::DOF5.3:EAR leaves, veins were surrounded by cells that had begun to lose the elongated shape characteristic of bundle-sheath cells (Fig. 5.5D,E,L). We conclude that DOF5.3 is able to activate functional *SHR* expression at early stages of vein development.

If DOF5.3 indeed were an activator of functional *SHR* expression in preprocambial cells, expression of the DOF5.3 protein should overlap with preprocambial activity of the *SHR* promoter. Consistent with the expression of a DOF5.3::erGFP transcriptional fusion (Gardiner et al., 2010; Lee et al., 2006) (Fig. 5.5M), a DOF5.3::DOF5.3:YFP translational fusion was expressed at early stages of vein development, including preprocambial stages—visible, for example, in second loops of 4-DAG first leaves (Donner et al., 2009; Gardiner et al., 2010, 2011; Odat et al., 2014; Sawchuk et al., 2007) (Chapter 2; Chapter 4)—(Fig. 5.5N). Moreover, the expression of DOF5.3::DOF5.3:YFP overlapped with that of SHR::nRFP in second loops of 4-DAG first leaves (Fig. 5.5O), suggesting that expression of the DOF5.3 protein overlaps with preprocambial activity of the *SHR* promoter.

Finally, we asked whether DOF5.3 bound in vivo the [-1638,-1516] region of the *SHR* promoter, which is required for functional *SHR* expression in preprocambial cells (Figs. 5.2–5.4). To address this question, we immunoprecipitated chromatin-crosslinked YFP in 4-DAG DOF5.3::DOF5.3:YFP seedlings and quantified levels of co-precipitated [-1707,-1493] *SHR* promoter region; to control for binding specificity, we quantified levels of a co-precipitated *UBQ10* promoter region that lacks putative DOF-binding sites. Levels of co-precipitated [-1707,-1493] *SHR* promoter region were ~2.5-fold higher than those of co-precipitated *UBQ10*

promoter region (Fig. 5.5P), suggesting that DOF5.3 binds in vivo the region of the *SHR* promoter that is required for functional *SHR* expression in preprocambial cells.

In conclusion, our results suggest that *DOF5.3* is a direct and positive regulator of both *SHR* expression at early stages of vein development and *SHR* function in bundle-sheath cell differentiation.

5.2.4 Genetic Analysis of *SHR* and *DOF* Genes

DOF5.3 is a direct and positive regulator of both *SHR* expression at early stages of vein development and *SHR* function in bundle-sheath cell differentiation (Fig. 5.5); however, such function of *DOF5.3* is redundant, as the shape of cells surrounding veins in mature leaves of *dof5.3* was no different from that of WT (Fig. 5.6).

DOF5.3 is most related to *DOF3.2* (Yanagisawa, 2002); therefore, we asked whether *DOF3.2* acted redundantly to *DOF5.3* in control of *SHR* function in bundle-sheath cell differentiation. To address this question, we expressed by the *UBQ10* promoter an RNA interference construct targeting *DOF3.2* (UBQ10::DOF3.2i), and compared the shape of cells surrounding veins in mature first leaves of WT, *dof5.3*, UBQ10::DOF3.2i, and UBQ10::DOF3.2i;*dof5.3*. The shape of cells surrounding veins of all those backgrounds was no different (Fig. 5.6); nevertheless, UBQ10::DOF3.2i;*dof5.3*, but not *dof5.3*, enhanced the defects in bundle-sheath cell differentiation of the weak *shr* allele *endodermal-amyloplast less1* (*eal1*) (Morita et al., 2007) (Fig. 5.6)—a finding which, in agreement with interpretations of similar genetic interactions in other organisms (Qiao et al., 1995; Smardon et al., 2000), is consistent with the redundant involvement of *DOF3.2* and *DOF5.3* in the pathway in which *SHR* acts.

The *DOF3.2*/*DOF5.3* pair is most related to the *DOF2.1*/*DOF5.6* pair (Lijavetzky et al., 2003; Yanagisawa, 2002). We therefore asked whether the *DOF2.1*/*DOF5.6* pair acted redundantly to the *DOF3.2*/*DOF5.3* pair in control of *SHR* function in bundle-sheath cell differentiation. To address this question, we compared the shape of cells surrounding veins in mature first leaves of *dof5.3*, UBQ10::DOF3.2i;*dof5.3*, *dof2.1*;*dof5.3*;*dof5.6*, and UBQ10::DOF3.2i;*dof2.1*;*dof5.3*;*dof5.6*. Mutation of the *DOF2.1*/*DOF5.6* pair enhanced the defects in bundle-sheath cell differentiation of UBQ10::DOF3.2i;*dof5.3*—but not those of *dof5.3*—to match the defects in bundle-sheath cell differentiation of *eal1* (Fig. 5.6). This

observation suggests that the *DOF2.1*/*DOF5.6* pair acts redundantly to the *DOF3.2*/*DOF5.3* pair in control of *SHR* function in bundle-sheath cell differentiation. Because the defects in bundle-sheath cell differentiation of UBQ10::DOF3.2i;*dof2.1*;*dof5.3*;*dof5.6* are weaker than those of a strong *shr* allele (Fig 5.6), it is possible that other *DOF* genes act redundantly to *DOF2.1*, *DOF3.2*, *DOF5.3,* and *DOF5.6* to control *SHR* function in bundle-sheath cell differentiation.

5.2.5 Conclusions

Our results suggest a molecular framework for control of bundle-sheath cell differentiation by vein-derived positional signals: *DOF5.3* directly and positively regulates *SHR* expression at early stages of vein development and, consequently, SHR-mediated bundle-sheath cell differentiation, which depends on such expression; such function of *DOF5.3* is redundant with that of *DOF2.1*, *DOF3.2*, *DOF5.6*, and other *DOF* genes. In the future, it will be interesting to understand which of the remaining 32 *DOF* genes in Arabidopsis (Yanagisawa, 2002) act redundantly with *DOF2.1*, *DOF3.2*, *DOF5.3,* and *DOF5.6* to control *SHR* expression and function at early stages of vein development; nevertheless, our results already provide long-awaited molecular details of how veins act as source of positional signals that specify fate of adjacent cells—positional signals which are so critical for the development of multicellular organisms such as plants, the cells of which, unlike those of animals, are unable to migrate.

5.3 Materials and Methods

5.3.1 Plants

Origin and nature of lines, genotyping strategies, and oligonucleotide sequences are in Tables 5.1–5.3. Unless otherwise stated, seeds were sterilized and germinated, and plants were grown and transformed as in (Sawchuk et al., 2008).

Table 5.1. Origin and Nature of Lines

Line	Origin/Nature
Q0990::erGFP	ABRC (CS9217); (Haseloff, 1999)
ATHB8::nYFP	(Sawchuk et al., 2007)
SHR::nYFP	(Gardiner et al., 2011) (Chapter 4)
SHR::nRFP	(Gardiner et al., 2011) (Chapter 4)
SHR::SHR:YFP	(Gardiner et al., 2011) (Chapter 4); rescues the bundle sheath (Fig. 5.3) defects of *shr*
SCL3::erGFP	(Ckurshumova et al., 2009)
SCR::nCFP	Transcriptional fusion of *SCR* (AT3G54220; -2165 to -1; primers: 'SCR-F' and 'SCR-R' to the sequence encoding ECFP-Nuc (Clontech Laboratories, Mountain View, CA)
SCR::nYFP	(Heidstra et al., 2004)
shr	ABRC (SALK_002744; *shr-6*); (Alonso et al., 2003; Dhondt et al., 2010)
[-2022, -16]::nYFP	Transcriptional fusion of *SHR* (AT4G37650; -2022 to -16; primers: 'SHR-2.0' and 'SHR-R') to the sequence encoding HTA6:EYFP (Zhang et al., 2005)
[-1515, -16]::nYFP	Transcriptional fusion of *SHR* (AT4G37650; -1515 to -16; primers: 'SHR-1.5' and 'SHR-R') to the sequence encoding HTA6:EYFP (Zhang et al., 2005)
[-1055, -16]::nYFP	Transcriptional fusion of *SHR* (AT4G37650; -1055 to -16; primers: 'SHR-1.0' and 'SHR-R') to the sequence encoding HTA6:EYFP (Zhang et al., 2005)

[-453, -16]::nYFP	Transcriptional fusion of *SHR* (AT4G37650; -453 to -16; primers: 'SHR-0.5' and 'SHR-R') to the sequence encoding HTA6:EYFP (Zhang et al., 2005)
[-1967, -16]::nYFP	Transcriptional fusion of *SHR* (AT4G37650; -1967 to -16; primers: '7AA' and 'SHR-R') to the sequence encoding HTA6:EYFP (Zhang et al., 2005)
[-1776, -16]::nYFP	Transcriptional fusion of *SHR* (AT4G37650; -1776 to -16; primers: '7AB' and 'SHR-R') to the sequence encoding HTA6:EYFP (Zhang et al., 2005)
[-1742, -16]::nYFP	Transcriptional fusion of *SHR* (AT4G37650; -1742 to -16; primers: '7AC' and 'SHR-R') to the sequence encoding HTA6:EYFP (Zhang et al., 2005)
[-1712, -16]::nYFP	Transcriptional fusion of *SHR* (AT4G37650; -1712 to -16; primers: '7AD' and 'SHR-R') to the sequence encoding HTA6:EYFP (Zhang et al., 2005)
[-1704, -16]::nYFP	Transcriptional fusion of *SHR* (AT4G37650; -1704 to -16; primers: '7M' and 'SHR-R') to the sequence encoding HTA6:EYFP (Zhang et al., 2005)
[-1638, -16]::nYFP	Transcriptional fusion of *SHR* (AT4G37650; -1638 to -16; primers: '7R' and 'SHR-R') to the sequence encoding HTA6:EYFP (Zhang et al., 2005)
[-1638, -1]::SHR:YFP	Translational fusion of *SHR* (AT4G37650; -1638 to +1586; primers: '7R SALI F' and

	'SHRgDNA BamHI Rev2') to a sequence encoding EYFP (primers: 'ECFP AflII F' and 'ECFP AflII R'); rescues the bundle-sheath defects of *shr* (Fig. 5.3)
[-1515, -1]::SHR:YFP	Translational fusion of *SHR* (AT4G37650; -1515 to +1586; primers: '7b SALI F' and 'SHRgDNA BamHI Rev2') to a sequence encoding EYFP (primers: 'ECFP AflII F' and 'ECFP AflII R'); fails to rescue the bundle-sheath defects of *shr* (Fig. 5.3)
[-1588, -16]::nYFP	Transcriptional fusion of *SHR* (AT4G37650; -1588 to -16; primers: '7S' and 'SHR-R') to the sequence encoding HTA6:EYFP (Zhang et al., 2005)
[-1552, -16]::nYFP	Transcriptional fusion of *SHR* (AT4G37650; -1552 to -16; primers: '7T' and 'SHR-R') to the sequence encoding HTA6:EYFP (Zhang et al., 2005)
mDBS1::nYFP	Transcriptional fusion of *SHR* (AT4G37650; -1638 to -16; primers: 'RmDOF FWD', 'Nested RmDOF FWD' and 'SHR-R') to the sequence encoding HTA6:EYFP (Zhang et al., 2005)
mDBS2,3::nYFP	Transcriptional fusion of *SHR* (AT4G37650; -1588 to -16; primers: 'SmDof Fwd', 'Nested SmDof Fwd' and 'SHR-R') to the sequence encoding HTA6:EYFP (Zhang et al., 2005)
mDBS4::nYFP	Transcriptional fusion of *SHR* (AT4G37650; -1552 to -16; primers: '7T mDOF','7T mDOF nested' and 'SHR-R') to the sequence

	encoding HTA6:EYFP (Zhang et al., 2005)
UBQ10::DOFi	Transcriptional fusion of *UBQ10* (AT4G05320; -1516 to -1; primers: 'UBQ10 HindIII Forw' and 'UBQ10 SmaI Rev') to a sequence encoding an RNA interference construct targeting the DOF DNA-binding domain of *DOF5.3* (AT5G60200; +265 to +418; primers: 'DOF RNAi EcoRI FWD' and 'DOF RNAi BamHI REV'; 'DOF RNAi HindIII FWD' and 'DOF RNAi KPNI REV')
dof5.3	ABRC (SALK_201987); (Alonso et al., 2003)
DOF5.3::DOF5.3:EAR	Translational fusion of DOF5.3 (AT5G60200; -3082 to +871; primers: 'DOF5.3 XhoI F' and 'DOF5.3 KpnI R') to the sequence encoding the EAR portable repressor domain (Hiratsu et al., 2003) (oligonucleotides: 'EAR KpnI SmaI PstI F' and 'EAR KpnI SmaI PstI R')
DOF5.3::erGFP	(Lee et al., 2006)
DOF5.3::DOF5.3:YFP	Translational fusion of *DOF5.3* (AT5G60200; -3082 to +871; primers: 'DOF5.3 XhoI F' and 'DOF5.3 KpnI R') to a sequence encoding EYFP (primers: 'ECFP AflII F' and 'ECFP AflII R')
UBQ10::DOF3.2i	Transcriptional fusion of *UBQ10* (AT4G05320; -1516 to –1; primers: 'UBQ10 HindIII Forw' and 'UBQ10 SmaI Rev') to a sequence encoding an RNA interference construct targeting *DOF3.2* (AT3G45610; +484 to +813 primers: '3.2 RNAi EcoRI FWD' and '3.2 RNAi BamHI REV'; '3.2

	RNAi HindIII FWD' and '3.2 RNAi KPNI REV')
eal1	(Morita et al., 2007)
dof2.1	NASC (N363677); (Kleinboelting et al., 2012)
dof5.6	NASC (N444662); (Kleinboelting et al., 2012)

[1]Unless otherwise indicated, all coordinates are relative to the translational start-site.

Table 5.2. Genotyping Strategies

Line	Strategy
shr	*SHR*: 'SALK_002744 FWD' and 'SALK_002744 REV'; *shr*: 'SALK_002744 REV' and 'LBb1.3'
dof5.3	*DOF5.3*: 'LP StongDOF5.3SALK_201987' and 'RP StongDOF5.3SALK_201987'; *dof5.3*: 'RP StongDOF5.3SALK_201987' and 'LBa1'
eal1	*EAL1*: 'SHR671F' and 'SHR936R'; *eal1*: 'eal1671F' and 'SHR936R' confirmed by the presence of defects in shoot agravitropism defects
dof2.1	*DOF2.1*: 'genespecific DOF2.1 FWD' and 'genespecific DOF2.1 REV'; *dof2.1*: 'genespecific DOF2.1 FWD' and 'o8409'
dof5.6	*DOF5.6*: 'DOF5.6 LP' and 'DOF5.6 RP' *dof5.6*: 'DOF5.6 RP' and 'o8409'

Table 5.3. Oligonucleotide Sequences

Name	Sequence (5' to 3')
SCR-F	GGGGACAAGTTTGTACAAAAAAGCAGGCTTAGATTGT GATCCTCTGCAAC
SCR-R	GGGGACCACTTTGTACAAGAAAGCTGGGTGGAGATTG AAGGGTTGTTGG
SHR-R	GGGGACCACTTTGTACAAGAAAGCTGGGTAATAAGAA AATGAATAGAAGAAAGGGAGACC
SHR HINDIII F	GAGAAGCTTGACAAAGAAGCAGAGCGTGG
SHR SALI R	TGGGTCGAC TTAATGAATAAGAAAATGAATAGAAGA AAGGG
SHR-SALI FORW2 F	AAAGTCGACCGAAGAAAGGGACAAAGAAGC
SHRgDNA BamHI Rev2	ATAGGATCCGTAGGTCGCCACGCACTAG
ECFP AflII F	TTACTTAAGGTGAGCAAGGGCGACGAGC
ECFP AflII R	AGACTTAAGATTGTACAGCTCGTCCATGCC
SALK_002744 FWD	AAATCCACCAAACCCATTCTC
SALK_002744 REV	ATCGTTGACAAACTTGTTGGC
LBb1.3	ATTTTGCCGATTTCGGAAC
SHR-2.0	GGGGACAAGTTTGTACAAAAAAGCAGGCTGGTTAATT AGAGGTTCGCATATAC
SHR-1.5	GGGGACAAGTTTGTACAAAAAAGCAGGCTCACTCACA CCTATGAACATTCTC
SHR-1.0	GGGGACAAGTTTGTACAAAAAAGCAGGCTGATTTAGG ATGCGTAAAGAGTC
SHR-0.5	GGGGACAAGTTTGTACAAAAAAGCAGGCTCTCAGTTA GCTATAGGGTTG
7AA	GGGGACAAGTTTGTACAAAAAAGCAGGCTCACACACA CCAAAAAAGTGGG

7AB	GGGGACAAGTTTGTACAAAAAAGCAGGCTCTGAGATA ATAATTACACACATTG
7AC	GGGGACAAGTTTGTACAAAAAAGCAGGCTGGTAAGAG AATATGACACATTGG
7AD	GGGGACAAGTTTGTACAAAAAAGCAGGCTCTTACGGG TAAATGTGAAG
7M	GGGGACAAGTTTGTACAAAAAAGCAGGCTTAAATGTG AAGAAAAAAAAATAG
7R	GGGGACAAGTTTGTACAAAAAAGCAGGCTGAAGAAG AGAGAAAAGGG
7R SALI F	GGGGTCGACGAAGAAGAGAGAAAAGGG
7b SALI F	AAAGTCGACCACTCACACCTATGAACATTCTC
7S	GGGGACAAGTTTGTACAAAAAAGCAGGCTGAGGCAA AGGCAAATGTGGAG
7T	GGGGACAAGTTTGTACAAAAAAGCAGGCTTGCACGCC GTCAGCTTTTC
RmDOF FWD	GGGGACAAGTTTGTACAAAAAAGCAGGCTGAAGAAGA GAGAAGAAGG
Nested RmDOF FWD	GTACAAAAAAGCAGGCTGAAGAAGAGAGAAGAAGGA AAAATAGTG
SmDof Fwd	GGGGACAAGTTTGTACAAAAAAGCAGGCTGAGGCAG AAGCAAATGTGGAGTTC
Nested SmDof Fwd	GTACAAAAAAGCAGGCTGAGGCAGAAGCAAATGTGG AGTTCTGATGATGTTG
7T mDOF	GGGGACAAGTTTGTACAAAAAAGCAGGCTTGCACGCC GTCAGTTCTTC
7T mDOF nested	GTACAAAAAAGCAGGCTTGCACGCCGTCAGTTCTTCTC CACGCC
UBQ10 HindIII Forw	CTCAAGCTTTCCCATGTTTCTCGTCTGTC

UBQ10 SmaI Rev	CGACCCGGGCTGTTAATCAGAAAAACTCAG
DOF RNAi EcoRI FWD	TCAGAATTCCAGGTGTCCACGTTGCGACTC
DOF RNAi BamHI REV	TTGGGATCCTTTCCGGCAGCCTCCACCCACG
DOF RNAi HindIII FWD	TCAAAGCTTCAGGTGTCCACGTTGCGACTC
DOF RNAi KPNI REV	TCTGGTACCTTTCCGGCAGCCTCCACCCACG
LP StongDOF5.3SALK_201987	ACAAAGCAAGAGAAGCAATGG
RP StongDOF5.3SALK_201987	GTTCATTCCAGAAGCCATTTG
LBa1	TGGTTCACGTAGTGGGCCATCG
DOF5.3 XhoI F	TATCTCGAGCCGAATTAGCATTAGGTCGAATAGG
DOF5.3 KpnI R	GCCGGTACCCATTAAAGCACCAGAATTAATGTAGTTC
EAR KpnI SmaI PstI F	CCTAGATCTGGATCTAGAACTCCGTTTGGGTTTCGCTT AACCCGGGCTGCA
EAR KpnI SmaI PstI R	GCCCGGGTTAAGCGAAACCCAAACGGAGTTCTAGATC CAGATCTAGGGTAC
3.2 RNAi EcoRI FWD	TTGGAATTCGCACCAGTATTAATGTAGTTGACAGT
3.2 RNAi BamHI REV	TTGGGATCCGATGGAGCTTGGGTTAGCATA
3.2 RNAi HindIII FWD	TTGAAGCTTGCACCAGTATTAATGTAGTTGACAGT
3.2 RNAi KPNI REV	TTA GGTACCGATGGAGCTTGGGTTAGCATA
SHR671F	CTGTACTAAAGTTCCAAGAA
SHR936R	TCCGATCTCTTTCATCATCC
eal1671F	CTGTACTAAAGTTCCAAGTT
genespecific DOF2.1 FWD	CGCCACGTACAACTAATCCG
genespecific DOF2.1 REV	CTCGTTTCCTTCCAAAGACATC
o8409	ATATTGACCATCATACTCATTGC
DOF5.6 LP	CTCAACCACACGAACACACAC
DOF5.6 RP	GTTAGGAATCCGAGTCATCAGG

5.3.2 Imaging

Developing leaves were mounted and imaged as in (Sawchuk et al., 2013); imaging parameters are in Table 5.4. Mature leaves were fixed in 3:1 ethanol:acetic acid, rehydrated in 70% ethanol and water, cleared briefly (few seconds to few minutes) in 0.4 M sodium hydroxide, washed in water, and mounted in 50% glycerol. Mounted leaves were imaged as in (Odat et al., 2014) (Chapter 2). Image brightness and contrast were adjusted by linear stretching of the histogram with ImageJ (Schneider et al., 2012). Images were cropped with Photoshop (Adobe Systems Inc. San Jose, CA) and assembled into figures with Canvas (ACD Systems International Inc. Victoria, Canada).

5.3.3 Chromatin Immunoprecipitation

Chromatin immunoprecipitation was performed as in (Donner et al., 2009) on 4-day-old DOF5.3::DOF5.3:YFP and MP::nYFP (Sawchuk et al., 2013) seedlings grown in half-strength Murashige and Skoog salts (Caisson Laboratories, North Logan, UT), 15 g l^{-1} sucrose (BioShop Canada Inc., Burlington, Canada), 0.5 g l^{-1} MES (BioShop Canada Inc.), pH 5.7, at 25°C under continuous light (~60 μmol m^{-2} s^{-1}) on a rotary shaker at 50 rpm. To control for binding of nuclear YFP to chromatin, levels of *SHR* (primers: 'SHR CHIP FWD Primer' and 'SHR CHIP REV Primer') and *UBQ10* (primers: 'jlg6UBQ10CHIP FWD' and 'jlg6UBQ10CHIP REV') promoter regions co-immunoprecipitated with YFP from DOF5.3::DOF5.3:YFP lysates were normalized to those from MP::nYFP lysates.

Table 5.4. **Imaging Parameters**

A. Single-fluorophore lines

Fluorophore	**Laser**	**Wavelength (nm)**	**Main dichroic beam splitter**	**First secondary dichroic beam splitter**	**Secondary dichroic beam splitter**	**Emission filter (detector)**
GFP	AR	488	HFT 405/488/594	NFT 545	NFT 490	BP505-530 (PMT3)
YFP	AR	514	HFT 405/514/594	NFT 595	NFT 515	BP 520-555 IR (PMT3)

B. Multi-fluorophore lines

Fluorophore		**Laser**	**Wavelength (nm)**	**Main dichroic beam splitter**	**First secondary dichroic beam splitter**	**Secondary dichroic beam splitter**	**Emission filter (detector)**
GFP/YFP	GFP	AR	458	HFT 458/514	MIRROR	NFT545	BP 475-525 (PMT2)
	YFP	AR	514	HFT 458/514	MIRROR	NFT 515	BP 560-615 IR (PMT3)

RFP/YFP	RFP	DI	543	HFT 458/543	MIRROR	MIRROR	BP 50-555 IR (PMT3)
	YFP	AR	514	HFT 458/543	MIRROR	NFT 545	BP 575-620 IR (PMT2)
CFP/YFP	CFP	DI	458	HFT 458/514	NFT 595	NFT 515	BP 480-520 (PMT2)
	YFP	AR	514	HFT 458/514	NFT 595	NFT 490	BP 520-555 IR (PMT3)

CHAPTER 6: GENERAL DISCUSSION

6.1 Conclusion Summary

Available evidence suggests that activation of the Class III *HOMEODOMAIN-LEUCINE ZIPPER* (*HD-ZIP III*) gene *ARABIDOPSIS THALIANA HOMEOBOX8* (*ATHB8*) expression in files of isodiametric, polygonal, ground cells of the leaf—"preprocambial cells" (Kang and Dengler, 2004; Sawchuk et al., 2007; Scarpella et al., 2004)—is the first indicator of the final vascular pattern of the leaf (Alonso-Peral et al., 2006; Carland and Nelson, 2004; Carland et al., 2010; Ckurshumova et al., 2011; Cnops et al., 2006; Gardiner et al., 2010, 2011; Garrett et al., 2012; Hou et al., 2010; Kang and Dengler, 2004; Koizumi et al., 2000; Krogan et al., 2012; Petricka and Nelson, 2007; Pineau et al., 2005; Pullen et al., 2010; Robles et al., 2010; Sawchuk et al., 2007; Scarpella et al., 2004; Tsugeki et al., 2009) (Chapter 4), and therefore that identification of the regulatory elements required for preprocambial expression of *ATHB8* and other genes the expression of which is activated in preprocambial cells, and identification of the transcription factors binding to these elements should identify transcriptional controls of vascular strand development; the scope of my Ph.D. thesis was to identify such controls by understanding how preprocambial gene expression is transcriptionally activated.

My results suggest that *ATHB8* preprocambial expression is activated by a MONOPTEROS (MP)-dependent incoherent feed-forward loop (Chapter 3): MP activates *ATHB8* expression by binding to a low-affinity MP-binding site in the *ATHB8* promoter (Donner et al., 2009), but MP also activates expression of *INDOLE-3-ACETIC ACID INDUCIBLE12*/*BODENLOS (BDL)* (Krogan et al., 2014; Lau et al., 2011), which inhibits MP-mediated activation of *ATHB8* expression.

My results also suggest that expression of *SHORT-ROOT* (*SHR*), which encodes a GIBBERELLIC ACID INSENSITIVE, REPRESSOR OF *gibberellic acid1-3,* AND SCARECROW (GRAS) transcription factor, is activated simultaneously with that of *ATHB8* in

preprocambial cells, that activation of *SHR* preprocambial expression is required for SHR-mediated differentiation of the bundle-sheath—the cell layer adjacent to leaf vascular strands—and that both *SHR* preprocambial expression and *SHR* function in bundle-sheath differentiation are directly and positively controlled by a group of previously functionally uncharacterized transcription factors of the DNA-BINDING WITH ONE FINGER (DOF) family (Gardiner et al., 2011) (Chapter 4; Chapter 5).

In the Discussion section of the respective chapters, I provided an account of how I reached these conclusions from the experimental data, how these conclusions could be integrated with one another and with those in studies of others to advance our understanding of vascular development, and what the implications of such conclusions are for aspects of plant development beyond the formation of leaf vascular strand. Here I instead wish to propose and discuss two non-mutually exclusive hypotheses that attempt to integrate the transcriptional control of *SHR* preprocambial expression with that of *ATHB8* preprocambial expression. These hypotheses should be understood as an attempt to develop a conceptual framework to guide future experimentation and not as an exhaustive mechanistic account.

6.1.1 Hypothesis I: MP Directly and Positively Controls *DOF5.3* Expression

I hypothesize that MP directly and positively controls *DOF5.3* expression. Three predictions made by this hypothesis are supported by available evidence.

i) MP indirectly and positively controls *SHR* expression and, therefore is required for bundle-sheath differentiation

mp lacks bundle-sheath cells (Przemeck et al., 1996).

ii) *DOF5.3* expression levels are reduced in *mp*

DOF5.3 transcripts are reduced in *mp* compared to wild type (Ckurshumova et al., 2011).

iii) Domains of MP protein expression and *DOF5.3* gene expression overlap

MP translational fusions and *DOF5.3* transcriptional fusions are expressed in similar regions of the leaf at similar stages (Donner et al., 2009; Gardiner et al., 2010; Krogan et al., 2012) (Chapter 5).

However, currently there is no evidence supporting three key predictions of this hypothesis.

i) MP binds the *DOF5.3* promoter

MP fails to bind any of the putative MP-binding sites in the 652-bp region upstream of the *DOF5.3* start codon (Schlereth et al., 2010); however, many more putative MP-binding sites exist in the *DOF5.3* promoter upstream of this region. I propose to test by chromatin immunoprecipitation whether MP binds these other putative MP-binding sites.

ii) Defects in bundle-sheath cells differentiation of *mp* are rescued by restoring *DOF5.3* expression in the *mp* background

I propose to test this prediction by expressing *DOF5.3* by an MP-independent vascular specific promoter in the *mp* background and by analyzing bundle-sheath cell shape in the resulting genotype.

iii) Defects in bundle-sheath cell differentiation caused by partial loss of *MP* function might be enhanced by additional loss of *DOF5.3* function

Because mutants that completely lack *MP* function also lack bundle-sheath cells (Przemeck et al., 1996), testing this prediction would require a mutant background in which *MP* function is only partially lost and in which such partial loss of *MP* function leads to weak defects in bundle-sheath cell differentiation—weak defects that could be enhanced to lead, for example, to loss of bundle-sheath cells.

The most readily available background for this test would be the weak *mp* allele *mp-11* (Odat et al., 2014) (Chapter 2). Should *mp-11* lack bundle-sheath cells, I propose to express by an MP-independent vascular-specific promoter an RNA interference construct targeting *MP;* different transgenic lines of this construct could be screened to identify a background with weak defects in bundle-sheath cell differentiation. Once a background with weak defects in bundle-sheath cell differentiation—be it *mp-11* or MPi—had been identified, it could be combined with the *dof5.3* mutation, and bundle-sheath cell shape could be analyzed in the resulting genotype.

6.1.2 Hypothesis II: SHR Directly and Positively Regulates *microRNA165/6* Expression in Leaf Veins

Mature vascular strands are composed of two vascular tissues that differentiate on opposite sides of a central procambium core: xylem, which transports water and minerals from the root, where they are absorbed from the soil, to the leaf; and phloem, which transports photosynthesis products from source organs, such as leaves, to sink organs, such as roots (Hopkins and Hüner, 2004).

The root vascular strand—the vascular cylinder—contains of two types of xylem: protoxylem, which is found at the periphery of the vascular cylinder and the elements of which have annular or spiral cell wall thickenings; and metaxylem, which is found in the center of the vascular cylinder and the elements of which have pitted secondary walls (Esau, 1965). Protoxylem and metaxylem are formed from the same procambial precursors, but protoxylem fate is specified earlier (Mahonen et al., 2000). The formation of protoxylem at the expense of metaxylem is promoted by the *micorRNA165/6 (miR165/6)*-mediated downregulation of expression of *HD-ZIP III* genes, including *ATHB8* (Carlsbecker et al., 2010).

In cells of the vascular cylinder, SHR directly binds the *miR165/6* promoter to activate *miR165*/*6* expression; in turn, *miR165*/*6* negatively regulates expression of *HD-ZIP III* genes, including *ATHB8*. Therefore, SHR indirectly and negatively regulates expression of *HD-ZIP III* genes, including *ATHB8*; I hypothesize that the same occurs in the leaf. One prediction made by this hypothesis fails to be supported by available evidence.

i) Loss-of-function mutants of *SHR* and gain-of-function mutants of *HD-ZIP III* genes, in which *HD-ZIP III* expression is insensitive to *miR165*/*6*-mediated downregulation, have similar leaf defects

In mature leaf vascular strands (“veins”), the that xylem is on the upper—adaxial— side while phloem is on the lower—abaxial—side, a vascular tissue arrangement referred to as “collateral” (Esau, 1965).

In veins of gain-of-function mutants of at least two of the five *HD-ZIP III* genes (for the other three *HD-ZIP III* genes this information is lacking), an outer layer of xylem surrounds a phloem core—a vascular tissue arrangement referred to as “amphivasal” (McConnell and Barton,

1998; Zhong and Ye, 2004); in *shr* veins however, the vascular tissue arrangement remains collateral, and bundle-sheath cells fail to differentiate at both the adaxial and abaxial sides of the vein (Cui et al., 2014).

Though this prediction fails to be supported by available evidence, currently there is no evidence supporting five key predictions of this hypothesis.

i) Domains of SHR protein expression and *miR165/6* gene expression overlap

To test this prediction, I propose to analyze expression of transcriptional fusions in each of the nine *miRNA165/6* genes in a background in a background expression a *SHR* translational fusion.

ii) *miRNA165/6* expression levels are reduced in *shr*

To test this prediction, I propose to quantify by qRT-PCR *miR165/6* transcript levels in *shr* and wild type. It is possible, however, that effects of *shr* on *miR165/6* expression levels are masked by functional redundancy between *SHR* and other *GRAS* genes. To test this possibility, I propose to quantify *miR165/6* expression levels in a transgenic line expressing SHR::SHR:EAR, which will act as a constitutive repressor of all targets of SHR, irrespective of redundancy.

iii) *HD-ZIP III* expression levels are increased in *shr*

To test this prediction, I propose to quantify by qRT-PCR *HD-ZIP III* transcript levels in *shr,* or—if redundancy is expected—SHR::SHR:EAR, and wild type.

iv) Vascular tissues are organized in collateral veins in *shr* (Cui et al., 2014); however, it is possible that SHR function in organization of leaf vascular tissues is redundant. In this case, vascular tissues should be organized in amphivasal veins in SHR::SHR:EAR, as in gain-of-function mutants of *HD-ZIPIII* genes

To test if this prediction, I propose to cross-section SHR::SHR:EAR leaves and analyze their vascular tissue organization by light microscopy.

v) Defects in vascular tissue organization in leaves of SHR::SHR:EAR are rescued by loss-of-function mutation of *HD-ZIP III* genes

To test this prediction, I propose to express SHR::SHR:EAR in loss-of-function mutants of *REV*—the only *HD-ZIP III* with non-redundant functions—and compare vascular tissue organization in leaves of this background with that of SHR::SHR:EAR.

6.2 Unresolved Questions and Future Approaches

Even though future experimental tests, including those suggested above, were to support one of both the hypothesis I proposed, many questions would remain to be addressed. For example, the same regulatory elements are often assumed to control the transcription of co-expressed genes (Niehrs and Pollet, 1999); however, *ATHB8* preprocambial expression depends on a single low-affinity MP-binding site (Donner and Scarpella, 2009) (Chapter 3), while *SHR* preprocambial expression depends on four high-affinity DOF-binding sites (Chapter 5). These findings seem to suggest that different regulatory elements control preprocambial gene expression, a redundancy in the regulatory code that has also been observed in animals [e.g., (Brown et al., 2007; Ramialison et al., 2012; Zinzen et al., 2009)]. Nevertheless, even though the molecular details are different, it is still possible that the regulatory logic of *ATHB8* and *SHR* preprocambial expression is the same: in both cases, narrow domains of gene expression (*ATHB8* or *SHR*) are activated by transcription factors expressed in broad domains (MP or DOF5.3), and incoherent feed-forward loops such as that which controls *ATHB8* preprocambial expression are the most frequent regulatory logic by which gene expression in narrow domains is activated in animals by broadly expressed transcription factors (Cotterell and Sharpe, 2010). However, it will be difficult—if not altogether impossible—to design informative experimental tests to probe whether the incoherent-feed-forward-loop logic that regulates *ATHB8* preprocambial expression also applies to *SHR* preprocambial expression, and to evaluate intuitively the results of those tests; a more precise formulation—a mathematical one, one that can be simulated computationally—will be necessary. Iterative cycles of computer simulations and experimentation will clarify whether the same the regulatory logic applies to both *ATHB8* and *SHR* preprocambial expression, thus taking us one step closer to understanding how regulation of gene expression in plants compares to that in animals—a key question to address if we are to understand how multicellular organisms develop and function.

LITERATURE CITED

Aloni, R. (1987). Differentiation of Vascular Tissues. Annu. Rev. Plant Physiol. *38*, 179–204.

Alonso, J.M., Stepanova, A.N., Leisse, T.J., Kim, C.J., Chen, H., Shinn, P., Stevenson, D.K., Zimmerman, J., Barajas, P., Cheuk, R., et al. (2003). Genome-wide insertional mutagenesis of Arabidopsis thaliana. Science *301*, 653–657.

Alonso-Peral, M.M., Candela, H., del Pozo, J.C., Martínez-Laborda, A., Ponce, M.R., and Micol, J.L. (2006). The HVE/CAND1 gene is required for the early patterning of leaf venation in Arabidopsis. Development *133*, 3755–3766.

Ariel, F.D., Manavella, P.A., Dezar, C.A., and Chan, R.L. (2007). The true story of the HD-Zip family. Trends Plant Sci. *12*, 419–426.

Ashe, H.L., and Briscoe, J. (2006). The interpretation of morphogen gradients. Development *133*, 385–394.

Bailey-Serres, J., Sorenson, R., and Juntawong, P. (2009). Getting the message across: cytoplasmic ribonucleoprotein complexes. Trends Plant Sci. *14*, 443–453.

Baima, S., Nobili, F., Sessa, G., Lucchetti, S., Ruberti, I., and Morelli, G. (1995). The expression of the Athb-8 homeobox gene is restricted to provascular cells in Arabidopsis thaliana. Development *121*, 4171–4182.

Baima, S., Possenti, M., Matteucci, A., Wisman, E., Altamura, M.M., Ruberti, I., and Morelli, G. (2001). The arabidopsis ATHB-8 HD-zip protein acts as a differentiation-promoting transcription factor of the vascular meristems. Plant Physiol. *126*, 643–655.

Baima, S., Forte, V., Possenti, M., Peñalosa, A., Leoni, G., Salvi, S., Felici, B., Ruberti, I., Morelli, G., Peñalosa, A., et al. (2014). Negative feedback regulation of auxin signaling by ATHB8/ACL5-BUD2 transcription module. Mol. Plant *7*, 1006–1025.

Band, L.R., Wells, D.M., Larrieu, A., Sun, J., Middleton, A.M., French, A.P., Brunoud, G., Sato, E.M., Wilson, M.H., Peťet, B., et al. (2012). Root gravitropism is regulated by a transient lateral auxin gradient controlled by a tipping-point mechanism. Proc. Natl. Acad. Sci. U. S. A. *109*, 4668–4673.

Band, L.R., Wells, D.M., Fozard, J. a, Ghetiu, T., French, A.P., Pound, M.P., Wilson, M.H., Yu, L., Li, W., Hijazi, H.I., et al. (2014). Systems analysis of auxin transport in the Arabidopsis root

apex. Plant Cell *26*, 862–875.
Beeckman, T., Przemeck, G.K.H., Stamatiou, G., Lau, R., Terryn, N., De Rycke, R., Inze, D., and Berleth, T. (2002). Genetic complexity of cellulose synthase A gene function in Arabidopsis embryogenesis. Plant Physiol. *130*, 1883–1893.
Belostotsky, D.A., and Sieburth, L.E. (2009). Kill the messenger: mRNA decay and plant development. Curr. Opin. Plant Biol. *12*, 96–102.
Benfey, P.N., Linstead, P.J., Roberts, K., Schiefelbein, J.W., Hauser, M.-T., and Aeschbacher, R.A. (1993). Root development in *Arabidopsis*: four mutants with dramatically altered root morphogenesis. Development *119*, 57–70.
Benková, E., Michniewicz, M., Sauer, M., Teichmann, T., Seifertová, D., Jürgens, G., and Friml, J. (2003). Local, Efflux-Dependent Auxin Gradients as a Common Module for Plant Organ Formation. Cell *115*, 591–602.
van den Berg, C., Willemsen, V., Hage, W., Weisbeek, P., and Scheres, B. (1995). Cell fate in the Arabidopsis root meristem determined by directional signalling. Nature *378*, 62–65.
van den Berg, C., Willemsen, V., Hendriks, G., Weisbeek, P., and Scheres, B. (1997). Short-range control of cell differentiation in the Arabidopsis root meristem. Nature *390*, 287–289.
Berleth, T., and Jürgens, G. (1993). The role of the monopteros gene in organising the basal body region of the Arabidopsis embryo. Development *118*, 575–587.
Berleth, T., and Sachs, T. (2001). Plant morphogenesis: long-distance coordination and local patterning. Curr. Opin. Plant Biol. *4*, 57–62.
Berleth, T., Mattsson, J., and Hardtke, C.S. (2000). Vascular continuity and auxin signals. Trends Plant Sci. *5*, 387–393.
Bezhani, S., Sherameti, I., Pfannschmidt, T., and Oelmüller, R. (2001). A repressor with similarities to prokaryotic and eukaryotic DNA helicases controls the assembly of the CAAT box binding complex at a photosynthesis gene promoter. J. Biol. Chem. *276*, 23785–23789.
Birkenbihl, R.P., Jach, G., Saedler, H., and Huijser, P. (2005). Functional dissection of the plant-specific SBP-domain: overlap of the DNA-binding and nuclear localization domains. J. Mol. Biol. *352*, 585–596.
Birnbaum, K., Shasha, D.E., Wang, J.Y., Jung, J.W., Lambert, G.M., Galbraith, D.W., and Benfey, P.N. (2003). A gene expression map of the Arabidopsis root. Science *302*, 1956–1960.

Bolle, C. (2004). The role of GRAS proteins in plant signal transduction and development. Planta *218*, 683–692.

Bolle, C., Koncz, C., and Chua, N.H. (2000). PAT1, a new member of the GRAS family, is involved in phytochrome A signal transduction. Genes Dev. *14*, 1269–1278.

Brady, S.M., Zhang, L., Megraw, M., Martinez, N.J., Jiang, E., Yi, C.S., Liu, W., Zeng, A., Taylor-Teeples, M., Kim, D., et al. (2011). A stele-enriched gene regulatory network in the Arabidopsis root. Mol. Syst. Biol. *7*, 459.

Brown, C.D., Johnson, D.S., and Sidow, A. (2007). Functional architecture and evolution of transcriptional elements that drive gene coexpression. Science *317*, 1557–1560.

Brunoud, G., Wells, D.M., Oliva, M., Larrieu, A., Mirabet, V., Burrow, A.H., Beeckman, T., Kepinski, S., Traas, J., Bennett, M.J., et al. (2012). A novel sensor to map auxin response and distribution at high spatio-temporal resolution. Nature *482*, 103–106.

Candela, H., Martínez-Laborda, A., and Luis Micol, J. (1999). Venation Pattern Formation in Arabidopsis thaliana Vegetative Leaves. Dev. Biol. *205*, 205–216.

Caño-Delgado, A., Lee, J.-Y., and Demura, T. (2010). Regulatory mechanisms for specification and patterning of plant vascular tissues. Annu. Rev. Cell Dev. Biol. *26*, 605–637.

Capron, A., Chatfi, S., Provart, N., Berleth, T., and Chatfield, S. (2009). Embryogenesis: Pattern Formation from a Single Cell. Arabidopsis Book *7*, e0126. doi:10.1199/tab.0126.

Carland, F.M., and Nelson, T. (2004). Cotyledon vascular pattern2-mediated inositol (1,4,5) triphosphate signal transduction is essential for closed venation patterns of Arabidopsis foliar organs. Plant Cell *16*, 1263–1275.

Carland, F.M., and Nelson, T. (2009). CVP2- and CVL1-mediated phosphoinositide signaling as a regulator of the ARF GAP SFC/VAN3 in establishment of foliar vein patterns. Plant J. *59*, 895–907.

Carland, F.M., Fujioka, S., and Nelson, T. (2010). The sterol methyltransferases SMT1, SMT2, and SMT3 influence Arabidopsis development through nonbrassinosteroid products. Plant Physiol. *153*, 741–756.

Carlsbecker, A., Lee, J.-Y., Roberts, C.J., Dettmer, J., Lehesranta, S., Zhou, J., Lindgren, O., Moreno-Risueno, M. a, Vatén, A., Thitamadee, S., et al. (2010). Cell signalling by microRNA165/6 directs gene dose-dependent root cell fate. Nature *465*, 316–321.

Chapman, E.J., and Estelle, M. (2009). Mechanism of auxin-regulated gene expression in plants. Annu. Rev. Genet. *43*, 265–285.
Cheng, Y., Dai, X., and Zhao, Y. (2006). Auxin biosynthesis by the YUCCA flavin monooxygenases controls the formation of floral organs and vascular tissues in Arabidopsis. Genes Dev. *20*, 1790–1799.
Chomczynski, P., and Sacchi, N. (1987). Single-Step Method of RNA Isolation by Acid Guanidinium Thiocyanate-Phenol-Chloroform Extraction. Anal. Biochem. *162*, 156–159.
Ckurshumova, W., Koizumi, K., Chatfield, S.P., Sanchez-Buelna, S.U., Gangaeva, A.E., McKenzie, R., and Berleth, T. (2009). Tissue-specific GAL4 expression patterns as a resource enabling targeted gene expression, cell type-specific transcript profiling and gene function characterization in the arabidopsis vascular system. Plant Cell Physiol. *50*, 141–150.
Ckurshumova, W., Scarpella, E., Goldstein, R.S., and Berleth, T. (2011). Double-filter identification of vascular-expressed genes using Arabidopsis plants with vascular hypertrophy and hypotrophy. Plant Sci. *181*, 96–104.
Clouse, S.D., and Sasse, J.M. (1998). BRASSINOSTEROIDS: Essential Regulators of Plant Growth and Development. Annu. Rev. Plant Physiol. Plant Mol. Biol. *49*, 427–451.
Cnops, G., Neyt, P., Raes, J., Petrarulo, M., Nelissen, H., Malenica, N., Luschnig, C., Tietz, O., Ditengou, F., Palme, K., et al. (2006). The TORNADO1 and TORNADO2 genes function in several patterning processes during early leaf development in Arabidopsis thaliana. Plant Cell *18*, 852–866.
Cole, M., Chandler, J., Weijers, D., Jacobs, B., Comelli, P., and Werr, W. (2009). DORNROSCHEN is a direct target of the auxin response factor MONOPTEROS in the Arabidopsis embryo. Development *136*, 1643–1651.
Cotterell, J., and Sharpe, J. (2010). An atlas of gene regulatory networks reveals multiple three-gene mechanisms for interpreting morphogen gradients. Mol. Syst. Biol. *6*, 425.
Cui, H., Kong, D., Liu, X., and Hao, Y. (2014). SCARECROW, SCR-LIKE 23 and SHORT-ROOT control bundle sheath cell fate and function in Arabidopsis thaliana. Plant J. *78*, 319–327.
Demandolx, D., and Davoust, J. (1997). Multicolour analysis and local image correlation in confocal microscopy. J. Microsc. *185*, 21–36.
Dengler, N., and Kang, J. (2001). Vascular patterning and leaf shape. Curr. Opin. Plant Biol. *4*,

50–56.
Dettmer, J., Elo, A., and Helariutta, Y. (2009). Hormone interactions during vascular development. Plant Mol. Biol. *69*, 347–360.
Dharmasiri, N., Dharmasiri, S., Weijers, D., Lechner, E., Yamada, M., Hobbie, L., Ehrismann, J.S., Jürgens, G., and Estelle, M. (2005). Plant development is regulated by a family of auxin receptor F box proteins. Dev. Cell *9*, 109–119.
Dhondt, S., Coppens, F., Winter, F. De, Swarup, K., Merks, R.M.H., Inze, D., Bennett, M.J., and Beemster, G.T.S. (2010). SHORT-ROOT and SCARECROW Regulate Leaf Growth in Arabidopsis by Stimulating S-Phase Progression of the Cell Cycle. Plant Physiol. *154*, 1183–1195.
Dill, A., and Sun, T.P. (2001). Synergistic derepression of gibberellin signaling by removing RGA and GAI function in Arabidopsis thaliana. Genetics *159*, 777–785.
Donner, T.J., and Scarpella, E. (2009). Auxin-transport-dependent leaf vein formation. Botany *87*, 678–684.
Donner, T.J., and Scarpella, E. (2013). Transcriptional control of early vein expression of CYCA2; 1 and CYCA2;4 in Arabidopsis leaves. Mech. Dev. *130*, 14–24.
Donner, T.J., Sherr, I., and Scarpella, E. (2009). Regulation of preprocambial cell state acquisition by auxin signaling in Arabidopsis leaves. Development *136*, 3235–3246.
Emery, J.F., Floyd, S.K., Alvarez, J., Eshed, Y., Hawker, N.P., Izhaki, A., Baum, S.F., and Bowman, J.L. (2003). Radial Patterning of Arabidopsis Shoots by Class III HD-ZIP and KANADI Genes. Curr. Biol. *13*, 1768–1774.
Esau, K. (1943). Origin and development of primary vascular tissues in plants. Bot. Rev. *9*, 125–206.
Esau, K. (1965). Plant anatomy (New York, NY, USA: John Wiley).
Eshed, Y., Baum, S.F., and Bowman, J.L. (2001). Establishment of polarity in lateral organs of plants. Curr. Biol. *11*, 1251–1260.
Esteve-Bruna, D., Pérez-Pérez, J.M., Ponce, M.R., and Micol, J.L. (2013). incurvata13, a novel allele of AUXIN RESISTANT6, reveals a specific role for auxin and the SCF complex in Arabidopsis embryogenesis, vascular specification, and leaf flatness. Plant Physiol. *161*, 1303–1320.

Etchells, J.P., Provost, C.M., Mishra, L., and Turner, S.R. (2013). WOX4 and WOX14 act downstream of the PXY receptor kinase to regulate plant vascular proliferation independently of any role in vascular organisation. Development *140*, 2224–2234.

Fode, B., Siemsen, T., Thurow, C., Weigel, R., and Gatz, C. (2008). The Arabidopsis GRAS protein SCL14 interacts with class II TGA transcription factors and is essential for the activation of stress-inducible promoters. Plant Cell *20*, 3122–3135.

Foster, A. (1952). Foliar venation in angiosperms from an ontogenetic standpoint. Am. J. Bot. *39*, 752–766.

Friml, J., Vieten, A., Sauer, M., Weijers, D., Schwarz, H., Hamann, T., Offringa, R., and Jürgens, G. (2003). Efflux-dependent auxin gradients establish the apical-basal axis of Arabidopsis. Nature *426*, 147–153.

Fu, X., Richards, D.E., Fleck, B., Xie, D., Burton, N., and Harberd, N.P. (2004). The Arabidopsis mutant sleepy1 gar2-1 protein promotes plant growth by increasing the affinity of the SCF SLY1 E3 ubiquitin ligase for DELLA protein substrates. Plant Cell *16*, 1406–1418.

Fukaki, H., Wysocka-Diller, J., Kato, T., Fujisawa, H., Benfey, P.N., and Tasaka, M. (1998). Genetic evidence that the endodermis is essential for shoot gravitropism in Arabidopsis thaliana. Plant J. *14*, 425–430.

Fukuda, H. (2004). Signals that control plant vascular cell differentiation. Nat. Rev. Mol. Cell Biol. *5*, 379–391.

Furuta, K.M., Hellmann, E., and Helariutta, Y. (2014). Molecular Control of Cell Specification and Cell Differentiation During Procambial Development. Annu. Rev. Plant Biol. *65*, 607–638.

Gallagher, K.L., Paquette, A.J., Nakajima, K., and Benfey, P.N. (2004). Mechanisms Regulating SHORT-ROOT Intercellular Movement. Curr. Biol. *14*, 1847–1851.

Gardiner, J., Sherr, I., and Scarpella, E. (2010). Expression of DOF genes identifies early stages of vascular development in Arabidopsis leaves. Int. J. Dev. Biol. *54*, 1389–1396.

Gardiner, J., Donner, T.J., and Scarpella, E. (2011). Simultaneous activation of SHR and ATHB8 expression defines switch to preprocambial cell state in Arabidopsis leaf development. Dev. Dyn. *240*, 261–270.

Garrett, J.J.T., Meents, M.J., Blackshaw, M.T., Blackshaw, L.C., Hou, H., Styranko, D.M., Kohalmi, S.E., and Schultz, E. a (2012). A novel, semi-dominant allele of MONOPTEROS

provides insight into leaf initiation and vein pattern formation. Planta *236*, 297–312.
Gong, X., Flores-Vergara, M.A., Hong, J.H., Chu, H., Lim, J., Franks, R.G., Liu, Z., and Xu, J. (2016). SEUSS integrates gibberellin signaling with transcriptional inputs from the SHR-SCR-SCL3 module to regulate middle cortex formation in the Arabidopsis root. Plant Physiol. *170*, 1675–1683.
Gordon, S.P., Heisler, M.G., Reddy, G.V., Ohno, C., Das, P., and Meyerowitz, E.M. (2007). Pattern formation during de novo assembly of the Arabidopsis shoot meristem. Development *134*, 3539–3548.
Gray, W.M., Pozo, J.C., Walker, L., Hobbie, L., Risseeuw, E., Banks, T., Crosby, W.L., Yang, M., Ma, H., and Estelle, M. (1999). Identification of an SCF ubiquitin – ligase complex required for auxin response in Arabidopsis thaliana. Genes Dev. *13*, 1678–1691.
Gray, W.M., Kepinski, S., Rouse, D., Leyser, O., and Estelle, M. (2001). Auxin regulates SCF(TIR1)-dependent degradation of AUX/IAA proteins. Nature *414*, 271–276.
Greb, T., Clarenz, O., Schafer, E., Muller, D., Herrero, R., Schmitz, G., and Theres, K. (2003). Molecular analysis of the LATERAL SUPPRESSOR gene in Arabidopsis reveals a conserved control mechanism for axillary meristem formation. Genes Dev. 1175–1187.
Guilfoyle, T.J., and Hagen, G. (2007). Auxin Response Factors. Curr. Opin. Plant Biol. *10*, 453–460.
Guilfoyle, T.J., and Hagen, G. (2012). Getting a grasp on domain III/IV responsible for Auxin Response Factor-IAA protein interactions. Plant Sci. *190*, 82–88.
Hamann, T., Mayer, U., and Jürgens, G. (1999). The auxin-insensitive bodenlos mutation affects primary root formation and apical-basal patterning in the Arabidopsis embryo. Development *126*, 1387–1395.
Hamann, T., Benkova, E., Bäurle, I., Kientz, M., and Jürgens, G. (2002). The Arabidopsis BODENLOS gene encodes an auxin response protein inhibiting MONOPTEROS-mediated embryo patterning. Genes Dev. *16*, 1610–1615.
Hardtke, C.S., and Berleth, T. (1998). The Arabidopsis gene MONOPTEROS encodes a transcription factor mediating embryo axis formation and vascular development. EMBO J. *17*, 1405–1411.
Hardtke, C.S., Ckurshumova, W., Vidaurre, D.P., Singh, S.A., Stamatiou, G., Tiwari, S.B.,

Hagen, G., Guilfoyle, T.J., and Berleth, T. (2004). Overlapping and non-redundant functions of the Arabidopsis auxin response factors MONOPTEROS and NONPHOTOTROPIC HYPOCOTYL 4. Development *131*, 1089–1100.

Haseloff, J. (1999). GFP variants for multispectral imaging of living cells. Methods Cell Biol. *58*, 139–151.

Heidstra, R., Welch, D., and Scheres, B. (2004). Mosaic analyses using marked activation and deletion clones dissect Arabidopsis SCARECROW action in asymmetric cell division. Genes Dev. *18*, 1964–1969.

Helariutta, Y., Fukaki, H., Wysocka-Diller, J., Nakajima, K., Jung, J., Sena, G., Hauser, M.T., and Benfey, P.N. (2000). The SHORT-ROOT gene controls radial patterning of the Arabidopsis root through radial signaling. Cell *101*, 555–567.

Hirakawa, Y., Kondo, Y., and Fukuda, H. (2010). TDIF peptide signaling regulates vascular stem cell proliferation via the WOX4 homeobox gene in Arabidopsis. Plant Cell *22*, 2618–2629.

Hiratsu, K., Matsui, K., Koyama, T., and Ohme-Takagi, M. (2003). Dominant repression of target genes by chimeric repressors that include the EAR motif, a repression domain, in Arabidopsis. Plant J. *34*, 733–739.

Hironaka, K. ichi, and Morishita, Y. (2012). Encoding and decoding of positional information in morphogen-dependent patterning. Curr. Opin. Genet. Dev. *22*, 553–561.

Hirota, A., Kato, T., Fukaki, H., Aida, M., and Tasaka, M. (2007). The auxin-regulated AP2/EREBP gene PUCHI is required for morphogenesis in the early lateral root primordium of Arabidopsis. Plant Cell *19*, 2156–2168.

Hirsch, S., and Oldroyd, G.E.D. (2009). GRAS-domain transcription factors that regulate plant development. Plant Signal. Behav. *4*, 698–700.

Hopkins, W.G., and Hüner, N.P.A. (2004). Introduction to Plant Physiology (Hoboken, NJ, USA: John Wiley & Sons, Inc.).

Hosoda, K., Imamura, A., Katoh, E., Hatta, T., Tachiki, M., Yamada, H., Mizuno, T., and Yamazaki, T. (2002). Molecular Structure of the GARP Family of Plant Myb-Related DNA Binding Motifs of the Arabidopsis Response Regulators. Plant Cell *14*, 2015–2029.

Hou, H., Erickson, J., Meservy, J., and Schultz, E.A. (2010). FORKED1 encodes a PH domain protein that is required for PIN1 localization in developing leaf veins. Plant J. *63*, 960–973.

Ilegems, M., Douet, V., Meylan-Bettex, M., Uyttewaal, M., Brand, L., Bowman, J.L., and Stieger, P.A. (2010). Interplay of auxin, KANADI and Class III HD-ZIP transcription factors in vascular tissue formation. Development *137*, 975–984.

Imamura, A., Hanaki, N., Nakamura, A., Suzuki, T., Taniguchi, M., Kiba, T., Ueguchi, C., Sugiyama, T., and Mizuno, T. (1999). Compilation and characterization of Arabidopsis thaliana response regulators implicated in His-Asp phosphorelay signal transduction. Plant Cell Physiol. *40*, 733–742.

Inoue, T., Higuchi, M., Hashimoto, Y., and Seki, M. (2001). Identification of CRE1 as a cytokinin receptor from Arabidopsis. Nature *409*, 1060–1063.

Dello Ioio, R., Linhares, F.S., Scacchi, E., Casamitjana-Martinez, E., Heidstra, R., Costantino, P., and Sabatini, S. (2007). Cytokinins Determine Arabidopsis Root-Meristem Size by Controlling Cell Differentiation. Curr. Biol. *17*, 678–682.

Ishida, K., Yamashino, T., Yokoyama, A., and Mizuno, T. (2008). Three type-B response regulators, ARR1, ARR10 and ARR12, play essential but redundant roles in cytokinin signal transduction throughout the life cycle of Arabidopsis thaliana. Plant Cell Physiol. *49*, 47–57.

Ito, T., Sakai, H., and Meyerowitz, E.M. (2003). Whorl-Specific Expression of the SUPERMAN Gene of Arabidopsis Is Mediated by cis Elements in the Transcribed Region. Curr. Biol. *13*, 1524–1530.

Jaeger, J., Irons, D., and Monk, N. (2008). Regulative feedback in pattern formation: towards a general relativistic theory of positional information. Development *135*, 3175–3183.

Jakoby, M., Weisshaar, B., Dröge-Laser, W., Vicente-Carbajosa, J., Tiedemann, J., Kroj, T., and Parcy, F. (2002). bZIP transcription factors in Arabidopsis. Trends Plant Sci. *7*, 106–111.

Jankovsky, J.P., Smith, L.G., and Nelson, T. (2001). Specification of bundle sheath cell fates during maize leaf development: roles of lineage and positional information evaluated through analysis of the tangled1 mutant. Development *128*, 2747–2753.

Ji, J., Strable, J., Shimizu, R., Koenig, D., Sinha, N., and Scanlon, M.J. (2010). Wox4 promotes procambial development. Plant Physiol. *152*, 1346–1356.

Kang, J., and Dengler, N. (2002). Cell cycling frequency and expression of the homeobox gene ATHB-8 during leaf vein development in Arabidopsis. Planta *216*, 212–219.

Kang, J., and Dengler, N. (2004). Vein pattern development in adult leaves of arabidopsis

thaliana. Int. J. Plant Sci. *165*, 231–242.
Kang, J., Mizukami, Y., Wang, H., Fowke, L., and Dengler, N.G. (2007). Modification of cell proliferation patterns alters leaf vein architecture in Arabidopsis thaliana. Planta *226*, 1207–1218.
Katayama, H., Iwamoto, K., Kariya, Y., Asakawa, T., Kan, T., Fukuda, H., and Ohashi-Ito, K. (2015). A negative feedback loop controlling bHLH complexes is involved in vascular cell division and differentiation in the root apical meristem. Curr. Biol. *25*, 3144–3150.
Kerstetter, R. a, Bollman, K., Taylor, R. a, Bomblies, K., and Poethig, R.S. (2001). KANADI regulates organ polarity in Arabidopsis. Nature *411*, 706–709.
Kidner, C., Sundaresan, V., Roberts, K., and Dolan, L. (2000). Clonal analysis of the Arabidopsis root confirms that position, not lineage, determines cell fate. Planta *211*, 191–199.
Kinsman, E. a, and Pyke, K. a (1998). Bundle sheath cells and cell-specific plastid development in Arabidopsis leaves. Development *125*, 1815–1822.
Kleinboelting, N., Huep, G., Kloetgen, A., Viehoever, P., and Weisshaar, B. (2012). GABI-Kat SimpleSearch: New features of the Arabidopsis thaliana T-DNA mutant database. Nucleic Acids Res. *40*, 1211–1215.
Koizumi, K., Sugiyama, M., and Fukuda, H. (2000). A series of novel mutants of Arabidopsis thaliana that are defective in the formation of continuous vascular network: calling the auxin signal flow canalization hypothesis into question. Development *127*, 3197–3204.
Kondo, Y., Fujita, T., Sugiyama, M., and Fukuda, H. (2015). A novel system for xylem cell differentiation in arabidopsis thaliana. Mol. Plant *8*, 612–621.
Konishi, M., and Yanagisawa, S. (2007). Sequential activation of two Dof transcription factor gene promoters during vascular development in Arabidopsis thaliana. Plant Physiol. Biochem. *45*, 623–629.
Konishi, M., and Yanagisawa, S. (2015). Transcriptional repression caused by Dof5.8 is involved in proper vein network formation in Arabidopsis thaliana leaves. J. Plant Res. *128*, 653–652.
Konishi, M., Donner, T.J., Scarpella, E., and Yanagisawa, S. (2015). MONOPTEROS directly activates the auxin-inducible promoter of the Dof5.8 transcription factor gene in Arabidopsis thaliana leaf provascular cells. J. Exp. Bot. *66*, 283–291.
Kosugi, S., and Ohashi, Y. (2000). Cloning and DNA-binding properties of a tobacco Ethylene-

Insensitive3 (EIN3) homolog. Nucleic Acids Res. *28*, 960–967.
Krämer, H., Cagan, R.L., and Zipursky, S.L. (1991). Interaction of bride of sevenless membrane-bound ligand and the sevenless tyrosine-kinase receptor. Nature *352*, 207–212.
Krogan, N.T., Ckurshumova, W., Marcos, D., Caragea, A.E., and Berleth, T. (2012). Deletion of MP/ARF5 domains III and IV reveals a requirement for Aux/IAA regulation in Arabidopsis leaf vascular patterning. New Phytol. *194*, 391–401.
Krogan, N.T., Yin, X., Ckurshumova, W., and Berleth, T. (2014). Distinct subclades of Aux/IAA genes are direct targets of ARF5/MP transcriptional regulation. New Phytol. *204*, 474–483.
Langdale, J.A., and Nelson, T. (1991). Spatial regulation of photosynthetic development in C4 plants. Trends Genet. *7*, 191–196.
Langdale, J.A., Metzler, M.C., and Nelson, T. (1987). The argentia mutation delays normal development of photosynthetic cell-types in Zea mays. Dev. Biol. *122*, 243–255.
Langdale, J.A., Rothermel, B.A., and Nelson, T. (1988a). Cellular patterns of photosynthetic gene expression in developing maize leaves. Genes Dev. *2*, 106–115.
Langdale, J.A., Zelitch, I., Miller, E., and Nelson, T. (1988b). Cell position and light influence C4 versus C3 patterns of photosynthetic gene expression in maize. EMBO J. *7*, 3643–3651.
Lau, S., De Smet, I., Kolb, M., Meinhardt, H., and Jürgens, G. (2011). Auxin triggers a genetic switch. Nat. Cell Biol. *13*, 611–615.
Di Laurenzio, L., Wysocka-Diller, J., Malamy, J.E., Pysh, L., Helariutta, Y., Freshour, G., Hahn, M.G., Feldmann, K., A., and Benfey, P.N. (1996). The SCARECROW gene regulates an asymmetric cell division that is essential for generating the radial organization of the Arabidopsis root. Cell *86*, 423–433.
Lee, J.-Y., Colinas, J., Wang, J.Y., Mace, D., Ohler, U., and Benfey, P.N. (2006). Transcriptional and posttranscriptional regulation of transcription factor expression in Arabidopsis roots. Proc. Natl. Acad. Sci. U. S. A. *103*, 6055–6060.
Lee, M.-H.M.M., Kim, B., Song, S.-K., Heo, J.-O., Yu, N.-I., Lee, S.A., Kim, M., Kim, D.G., Sohn, S.O., Lim, C.E., et al. (2008). Large-scale analysis of the GRAS gene family in Arabidopsis thaliana. Plant Mol. Biol. *67*, 659–670.
Lee, S., Cheng, H., King, K.E., Wang, W., He, Y., Hussain, A., Lo, J., Harberd, N.P., and Peng, J. (2002). Gibberellin regulates Arabidopsis seed germination via RGL2,a GAI/RGA-like gene

whose expression is up-regulated following imbibition. Genes Dev. *16*, 646–658.
Levesque, M.P., Vernoux, T., Busch, W., Cui, H., Wang, J.Y., Blilou, I., Hassan, H., Nakajima, K., Matsumoto, N., Lohmann, J.U., et al. (2006). Whole-genome analysis of the short-root developmental pathway in Arabidopsis. PLoS Biol. *4*, 739–752.
Leyser, O. (2010). The power of auxin in plants. Plant Physiol. *154*, 501–505.
Li, H., Tiwari, S.B., Hagen, G., and Guilfoyle, T.J. (2011). Identical amino acid substitutions in the repression domain of auxin/indole-3-acetic acid proteins have contrasting effects on auxin signaling. Plant Physiol. *155*, 1252–1263.
Lijavetzky, D., Carbonero, P., and Vicente-Carbajosa, J. (2003). Genome-wide comparative phylogenetic analysis of the rice and Arabidopsis Dof gene families. BMC Evol. Biol. *3*.
Lippuner, V., Chou, I., Scott, S., Ettinger, W., Theg, S., and Gasser, C. (1994). Cloning and characterization of chloroplast and cytosolic forms of cyclophilin from Arabidopsis thaliana. J. Biol. Chem. *269*, 7863–7868.
Louis, J. (1935). L'ontogenese du systeme conducteur dans la pousse feuillee des Dicotyles et des Gymnospermes. Cellule *44*, 87–172.
Mahonen, A.P., Bonke, M., Kauppinen, L., Riikonen, M., Benfey, P.N., and Helariutta, Y. (2000). A novel two-component hybrid molecule regulates vascular morphogenesis of the Arabidopsis root. Genes Dev. *14*, 2938–2943.
Mansfield, S.G., and Briarty, L.G. (1991). Early Embryogenesis in Arabidopsis-Thaliana .II. the Developing Embryo. Can. J. Bot. Can. Bot. *69*, 461–476.
Mason, M.G., Li, J., Mathews, D.E., Kieber, J.J., and Schaller, G.E. (2004). Type-B Response Regulators Display Overlapping Expression Patterns in Arabidopsis. Plant Physiol. *135*, 927–937.
Mattsson, J., Sung, Z.R., and Berleth, T. (1999). Responses of plant vascular systems to auxin transport inhibition. Development *126*, 2979–2991.
Mattsson, J., Ckurshumova, W., and Berleth, T. (2003). Auxin Signaling in Arabidopsis Leaf Vascular Development. Plant Physiol. *131*, 1327–1339.
Mayer, U., Büttner, G., and Jürgens, G. (1993). Apical-basal pattern formation in the Arabidopsis embryo. Development *117*, 149–162.
McAbee, J.M., Hill, T.A., Skinner, D.J., Izhaki, A., Hauser, B.A., Meister, R.J., Venugopala

Reddy, G., Meyerowitz, E.M., Bowman, J.L., and Gasser, C.S. (2006). Aberrant testa shape encodes a KANADI family member, linking polarity determination to separation and growth of Arabidopsis ovule integuments. Plant J. *46*, 522–531.
McConnell, J.R., and Barton, M.K. (1998). Leaf polarity and meristem formation in Arabidopsis. Development *125*, 2935–2942.
McConnell, J.R., Emery, J.F., Eshed, Y., Bao, N., Bowman, J.L., and Barton, M.K. (2001). Role of PHABULOSA and PHAVOLUTA in determining radial patterning in shoots. Nature *411*, 709–713.
Michniewicz, M., Zago, M.K., Abas, L., Weijers, D., Schweighofer, A., Meskiene, I., Heisler, M.G., Ohno, C., Zhang, J., Huang, F., et al. (2007). Antagonistic Regulation of PIN Phosphorylation by PP2A and PINOID Directs Auxin Flux. Cell *130*, 1044–1056.
Mockaitis, K., and Estelle, M. (2008). Auxin receptors and plant development: a new signaling paradigm. Annu. Rev. Cell Dev. Biol. *24*, 55–80.
Morita, M.T., Saito, C., Nakano, A., and Tasaka, M. (2007). endodermal-amyloplast less 1 is a novel allele of SHORT-ROOT. Adv. Sp. Res. *39*, 1127–1133.
Müller, C.J., Valdés, A.E., Wang, G., Ramachandran, P., Beste, L., Uddenberg, D., and Carlsbecker, A. (2016). PHABULOSA Mediates an Auxin Signaling Loop to Regulate Vascular Patterning in Arabidopsis. Plant Physiol. *170*, 956–970.
Mustroph, A., Zanetti, M.E., Jang, C.J.H., Holtan, H.E., Repetti, P.P., Galbraith, D.W., Girke, T., and Bailey-Serres, J. (2009). Profiling translatomes of discrete cell populations resolves altered cellular priorities during hypoxia in Arabidopsis. Proc. Natl. Acad. Sci. U. S. A. *106*, 18843–18848.
Nakajima, K., Sena, G., Nawy, T., and Benfey, P.N. (2001). Intercellular movement of the putative transcription factor SHR in root patterning. Nature *413*, 307–311.
Nelson, T., and Dengler, N. (1997). Leaf Vascular Pattern Formation. Plant Cell *9*, 1121–1135.
Niehrs, C., and Pollet, N. (1999). Synexpression groups in eukaryotes. Nature *402*, 483–487.
Nishal, B., Tantikanjana, T., and Sundaresan, V. (2005). An inducible targeted tagging system for localized saturation mutagenesis in Arabidopsis. Plant Physiol. *137*, 3–12.
Normanly, J. (2010). Approaching cellular and molecular resolution of auxin biosynthesis and metabolism. Cold Spring Harb. Perspect. Biol. *2*, 1–18.

Norris, S.R., Meyer, S.E., and Callis, J. (1993). The intron of Arabidopsis thaliana polyubiquitin genes is conserved in location and is a quantitative determinant of chimeric gene expression. Plant Mol. Biol. *21*, 895–906.

Ochando, I., González-Reig, S., Ripoll, J.J., Vera, A., and Martínez-Laborda, A. (2008). Alteration of the shoot radial pattern in Arabidopsis thaliana by a gain-of-function allele of the class III HD-Zip gene INCURVATA4. Int. J. Dev. Biol. *52*, 953–961.

Odat, O., Gardiner, J., Sawchuk, M.G., Verna, C., Donner, T.J., and Scarpella, E. (2014). Characterization of an allelic series in the MONOPTEROS gene of arabidopsis. Genesis *52*, 127–133.

Ohashi-Ito, K., and Bergmann, D.C. (2007). Regulation of the Arabidopsis root vascular initial population by LONESOME HIGHWAY. Development *134*, 2959–2968.

Ohashi-Ito, K., Oguchi, M., Kojima, M., Sakakibara, H., and Fukuda, H. (2013). Auxin-associated initiation of vascular cell differentiation by LONESOME HIGHWAY. Development *140*, 765–769.

Okushima, Y., Overvoorde, P.J., Arima, K., M, A.J., Chan, A., Chang, C., Ecker, J.R., Hughes, B., Lui, A., Nguyen, D., et al. (2005). Functional genomic analysis of the AUXIN RESPONSE FACTOR gene family members in Arabidopsis thaliana: unique and overlapping functions of ARF7 and ARF19. Plant Cell *17*, 444–463.

Otsuga, D., DeGuzman, B., Prigge, M.J., Drews, G.N., and Clark, S.E. (2001). REVOLUTA regulates meristem initiation at lateral positions. Plant J. *25*, 223–236.

Overvoorde, P., Okushima, Y., Alonso, J.M., Chan, A., Chang, C., Ecker, J.R., Hughes, B., Liu, A., Onodera, C., Quach, H., et al. (2005). Functional genomic analysis of the AUXIN/INDOLE-3-ACETIC ACID gene family members in Arabidopsis thaliana. Plant Cell *17*, 3282–3300.

Peng, J., Carol, P., Richards, D.E., King, K.E., Cowling, R.J., Murphy, G.P., and Hardberd, N.P. (1997). The Arabidopsis GAI gene defines a signalling pathway that negatively regulates gibberellin responses. Genes Dev *11*, 3194–3205.

Petrásek, J., and Friml, J. (2009). Auxin transport routes in plant development. Development *136*, 2675–2688.

Petricka, J.J., and Nelson, T.M. (2007). Arabidopsis nucleolin affects plant development and patterning. Plant Physiol. *144*, 173–186.

Pineau, C., Freydier, A., Ranocha, P., Jauneau, A., Turner, S., Lemonnier, G., Renou, J.-P., Tarkowski, P., Sandberg, G., Jouanin, L., et al. (2005). hca: an Arabidopsis mutant exhibiting unusual cambial activity and altered vascular patterning. Plant J. *44*, 271–289.

Pray, T.R. (1955). Foliar Venation of Angiosperms . II . Histogenesis of the Venation of Liriodendron. Am. J. Bot. *42*, 18–27.

Prigge, M.J., Otsuga, D., Alonso, J.M., Ecker, J.R., Drews, G.N., and Clark, S.E. (2005). Class III homeodomain-leucine zipper gene family members have overlapping, antagonistic, and distinct roles in Arabidopsis development. Plant Cell *17*, 61–76.

Prouse, M.B., and Campbell, M.M. (2012). The interaction between MYB proteins and their target DNA binding sites. Biochim. Biophys. Acta *1819*, 67–77.

Przemeck, G., Mattsson, J., Hardtke, C.S., Sung, Z.R., and Berleth, T. (1996). Studies on the role of the Arabidopsis gene MONOPTEROS in vascular development and plant cell axialization. Planta *200*, 229–237.

Pullen, M., Clark, N., Zarinkamar, F., Topping, J., and Lindsey, K. (2010). Analysis of vascular development in the hydra sterol biosynthetic mutants of Arabidopsis. PLoS One *5*, e12227.

Pysh, L.D., Wysocka-Diller, J.W., Camilleri, C., Bouchez, D., and Benfey, P.N. (1999). The GRAS gene family in Arabidopsis: sequence characterization and basic expression analysis of the SCARECROW-LIKE genes. Plant J. *18*, 111–119.

Qiao, L., Lissemore, J.L., Shu, P., Smardon, A., Gelber, M.B., and Maine, E.M. (1995). Enhancers of glp-1, a gene required for cell-signaling in Caenorhabditis elegans, define a set of genes required for germline development. Genetics *141*, 551–569.

Ramialison, M., Reinhardt, R., Henrich, T., Wittbrodt, B., Kellner, T., Lowy, C.M., and Wittbrodt, J. (2012). Cis-regulatory properties of medaka synexpression groups. Development *139*, 917–928.

Raven, J.A. (1975). Transport of Indoleacetic Acid in Plant Cells in Relation to pH and Electrical Potential Gradients , and its Significance for Polar IAA Transport. New Phytol. *74*, 163–172.

Reeves, G.T., and Stathopoulos, A. (2009). Graded dorsal and differential gene regulation in the Drosophila embryo. Cold Spring Harb. Perspect. Biol. *1*, a000836.

Reyes, J., Muro-Pastor, M., and Florencio, F. (2004). The GATA family of transcription factors in Arabidopsis and rice. Plant Physiol. *134*, 1718–1732.

Riechmann, J.L., Heard, J., Martin, G., Reuber, L., Jiang, C.Z., Keddie, J., Adam, L., Pineda, O., Ratcliffe, O.J., Samaha, R.R., et al. (2000). Arabidopsis Transcription Factors: Genome-Wide Comparative Analysis Among Eukaryotes. Science *290*, 2105–2110.

Robles, P., Fleury, D., Candela, H., Cnops, G., Alonso-Peral, M.M., Anami, S., Falcone, A., Caldana, C., Willmitzer, L., Ponce, M.R., et al. (2010). The RON1/FRY1/SAL1 gene is required for leaf morphogenesis and venation patterning in Arabidopsis. Plant Physiol. *152*, 1357–1372.

Rogers, K.W., and Schier, A.F. (2011). Morphogen Gradients: From Generation to Interpretation. Annu. Rev. Cell Dev. Biol. *27*, 377–407.

Rubery, P., and Sheldrake, A. (1974). Carrier-mediated auxin transport. Planta *118*, 101–121.

Rubio, V., Linhares, F., Solano, R., Martín, A.C., Iglesias, J., Leyva, A., and Paz-ares, J. (2001). A conserved MYB transcription factor involved in phosphate starvation signaling both in vascular plants and in unicellular algae. Genes Dev. *15*, 2122–2133.

Rybel, B. De, Mo, B., Yoshida, S., Grabowicz, I., Reuille, P.B. De, Boeren, S., Smith, R.S., Borst, J.W., and Weijers, D. (2013). Article A bHLH Complex Controls Embryonic Vascular Tissue Establishment and Indeterminate Growth in Arabidopsis. Dev. Cell *24*, 426–437.

Sachs, T. (1975). The Control of the Differentiation of Vascular Networks. Ann. Bot. *39*, 197–204.

Sachs, T. (1981). The control of the patterned differentiation of vascular tissues. Adv Bot Res *9*, 151–262.

Sachs, T. (1989). The development of vascular networks during leaf development. Curr. Top. Plant Biochem. Physiol. *8*, 168–183.

Sachs, T. (1991). Cell polarity and tissue patterning in plants. Dev. Suppl. *1*, 83–93.

Sachs, T. (2000). Integrating cellular and organismic aspects of vascular differentiation. Plant Cell Physiol. *41*, 649–656.

Santuari, L., Scacchi, E., Rodriguez-Villalon, A., Salinas, P., Dohmann, E.M.N., Brunoud, G., Vernoux, T., Smith, R.S., and Hardtke, C.S. (2011). Positional information by differential endocytosis splits auxin response to drive arabidopsis root meristem growth. Curr. Biol. *21*, 1918–1923.

Satoh, R., Fujita, Y., Nakashima, K., Shinozaki, K., and Yamaguchi-Shinozaki, K. (2004). A novel subgroup of bZIP proteins functions as transcriptional activators in hypoosmolarity-

responsive expression of the ProDH gene in Arabidopsis. Plant Cell Physiol. *45*, 309–317.
Sauer, M., Balla, J., Luschnig, C., Wiśniewska, J., Reinöhl, V., Friml, J., and Benková, E. (2006). Canalization of auxin flow by Aux/IAA-ARF-dependent feedback regulation of PIN polarity. Genes Dev. *20*, 2902–2911.
Sawchuk, M.G., Head, P., Donner, T.J., and Scarpella, E. (2007). Time-lapse imaging of Arabidopsis leaf development shows dynamic patterns of procambium formation. New Phytol. *176*, 560–571.
Sawchuk, M.G., Donner, T.J., Head, P., and Scarpella, E. (2008). Unique and overlapping expression patterns among members of photosynthesis-associated nuclear gene families in Arabidopsis. Plant Physiol. *148*, 1908–1924.
Sawchuk, M.G., Edgar, A., and Scarpella, E. (2013). Patterning of leaf vein networks by convergent auxin transport pathways. PLoS Genet. *9*, e1003294.
Scarpella, E., Francis, P., and Berleth, T. (2004). Stage-specific markers define early steps of procambium development in Arabidopsis leaves and correlate termination of vein formation with mesophyll differentiation. Development *131*, 3445–3455.
Scarpella, E., Marcos, D., Friml, J., and Berleth, T. (2006). Control of leaf vascular patterning by polar auxin transport. Genes Dev. *20*, 1015–1027.
Schlereth, A., Möller, B., Liu, W., Kientz, M., Flipse, J., Rademacher, E.H., Schmid, M., Jürgens, G., and Weijers, D. (2010). MONOPTEROS controls embryonic root initiation by regulating a mobile transcription factor. Nature *464*, 913–916.
Schneider, C. a, Rasband, W.S., and Eliceiri, K.W. (2012). NIH Image to ImageJ: 25 years of image analysis. Nat. Methods *9*, 671–675.
Sena, G., Jung, J.W., and Benfey, P.N. (2004). A broad competence to respond to SHORT ROOT revealed by tissue-specific ectopic expression. Development *131*, 2817–2826.
Sessions, A., Burke, E., Presting, G., Aux, G., Mcelver, J., Patton, D., Dietrich, B., Ho, P., Bacwaden, J., Ko, C., et al. (2002). A High-Throughput Arabidopsis Reverse Genetics System. Plant Cell *14*, 2985–2994.
Shaner, N.C., Campbell, R.E., Steinbach, P.A., Giepmans, B.N.G., Palmer, A.E., and Tsien, R.Y. (2004). Improved monomeric red, orange and yellow fluorescent proteins derived from Discosoma sp. red fluorescent protein. Nat. Biotechnol. *22*, 1567–1572.

Sieburth, L.E. (1999). Auxin is required for leaf vein pattern in Arabidopsis. Plant Physiol. *121*, 1179–1190.

Silverstone, A.L., Ciampaglio, C.N., and Sun, T. (1998). The Arabidopsis RGA gene encodes a transcriptional regulator repressing the gibberellin signal transduction pathway. Plant Cell *10*, 155–169.

Smardon, A., Spoerke, J.M., Stacey, S.C., Klein, M.E., MacKin, N., and Maine, E.M. (2000). EGO-1 is related to RNA-directed RNA polymerase and functions in germ-line development and RNA interference in C. elegans. Curr. Biol. *10*, 169–178.

De Smet, I., and Jürgens, G. (2007). Patterning the axis in plants--auxin in control. Curr. Opin. Genet. Dev. *17*, 337–343.

Steinmann, T., Geldner, N., Grebe, M., Mangold, S., Jackson, C.L., Paris, S., Gälweiler, L., Palme, K., and Jürgens, G. (1999). Coordinated Polar Localization of Auxin Efflux Carrier PIN1 by GNOM ARF GEF. Science *286*, 316–318.

Steynen, Q.J., and Schultz, E.A. (2003). The FORKED genes are essential for distal vein meeting in Arabidopsis. Development *130*, 4695–4708.

Suzuki, T., Miwa, K., Ishikawa, K., Yamada, H., Aiba, H., and Mizuno, T. (2001). The Arabidopsis sensor His-kinase, AHk4, can respond to cytokinins. Plant Cell Physiol. *42*, 107–113.

Swaminathan, K., Peterson, K., and Jack, T. (2008). The plant B3 superfamily. Trends Plant Sci. *13*, 647–655.

Szemenyei, H., Hannon, M., and Long, J.A. (2008). TOPLESS mediates auxin-dependent transcriptional repression during Arabidopsis embryogenesis. Science *319*, 1384–1386.

Tajima, Y., Imamura, A., Kiba, T., Amano, Y., Yamashino, T., and Mizuno, T. (2004). Comparative Studies on the Type-B Response Regulators Revealing their Distinctive Properties in the His-to-Asp Phosphorelay Signal Transduction of Arabidopsis thaliana. Plant Cell Physiol. *45*, 28–39.

Tan, X., Calderon-Villalobos, L.I. a, Sharon, M., Zheng, C., Robinson, C. V, Estelle, M., and Zheng, N. (2007). Mechanism of auxin perception by the TIR1 ubiquitin ligase. Nature *446*, 640–645.

Telfer, A., and Poethig, RS. (1994). Leaf development in Arabidopsis. In The Arabidopsis Book,

E.M. Meyerowitz, and C.R. Somerville, eds. (New York: Cold Spring Harbor Press.), p. 379–401.

Thomas, C.L., Schmidt, D., Bayer, E.M., Dreos, R., and Maule, A.J. (2009). Arabidopsis plant homeodomain finger proteins operate downstream of auxin accumulation in specifying the vasculature and primary root meristem. Plant J. *59*, 426–436.

Tiwari, S.S.B., Hagen, G., and Guilfoyle, T.J. (2003). The roles of auxin response factor domains in auxin-responsive transcription. Plant Cell *15*, 533–543.

Toledo-Ortiz, G., Huq, E., and Quail, P.H. (2003). The Arabidopsis Basic/Helix-Loop-Helix Transcription Factor Family. Plant Cell *15*, 1749–1770.

Torres-Galea, P., Huang, L.F., Chua, N.H., and Bolle, C. (2006). The GRAS protein SCL13 is a positive regulator of phytochrome-dependent red light signaling, but can also modulate phytochrome A responses. Mol. Genet. Genomics *276*, 13–30.

Toufighi, K., Brady, S.M., Austin, R., Ly, E., and Provart, N.J. (2005). The Botany Array Resource: e-Northerns, Expression Angling, and promoter analyses. Plant J. *43*, 153–163.

Triezenberg, S.J., Kingsbury, R.C., and McKnight, S.L. (1988). Functional dissection of VP16, the trans-activator of herpes simplex virus immediate early gene expression. Genes Dev. *2*, 718–729.

Tsuchisaka, A., and Theologis, A. (2004). Unique and Overlapping Expression Patterns among the Arabidopsis 1-Amino-Cyclopropane-1-Carboxylate Synthase Gene Family Members. Plant Physiol. *136*, 2982–3000.

Tsugeki, R., Ditengou, F.A., Sumi, Y., Teale, W., Palme, K., and Okada, K. (2009). NO VEIN mediates auxin-dependent specification and patterning in the Arabidopsis embryo, shoot, and root. Plant Cell *21*, 3133–3151.

Tyler, L., Thomas, S.G., Hu, J., Dill, A., Alonso, J.M., and Ecker, J.R. (2004). DELLA Proteins and Gibberellin-Regulated Seed Germination and Floral Development. Plant Physiol. *135*, 1008–1019.

Ueki, T., and Citovskytle, V. (2000). Intercellular RNA transport in plants. Curr. Top. Plant Biol. *2*, 167–179.

Ulmasov, T. (1997). ARF1, a Transcription Factor That Binds to Auxin Response Elements. Science *276*, 1865–1868.

Ulmasov, T., Murfett, J., Hagen, G., and Guilfoyle, T.J. (1997). Aux/lAA Proteins Repress Expression of Reporter Genes Containing Natural and Highly Active Synthetic Auxin Response Elements. Plant Cell *9*, 1963–1971.

Ulmasov, T., Hagen, G., and Guilfoyle, T.J. (1999a). Activation and repression of transcription by auxin- response factors. Proc. Natl. Acad. Sci. USA *96*, 5844–5849.

Ulmasov, T., Hagen, G., and Guilfoyle, T.J. (1999b). Dimerization and DNA binding of auxin response factors. Plant J. *19*, 309–319.

Vera-Sirera, F., Minguet, E.G., Singh, S.K., Ljung, K., Tuominen, H., Blázquez, M.A., and Carbonell, J. (2010). Role of polyamines in plant vascular development. Plant Physiol. Biochem. *48*, 534–539.

Verna, C., Sawchuk, M.G., Linh, N.M., and Scarpella, E. (2015). Control of vein network topology by auxin transport. BMC Biol. *13*, 94.

Vernoux, T., Brunoud, G., Farcot, E., Morin, V., Van den Daele, H., Legrand, J., Oliva, M., Das, P., Larrieu, A., Wells, D., et al. (2011). The auxin signalling network translates dynamic input into robust patterning at the shoot apex. Mol. Syst. Biol. *7*, 508.

Wang, J.-W., Wang, L.-J., Mao, Y.-B., Cai, W.-J., Xue, H.-W., and Chen, X.-Y. (2005). Control of root cap formation by MicroRNA-targeted auxin response factors in Arabidopsis. Plant Cell *17*, 2204–2216.

Weijers, D., Benkova, E., Jäger, K.E., Schlereth, A., Hamann, T., Kientz, M., Wilmoth, J.C., Reed, J.W., and Jürgens, G. (2005). Developmental specificity of auxin response by pairs of ARF and Aux/IAA transcriptional regulators. EMBO J. *24*, 1874–1885.

Wen, C.-K., and Chang, C. (2002). Arabidopsis RGL1 encodes a negative regulator of gibberellin responses. Plant Cell *14*, 87–100.

Wenzel, C.L., Schuetz, M.M., Yu, Q., and Mattsson, J. (2007). Dynamics of MONOPTEROS and PIN-FORMED1 expression during leaf vein pattern formation in Arabidopsis thaliana. Plant J. *49*, 387–398.

Werner, T., and Schmulling, T. (2009). Cytokinin action in plant development. Curr. Opin. Plant Biol. *12*, 527–538.

Woody, S.T., Austin-Phillips, S., Amasino, R.M., and Krysan, P.J. (2007). The WiscDsLox T-DNA collection: an arabidopsis community resource generated by using an improved high-

throughput T-DNA sequencing pipeline. J. Plant Res. *120*, 157–165.
Worley, C.K., Zenser, N., Ramos, J., Rouse, D., Leyser, O., Theologis, A., and Callis, J. (2000). Degradation of Aux / IAA proteins is essential for normal auxin signalling. Plant J. *21*, 553–562.
Wykoff, D.D., Grossman, A.R., Weeks, D.P., Usuda, H., and Shimogawara, K. (1999). Psr1, a nuclear localized protein that regulates phosphorus metabolism in Chlamydomonas. Proc. Natl. Acad. Sci. U. S. A. *96*, 15336–15341.
Wysocka-Diller, J.W., Helariutta, Y., Fukaki, H., Malamy, J.E., and Benfey, P.N. (2000). Molecular analysis of SCARECROW function reveals a radial patterning mechanism common to root and shoot. Development *127*, 595–603.
Yanagisawa, S. (2002). The Dof family of plant transcription factors. Trends Plant Sci. *7*, 555–560.
Yanagisawa, S., and Schmidt, R.J. (1999). Diversity and similarity among recognition sequences of Dof transcription factors. Plant J. *17*, 209–214.
Yokoyama, A., Yamashino, T., Amano, Y.I., Tajima, Y., Imamura, A., Sakakibara, H., and Mizuno, T. (2007). Type-B ARR transcription factors, ARR10 and ARR12, are implicated in cytokinin-mediated regulation of protoxylem differentiation in roots of Arabidopsis thaliana. Plant Cell Physiol. *48*, 84–96.
Zenser, N., Ellsmore, a, Leasure, C., and Callis, J. (2001). Auxin modulates the degradation rate of Aux/IAA proteins. Proc. Natl. Acad. Sci. U. S. A. *98*, 11795–11800.
Zhang, C., Gong, F.C., Lambert, G.M., and Galbraith, D.W. (2005). Cell type-specific characterization of nuclear DNA contents within complex tissues and organs. Plant Methods *1*, 7.
Zhang, S., Raina, S., Li, H., Li, J., Dec, E., Ma, H., Huang, H., and Fedoroff, N. V (2003). Resources for targeted insertional and deletional mutagenesis in Arabidopsis. Plant Mol. Biol. *53*, 133–150.
Zhao, Y. (2010). Auxin Biosynthesis and Its Role in Plant Development. Annu. Rev. Plant Biol. *61*, 49–64.
Zhong, R., and Ye, Z.-H. (2004). amphivasal vascular bundle 1, a Gain-of-Function Mutation of the IFL1/REV Gene, Is Associated with Alterations in the Polarity of Leaves, Stems and Carpels. Plant Cell Physiol. *45*, 369–385.
Zhou, G.-K., Kubo, M., Zhong, R., Demura, T., and Ye, Z.-H. (2007). Overexpression of

miR165 affects apical meristem formation, organ polarity establishment and vascular development in Arabidopsis. Plant Cell Physiol. *48*, 391–404.
Zinzen, R.P., Girardot, C., Gagneur, J., Braun, M., and Furlong, E.E.M. (2009). Combinatorial binding predicts spatio-temporal cis-regulatory activity. Nature *462*, 65–70.